Universidade de Lisboa

Faculdade de Medicina de Lisboa

Magnetic resonance imaging of the *substantia nigra* in Parkinson's disease

Neuromelanin, iron and diffusion tensor imaging

SOFIA PEREIRA COUTINHO REIMÃO

Orientador: Professor Doutor Jorge Guedes Campos
Co-Orientador: Professor Doutor Joaquim Ferreira

Doutoramento em Medicina
Especialidade de Imagiologia

A impressão desta dissertação foi aprovada pelo Conselho Científico da Faculdade de Medicina de Lisboa em reunião de 24 de Março de 2015.

CONTENTS

ACKNOWLEDGEMENTS

We express our gratitude to all who directly or indirectly made this work possible, with a very special recognition to Professor Doutor Jorge Guedes Campos and Professor Doutor Joaquim Ferreira for their inestimable guidance, tireless and permanent support given to the concretization of this work. Their example taught us lessons we will treasure for life.

We are extremely grateful to the multidisciplinary team that collaborated with us and are an intrinsic support of this work.

A special word of recognition to Professora Doutora Rita Nunes and the members of Instituto de Biofísica e Engenharia Biomédica (IBEB) of Faculdade de Ciências da Universidade de Lisboa, for their participation in imaging analysis and post-processing tools development, without which we could not have achieved these results. To all the IBEB master's students who participated in this project our appreciation for the commitment to this project and all the developed work.

To Dr. Patrícia Pita Lobo and Dr. Dulce Neutel a recognized word for all the help and expertise in the clinical evaluations. We are also thankful to all the staff of Unidade de Doenças do Movimento of Serviço de Neurologia do Centro Hospitalar Lisboa Norte, EP – Hospital de Santa Maria.

We are also very grateful to the Sociedade Portuguesa de Ressonância Magnética, in the person of its Clinical Director, Dra. Alexandra Covas de Lima, by all the support. To all the imagiology technicians who performed the MR examinations in SPRM and Serviço de Imagiologia Neurológica do Centro Hospitalar Lisboa Norte, EP – Hospital de Santa Maria, our recognition for the competence and professionalism.

To MsC. Daisy Abreu and MsC. Nilza Gonçalves our gratitude for all the help and expertise in the statistical analysis as well as to Ana Teresa Santos for all the support.

We are also thankful to Phillips in the person of Eng. Manuel Eugénio for the support and to engineer Nuno Loução for MRI sequence optimization.

We thank all of the patients and control subjects for their time and commitment to this research.

A last and very special word of gratitude to my parents without whose incentive from the beginning to the end of this long journey this work would not have been possible.

ABBREVIATIONS

PD Parkinson's disease

SN *Substantia nigra*

SNpc *Substantia nigra pars compacta*

SNpr *Substantia nigra pars reticulata*

LC *Locus coeruleus*

MR Magnetic resonance

DTI Diffusion tensor imaging

FA Fractional anisotropy

MD mean diffusivity

ET Essential tremor

MSA Multiple system atrophy

PSP Progressive supranuclear palsy

APS Atypical parkinsonian syndromes

α-Syn alpha-synuclein

TYR tyrosinase

TH tyrosine hydroxylase

DA dopamine

IR inversion-recovery

STIR short T1 inversion recovery

MT magnetization transfer

ROI region-of-interest

VBM voxel based morphometry

VBA voxel-based analysis

TBSS tract-based spatial statistics

ABSTRACT

In the last years, extensive developments in neuroimaging MR techniques have profoundly changed the study of Parkinson's disease (PD), evolving from the role of excluding secondary parkinsonism to the emergence as a disease biomarker. MR advanced sequences in high field magnets opened the possibility to visualize *in vivo* the *substantia nigra* (SN) and to investigate specific PD pathological changes, enabling the development of high accuracy tools for disease diagnosis in early stages and for the comprehension of disease pathophysiology.

Our work was centered on the application of new MR imaging techniques to study the SN in PD, early in the disease course, mainly focusing on untreated patients at the time of clinical diagnosis. The primary objectives were centered on the application of high field MR imaging sequences in two main areas: diagnosis of PD in early disease stages and differential diagnosis with Essential tremor (ET).

The development and application of neuromelanin sensitive MR imaging in 3.0 Tesla allowed the detection of significant changes in the SN of PD patients, with high sensitivity and specificity for disease diagnosis, even in early disease stages (namely at the time of clinical diagnosis). These imaging findings reproduced *in vivo* the characteristic pathological changes of PD with greater alteration in the ventrolateral SN region and preservation of the dorsal segment. These results were obtained with several image evaluation methods: semi-automated area assessments, manual width measurements and simple visual inspection by Neuroradiologists, corroborating the reproducibility of the data and enabling wider applications of this image technique in the clinical practice.

The MR correlation of neuromelanin with iron in the SN of PD patients allowed the *in vivo* investigation of the influence of local iron concentration in the SN on the signal of neuromelanin-sensitive sequences. A quantification T2-relaxometry study showed that the SN paramagnetic iron effects do not seem to influence significantly the neuromelanin MR signal reduction in PD patients.

Several studies with diffusion tensor MR imaging (DTI) have allowed the detection of microstructural changes in the SN of PD patients in early disease changes, emerging as a possible disease biomarker. So, the reproducibility of DTI metrics in this specific brain

area was particularly relevant for future applications of this MR technique. We conducted a reproducibility DTI study in PD patients that showed a good reproducibility of DTI metrics supporting the use of these measurements in further studies, namely longitudinal within-subject evaluation, and cross-sectional comparisons.

The differential diagnosis of PD with ET is particularly relevant and there was the need of high accurate tools to aid the clinical assessment. The application of neuromelanin-sensitive MR techniques was able to discriminate ET from early stage tremor-dominant PD with high sensitivity and specificity values, in the same range as nuclear medicine techniques and may become a useful clinical tool in the evaluation of tremor disorders.

Our research showed an important role of neuromelanin sensitive MR imaging for the diagnosis PD in early disease stages and its differential diagnosis with ET. A multi-modal MR approach with iron assessment and diffusion tensor imaging can further elucidate the SN disease changes and aid future research of disease pathophysiology.

Key-words: *Parkinson's disease, MRI, neuromelanin, iron, diffusion tensor imaging, Essential tremor*.

RESUMO

Nos últimos anos, o extenso desenvolvimento das técnicas de neuroimagem modificou profundamente a investigação da Doença de Parkinson (PD), evoluindo de um simples papel na exclusão de parkinsonismo secundário para a emergência de biomarcadores imagiológicos da doença. Sequências avançadas de RM em aparelhos de alto campo magnético abriram a possibilidade de visualizar *in vivo* a substantia nigra (SN) e a investigação de alterações patológicas específicas da PD, permitindo o desenvolvimento de ferramentas com elevada fiabilidade para o diagnóstico em fases precoces da evolução da doença e para a compreensão da sua fisiopatologia.

A nossa investigação centrou-se na aplicação de novas técnicas de imagem RM para estudar a SN na PD, em fases precoces da doença, com enfoque especial em doentes não tratados na altura do diagnóstico clínico. Os objectivos principais centraram-se na aplicação de sequências de RM em alto campo em duas áreas major: diagnóstico da PD em fases precoces da doença e o diagnóstico diferencial com o Tremor essencial (ET).

O desenvolvimento e aplicação da imagem RM sensível à neuromelanina em 3.0T permitiu a detecção de alterações significativas na SN de doentes com PD, com elevada sensibilidade e especificidade para o diagnóstico da doença, mesmo em fases precoces da sua evolução dela (nomeadamente na altura do diagnóstico clínico). Estes achados de imagem reproduziram *in vivo* as alterações patológicas características da PD, com uma maior alteração na região ventero-lateral da SN e preservação do segmento dorsal. Estes resultados foram obtidos com vários métodos de avaliação de imagem: avaliação semi-automática da área, medição manual da espessura e avaliação visual por neurorradiologistas, corroborando a reproductibilidade dos dados e permitindo uma aplicação abrangente desta técnica de imagem na prática clínica.

A correlação por RM da neuromelanina com o ferro, na SN de doentes com PD, permitiu a investigação *in vivo* da influência da concentração local de ferro na SN com o sinal das sequências sensíveis à neuromelanina. Um estudo quantitativo de relaxometria T2* mostrou que os efeitos paramagnéticos do ferro não influenciam significativamente a redução de sinal RM da neuromelanina em doentes com PD.

Vários estudos com tensores de difusão (DT) permitiram a detecção de alterações microestruturais na SN de doentes com PD em fases precoces de doença, emergindo como um possível biomarcador de doença. Assim, a reproductibilidade das métricas de DTI, nesta área específica do encéfalo, é particularmente relevante para aplicações futuras desta técnica de RM. Conduzimos um estudo de reproductibilidade de DTI em doentes com PD que demonstrou uma boa reproductibilidade das métricas de DTI, suportando a utilização destas medidas em estudos futuros, nomeadamente avaliações longitudinais "within-subject" e comparações "cross-sectional".

O diagnóstico diferencial da PD com ET é particularmente relevante e ferramentas fiáveis para auxiliar a avaliação clínica eram necessárias. A aplicação de técnicas de RM sensíveis à neuromelanina possibilitou a discriminação de ET de PD "tremor-dominant" em fases precoces com elevados valores de sensibilidade e especificidade, no mesmo espectro das técnicas de medicina nuclear e pode tornar-se uma ferramenta clínica útil para a avaliação do tremor.

A nossa investigação demonstrou um importante papel das técnicas de RM sensíveis à neuromelanina para o diagnóstico de PD em fases precoces da doença e para o seu diagnóstico diferencial com ET. Uma abordagem multi-modal de RM com avaliação do ferro e DTI pode, adicionalmente, permitir estudar as alterações da SN e auxiliar a investigação futura da fisiopatologia da doença.

Palavras-chave: *Doença de Parkinson, MRI, neuromelanina, ferro, imagem por tensores de difusão, Tremor essencial*.

INTRODUCTION

Extensive developments of neuroimaging techniques in the last years have profoundly changed the study of Parkinson's disease (PD). In the past, computed tomography (CT) and magnetic resonance (MR) in PD were almost exclusively confined to the detection of secondary causes of parkinsonism. However, advanced MR sequences and high field magnets have revolutionized the *in vivo* study of the brain parenchyma, increasing signal-to noise ratios, improving spacial and contrast resolutions and allowing microstructural evaluation.

Recent advances in the understanding of PD pathogenesis have stimulated a great interest in the development of potential disease modifying therapies, and therefore, a more urgent need to detect disease as early as possible, to develop biomarkers that can assess the result of the interventions, and even allow an *in vivo* assessment of the processes involved in disease pathogenesis.

The increased volume of research in the neuroimaging of PD, analyzing morphological and microstructural changes, opens a new path for the development of high accuracy diagnostic tools in early disease stages and for the comprehension of pathophysiological mechanisms, possibly allowing the development of imaging biomarkers with direct impact in the clinical practice. The increased interest in pre-manifest PD highlights the need to investigate pathological changes that occur very early in the course of the disease, before the beginning of clinical symptoms. MR imaging methods may significant contribute to study *in vivo* these changes and become very relevant in the detection of precocious disease alterations. Structural MR imaging appears also as the most promising marker of disease progression which may have a significant impact on the comprehension of disease progression, clinical correlations and the investigation of therapeutical effects.

The expected rise in PD incidence over the next years additionally motivates research in this area. Currently, PD has an estimated prevalence of 1% in the European population (1) and approximately 1,5 million in the United States (2). A recent study determined PD prevalence in Portugal to be around 18.000 patients (Nilza Gonçalves, Joaquim J. Ferreira, personal communication, February 26, 2015). The risk of developing PD increases significantly after 60 years of age and so, in the next 25 years, disease incidence is expected to significantly increase (2).

Parkinson's disease (PD), first described in 1817 by James Parkinson (3), was traditionally seen as a specific neurodegenerative chronic progressive disease with specific clinical presentation and pathological findings. However what is designated as "idiopathic PD" might in fact be a heterogeneous group of changes, with diverse susceptibility factors and a wide genetic and phenotypic heterogeneity (4)[1].

Although PD is characterized by cardinal motor symptoms of bradykinesia, rigidity, tremor and postural instability (5,6), non-motor symptoms are growingly relevant in disease associated morbidity (7,8). Olfactory changes, depression, cognitive impairment, autonomic dysfunction and sleep disorders reflect the global brain involvement of PD (7,8). Imaging studies can provide significant insights into the comprehension of motor and non-motor complications of PD unveiling the diffuse brain changes of the disease.

The characteristic topographic brain involvement of PD, with an ascending path from the brainstem to the neocortex (9) (Table 1), might be related to the susceptibility of neuronal types (9) to the accumulation of the inclusion **Lewy bodies**, abnormal aggregates mainly constituted of α-synuclein (α-Syn) and ubiquitin (10).

Table 1. Main evolution stages of pathology changes in PD (9)

Stages	Main structre involved	Location of the lesions on pathology studies
Stage 1	Medulla	Dorsal IX/X motor nucleus and/or intermediate reticular zone
Stage 2	Medulla and pons tegmentum	Stage 1 + raphe nuclei, gigantocellular reticular nucleus, and coeruleus-subcoeruleus complex
Stage 3	Midbrain	Stage 2 + midbrain lesions, in particular SNc
Stage 4	Prosencephalum and mesocortex	Stage 3 + prosencephalic lesions; mesocortex and allocortex
Stage 5	Neocortex	Stage 4 + sensory association areas of the neocortex and prefrontal neocortex
Stage 6	Neocortex	Stage 5 + sensory association areas of the neocortex and premotor areas, occasionally mild changes in primary sensory areas and the primary motor field

The characteristic depletion of *substantia nigra* (SN) dopaminergic and *locus coeruleus* (LC) noradrenergic neurons in PD (9,11-13) leads to a denervation of the striatum and

[1] In spite of the recent controversy regarding the precise meaning of the term "Parkinson's disease" and the most appropriate terminology to characterize disease variants (4) in this work we will use the term PD regardless of its variants, since there is no wide consensus as to the definitions in this field.

additionally to extensive extra-nigral pathology (9). In PD the SN changes are not uniform being characterized by a more pronounced reduction of dopaminergic cells in the ventrolateral segment (14) with a corresponding loss of dopaminergic innervation in the posterior putamen (15).

PD becomes clinically manifest when the SN pathological changes have reached an advanced stage (16) being estimated that a degeneration of more than 50% of the dopaminergic SN neurons occurs before the beginning of motor symptoms (17). So most of the disease process has already occurred by the time the patient has clinical complaints, emphasizing the need for early and even pre-manifest disease studies.

The diagnosis of PD in early disease stages has a great clinical relevance for the implementation of an adequate therapeutical plan, for prognostic definition and even for the appropriate selection of patients in clinical trials (18). But in spite of the established PD diagnostic clinical criteria (19), the differentiation with other causes of tremor and parkinsonism can be challenging, especially in early disease stages where a significant clinical overlap can occur (20). In atypical/uncertain cases the exclusive use of clinical criteria for PD diagnosis can have a high rate of misdiagnosis, even if performed by movement disorders specialized neurologists (21,22).

So, imaging techniques might be of great importance, aiding diagnosis in early or pre-manifest stages, helping to monitor disease progression and the therapeutical response and allowing the *in vivo* visualization of the characteristics disease patterns for the differentiation of parkinsonian syndromes (23).

MR imaging approaches, including anatomical studies of connectivity and shape analysis, the evaluation of iron deposition in-vivo or microstructural diffusion changes, are increasingly relevant in PD.

In this work we used a combined multimodal MR imaging protocol to study PD patients focusing on early-stage disease diagnosis and the differentiation of PD with essential tremor (ET). The study of neuromelanin with MR sensitive sequences assumed a particular relevance in PD early disease diagnosis, offering the possibility to image *in vivo* specific disease pathological changes and was complemented by a quantitative assessment of the iron content and microstructural diffusion tensor imaging, enabling a multifaceted study of PD pathological processes.

So we developed a multi-modal advanced MR imaging protocol focusing on the implementation, data analysis, evaluation of clinical impact and correlation with anatomical and pathophysiological PD changes of MR sensitive neuromelanin imaging for the diagnosis of early-stage PD patients, complementing this study with iron quantification and diffusion tensor imaging.

AIMS

The principal aim of this work was the implementation of a multimodal MR imaging protocol to study the SN in PD, focusing on early-stage patients at the time of clinical diagnosis, analyzing data in two main areas: disease diagnosis and differentiation with ET.

The specific aims of this work were:

- Analysis of MR neuromelanin changes in the SN of PD patients in early disease stages, determining the accuracy of this imaging technique for disease diagnosis;

- MR study of the iron content of the SN in PD patients and it's correlation with neuromelanin MR signal changes;

- Microstructural evaluation of the SN with diffusion tensor imaging, determining the reproducibility of this imaging technique in PD patients;

- Analysis of accuracy of MR SN neuromelanin imaging for the differential diagnosis of PD with ET;

- Development of post-processing tools and evaluation methods to allow the clinical usage of these imaging techniques.

PUBLICATIONS LIST

In agreement with Decreto-Lei 388/70, art. 8º, the results presented and discussed in this work were published, accepted or submitted for publication in the following scientific peer-reviewed journals:

- **Sofia Reimão**, Carlos Morgado, Lia Neto, Joaquim Ferreira, Miguel Coelho, Mário Miguel Rosa, Jorge Campos. Diffusion tensor imaging in movement disorders: review of major patterns and correlation with normal brainstem/cerebellar white matter. *The Neuroradiology Journal* 2011; 24: 177-186.

- **Sofia Reimão**, Patrícia Pita Lobo, Dulce Neutel, Leonor Correia Guedes, Miguel Coelho, Mário Miguel Rosa, Joana Ferreira, Daisy Abreu, Nilza Gonçalves, Carlos Morgado, Rita Nunes, Jorge Campos, Joaquim J Ferreira. Substantia nigra neuromelanin magnetic resonance imaging in "de novo" Parkinson's disease patients. *European Journal of Neurology (Eur J Neurol)* 2015 Mar;22(3):540-6. doi:10.1111/ene.12613. Epub 2014 Dec 22.

- **Sofia Reimão**, Patrícia Pita Lobo, Dulce Neutel, Leonor Correia Guedes, Miguel Coelho, Mário Miguel Rosa, Joana Ferreira, Daisy Abreu, Nilza Gonçalves, Carlos Morgado, Rita G Nunes, Jorge Campos, Joaquim J Ferreira. Quantitative analysis versus visual assessment of neuromelanin MR imaging for the diagnosis of Parkinson's disease. *Submitted for publication.*

- **Sofia Reimão**, Sara Ferreira, Rita G Nunes, Patrícia Pita Lobo, Dulce Neutel, Daisy Abreu, Nilza Gonçalves, Jorge Campos, Joaquim J Ferreira. MRI correlation of iron content with neuromelanin in the Substantia nigra of early stage Parkinson's disease. *Submitted for publication*.

- **Sofia Reimão**, Ana Morgado, Rita G Nunes, Patrícia Pita Lobo, Dulce Neutel, Daisy Abreu, Nilza Gonçalves, Jorge Campos, Joaquim J Ferreira. Reproducibility of diffusion tensor imaging (measurements) in early stage Parkinson's disease. *Submitted for publication*.

- **Sofia Reimão**, Patrícia Pita Lobo, Dulce Neutel, Leonor Correia Guedes, Miguel Coelho, Mário Miguel Rosa, Pedro Azevedo, Joana Ferreira, daisy Abreu, Nilza Gonçalves, Rita G Nunes, Jorge Campos, Joaquim Ferreira. Substantia nigra neuromelanin-MR imaging differentiates Essential tremor from Parkinson's disease. *Movement Disorders 2015* Mar 11. doi:10.1002/mds.26182 [Epub ahead of print].

1. MR IMAGING OF PARKINSON'S DISEASE

1.1. MR conventional sequences

Conventional MR sequences, T1- or T2-weighted, do not allow a clear morphological identification of the SN, do not separate the two anatomical and functionally distinct areas - the SN *pars compacta* (SNc) and SN *pars reticulata* (SNr) - and are not able to detect the SN PD pathological changes (24). In T2-weighted images the SN has a characteristic low signal compared to the surrounding midbrain, but this hypointense area does not correspond to the SNc (25), extending anteriorly into the antero-medial *crus cerebri*, indistinguishable from the sub-thalamic nucleus. Several MR techniques have tried to improve SN visualization, namely through the increase of contrast with inversion-recovery sequences (IR) (26,27), short T1 inversion recovery (STIR) (24) and magnetization transfer (MT) (28).

1.2. MR advanced sequences

In the last years a great number of MR advanced techniques have been used to investigate PD, accessing new morphological and structural information *in vivo*, especially in the evaluation of the SN and basal ganglia (29). However the data from the different studies are variable and have not allowed, in most cases, a significant accuracy for clinical application in disease diagnosis or progression monitoring.

Diffusion weighted imaging studies using different methodologies (either ROI or VBM) have not been able to detect consistent changes in the diffusivity of the SN or the basal ganglia in PD patients (29,30).

Spectroscopy studies in PD have also inconsistent findings which can be related with the low dimensions of the studied areas, namely in the SN, resulting in a great partial volume effect for each voxel (31). Very high field magnets, namely 7.0 or 9.0Tesla, increasing signal-to-noise ratios and spectrum resolution, might in the future allow the *in vivo* biochemical evaluation of the SN and other relevant areas for the study of PD.

Functional MR studies have been widely used in PD, investigating changes in the motor networks. Using different methods especially recently developed techniques of resting-state connectivity (32), these studies have depicted *in vivo* alterations of functional SN

connectivity. However in PD these imaging techniques are restricted almost exclusively to the clinical investigation field with reduced clinical implementation, which is also the case of perfusion studies with arterial RM de *arterial spin labeling* (33).

1.2.1. Neuromelanin sensitive MR imaging

In spite of the long known characteristic depigmentation of the SN in PD being related to the loss of the pigment neuromelanin (9), the investigation of the role of neuromelanin in the pathophysiology of PD is a new field of research. Projection neurons from the SNc and LC are characterized by the presence of a dark colored pigment, related to skin melanin, called **neuromelanin** (34).

Neuromelanin is a substance originating from dopamine and noradrenaline metabolism and is though to have a protective role of neurons from oxidative stress mediated by free metals or free radicals (34,35). Following neuronal death neuromelanin can be released from neuropil (a complex network of axonal arborizations, dendrites and glia that forms most of the grey matter) or engulfed by macrophages (36).

The role of neuromelanin in the etiology and pathophysiology of PD was highlighted by several epidemiology studies that described an increased incidence of melanoma in PD patients and *vice versa* (37-41). The largest prospective melanoma study in PD, with a total of 2106 patients, reported a seven times increase of the relative risk of melanomas in this population (38). Another study associated the diagnosis of melanoma to a 50% increased risk of subsequent PD development (42) and data from a study that included 160 000 individuals without neurological disease has shown that individuals with a familiar history of melanoma have more that a double risk of developping PD (40).

Epidemiology data additionally reports an increased incidence of PD (43-45) and of melanomas (46,47) in Caucasian populations compared to black individuals, indicating an increased vulnerability for the development of both skin tumors and PD associated with melanin skin concentration.

The notion that melanosis potentially protects against melanomas and PD is additionally supported by the negative association between tobacco smoke and the incidence of PD, consistently found in numerous studies over the last 50 years (48-50). Smoker's melanosis, a well documented phenomenon, is probably the result of increased melanin

synthesis related to the stimulation of melanocytes by nicotine or the bonding of melanin to noxious tobacco substances (51).

Although the association between PD and melanomas is well documented the mechanisms of this association are not yet entirely known. The most accepted hypothesis implicates α-Syn which is known to play a crucial role in melanoma pathogenesis and PD.

The relationship between melanin and α-Syn, which is expressed in normal skin (52) and in melanomas (53), has opened new perspectives in the pathophysiological research of PD. The melanin pigments are derived from the aminoacid tyrosine and the enzymes tyrosinase (TYR) and tyrosine hydroxylase (TH) are involved in the biosynthesis of melanin and dopamine initiated by the conversion of tyrosine to DOPA (54,55). These enzymes are present both in skin melanocytes and dopaminergic SN cells and exposure to ultra-violet light (UVB) enhances melanin synthesis and the activity of TYR and reduces extracelular DA in dopaminergic cells (56,57).

The finding that α-Syn can interact with TYR (58) and inhibit TH (54,59) raises the possibility that α-Syn can play a role in the regulation of the biosynthesis of both melanin and DA.

Therefore, in skin melanocytes of PD patients the increase in α-Syn inhibits TH decreasing melanin synthesis (53), with the consequent increase in melanoma risk. In dopaminergic neurons the interaction of TYR with increased levels of α-Syn changes the functions of this molecule inducing a toxic process with cytosolic DA and dopaquinone increased levels leading to mitochondrial damage and neuronal death (60). The association of α-Syn neurotoxicity with neuromelanin concentration changes (56,57) being the possible link between PD and melanoma has lead to a particular interest in the research of neuromelanin.

In 2006 a Japanese group first described the application of a recently developed MR sequence that allowed the visualization of neuromelanin to the study of PD patients (61). In these patients there was a marked reduction of signal intensity in the regions corresponding to the LC and SN (62,63).

We found this technique to be very promising for the direct visualization of pathological changes in PD. This imaging area was new and only initial reports had been published by the Japanese group, so we had to implement the MR sequence and the imaging analysis methodology. The initial MR sequence imaging parameters (61) had to be adjusted to the

available MR equipment (RM 3.0T Philips Achieva®) and in cooperation with Instituto de Biofísica e Engenharia Biomédica (IBEB) user interface tools were developed for imaging post-processing allowing the semi-authomated quantitative measurements of SN neuromelanin (Fig 1).

Fig 1. Graphic user interface developed for the evaluation of MR sensitive neuromelanin images, with semi-automated quantification tools for the SN high signal area (Matlab R2012a, The Math Works, Natick. Massachusetts, USA).

So, we investigated the application of this MR technique to evaluate the SN of early-stage PD patients focusing in the diagnostic accuracy and the *in vivo* detection power of the pathophysiological changes of the disease. The growing recognition of the role of neuromelanin the PD pathophysiology combined with the possibility of visualization of this pigment using high field MR motivated our study were we ascertained the feasibility and determined the sensitivity and specificity of this imaging technique for "early-stage" PD diagnosis.

The results of our study, with high accuracy of neuromelanin-sensitive MR imaging for early-stage PD diagnosis, opened the possibility for a wider use of this imaging techniques in further investigation trials with higher number of subjects but also in clinical practice. A wider use of this imaging technique needed easy and widely available imaging analyzing methods. So, we investigated the possible use of simple image analysis, comparing the visual inspection with a quantitative width analysis of the neuromelanin SN high signal area for PD diagnosis.

1.2.2. MR evaluation of brain iron content

Iron in the brain accumulates mainly as ferritin in oligodendrocytes, but can also be found in neurons and microglia, as shown in post-mortem studies, with higher concentration in the globus pallidus, SN, red nucleus, caudate and putamen (64). Dopaminergic neurons of the *substantia nigra* (SN) *pars compacta* (SNpc) and noradrenergic neurons of the *locus coeruleus* (LC) contain significant amounts of iron sequestered in neuromelanin granules (65). Approximately 20% of SN iron is bonded to neuromelanin in its ferric form (66) and the remainder is stored as ferritin and hemosiderin (67,68).

In PD the SN iron content is increased (69,70), as demonstrated by several post-mortem studies, with higher iron levels in the individual neuromelanin granules of the nigral neurons (71). But the loss of these functional nigral neurons early in the course of the disease results in a general decrease in the number of neuromelanin granules, with iron being sequestered in Lewy bodies in SNpc neurons (72) and with an increased loading of ferritin with iron (73).

Paramagnetic substances such as iron increase proton transverse relaxation rate (R_2), shortening T2 but these signal changes are dependent on several factors other than concentration (74). In the brain tissue multiple iron interactions occur, possibly explaining the poor correlation between T2 times and direct measures of iron and ferritin, with factors other than iron having a role in determining the transverse relaxation parameters (75).

Several MR techniques have been used to study the brain iron load, given the crucial role played by this element in a great number of biological processes namely DNA synthesis, gene expression, myelination or as a co-factor of several enzymes (such as TH), and its implication in neurodegeneration, including PD (76,77). MR studies with R2, R2* or R2' relaxometry, determined by the transversal relaxation rate (T2 or T2*), correlate with *post-mortem* iron concentration, being very sensitive to evaluate and quantify brain iron content *in vivo* (78).

A different MR imaging iron analysis with magnetic susceptibility weighted techniques (SWI) uses the information of magnetic susceptibility differences between regions to generate image contrast, combining both magnitude and phase information, and

although not allowing quantification, is very sensitive to alterations induced by the presence of paramagnetic substances such as iron (79).

Both techniques have been used to study PD, trying to identify changes in the regional iron distribution and differences in the deposition patterns compared to other parkinsonian syndromes. Relaxometry studies using high field MR magnets have identified an increase in iron deposition in the SN corresponding to the characteristic pathological changes of the disease (80,81). SWI studies in PD have described an increased magnetic susceptibility in the SN, greater in the caudal segment (82) that allowed the identification of pattern differences with other parkinsonian syndromes (83).

It is known that neuromelanin interacts with free iron in the SN and LC neurons acting as a strong protector in the delay of neuronal death (84-86). The interaction of neuromelanin with iron can render the SN dopaminergic neurons more susceptible to oxidative stress leading to neuronal damage (87-89).

The interaction of neuromelanin with iron had not yet been studied and this was pointed out as a limitation to the analysis of neuromelanin-sensitive MR studies since the implication of the iron content to the T1 high signal in the SN of PD patients was not known. To answer this question we performed a combined MR imaging analysis of iron content, using quantitative relaxometry (Fig 2) and a neuromelanin-sensitive sequence to study of their interaction, influence and correlation.

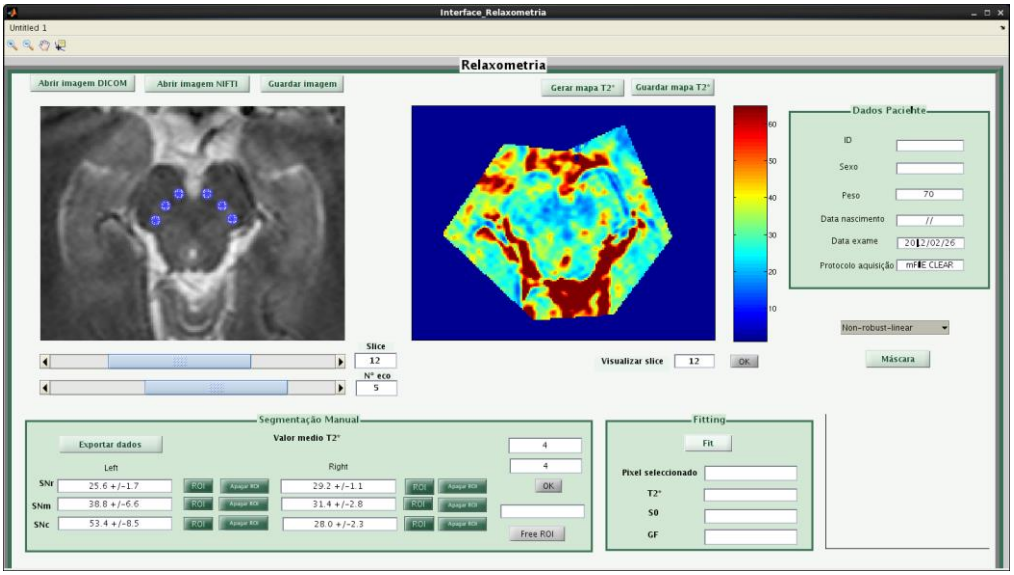

Fig 2. Graphic user interface developed for evaluation of MR relaxometry with quantification tools for the SN area (Matlab R2012a, The Math Works, Natick. Massachusetts, USA).

1.2.3. Diffusion tensor imaging

Diffusion tensor imaging (DTI) MR sequences have recently acquired a significant relevance in PD investigation. This technique is based in the analysis of water molecules diffusivity, using a mathematical tensor model to characterize diffusion in the 3D space, which has a variable degree according to the molecular characteristics of the tissue (90). DTI parameters allow an estimation of the degree of directionality through anisotropy (frequently fractional anisotropy [FA]) and the global movement of the molecules (mean diffusivity[MD] and apparent diffusion coefficient [ADC]). These measures can be obtained with multiple approaches either locally in predefined regions with ROI analysis or globally with voxel-based analysis (VBAA) or tract-based spatial statistics (TBSS). In the white matter diffusion is limited in certain directions being less dependent of direction in the grey matter where FA values are lower (90). Voxel-based DTI studies have been widely used to study white matter but also allow the detection of grey matter integrity changes (91).

Tissue microstructural changes such as occur in neurodegenerative processes can be associated with alterations in anisotropy and diffusivity measures (91) and animal model studies have positively correlated DTI parameters with SN dopaminergic neuronal loss (92), giving and indirect measure of degeneration.

A DTI study by Vaillancourt and colleagues (93) has gained a particular relevance because of the high sensitivity and specificity of the reported reduction of FA values in the SN for the distinction of early-stage PD patients from healthy controls; this data reproduced *in vivo* the pathology findings of selective dopaminergic neuronal loss in the ventrolateral and caudal segments of the SN (14). But several studies have used DTI to evaluate the SN in PD and the majority of the studies report an FA reduction in the SN, consistent with the characteristic pathological changes of the disease (23,94). Very recently a DTI study has even demonstrated microstructural SN changes in subjects chronically exposed to pesticides, which is a known risk factor associated with PD (95).

So, these data seem to indicate that MR studies with DTI can detect SN changes that occur before clinical manifestations of the disease aiding early and even pre-clinical diagnosis and identifying disease risk factors and its etiological implication with the potential to become a non-invasive biomarker of PD.

DTI techniques have additionally allowed the study not only of nigro-striatal pathways and its projections (94), but also of the diffuse brain involvement in PD, identifying changes in the olfactory areas (96), basal ganglia (97), frontal white matter (98) or the corpus callosum (99), among many other regions. DTI tractography studies have also enabled the investigation of structural connectivity between brain regions, with descriptions of a reduced connectivity between the SN and the putamen/ipsilateral thalamus in PD patients (100).

In spite of all the data, a recent meta-analysis of DTI studies in PD has concluded that there is still some inconsistency of the results in early-stage patients and that with the available data the conclusion as to the accuracy of this technique in terms of PD patient's identification can not be drawn (23).

Our imaging protocol included the microstructural study of the SN with DTI answering to the need to replicate the DTI data in the evaluation of SN changes in early-stage PD patients studying the reliability of the measurements with a reproducibility analysis. This had not yet been done in PD patients and this group of patients had specific characteristics that might influence diffusivity measurements.

1.2.3.1. ***Diffusion tensor imaging in movement disorders: review of major patterns and correlation with normal brainstem/cerebellar white matter.***

Reimão S, Morgado C, Neto L, Ferreira J, Coelho M, Rosa M, Campos J.

The Neuroradiology Journal 2011; 24: 177-186.

Diffusion tensor imaging in movement disorders: review of major patterns and correlation with normal brainstem/cerebellar white matter

Reimão S[1], Morgado C[1], Neto L[1], Ferreira JJ[2], Coelho M[2], Rosa M[2], Campos J[1]

Neurological Imaging Department[1] and Neurology Department[2] of Hospital Santa Maria. Lisbon.

Abstract: The authors reviewed the diffusion tensor imaging (DTI) and tractography (DTT) of the normal brainstem and cerebellar white matter in normal volunteers, correlating it with structural magnetic resonance (MR) imaging and DTI data obtained in patients evaluated in our department with parkinsonian movement disorders, including multisystem atrophy (MSA), spinocerebellar ataxia (SCA), Progressive Supra-nuclear palsy (PSP) and idiopathic Parkinson's disease (PD). Axial, sagital, coronal DTI and tractography data demonstrated major white-matter fibers within the brain stem and cerebellum, including cortico-spinal tracts, transverse pontine fibers, medial lemniscus and cerebellar peduncles. Visualization of the selective degeneration of these individual fibre tracts with DTI, in our cases, added qualitative data facilitating the differential diagnosis of movement disorders.

Introduction

Diffusion tensor imaging (DTI) and diffusion tensor tractography (DTT) have been used to map the normal anatomy of the brainstem/cerebellum, not only of the white matter but also allowing the study of gray matter structures (101). DTI data has enabled detailed imaging of major afferent and efferent pathways of the cerebellum and their connections with the brainstem (101,102). The increased sensitivity of DTI in demonstrating changes in the brainstem and cerebellum white matter has been shown in a wide number of pathologies. This information combined with structural MR imaging has proven useful in the detection of impairment in extra-pyramidal circuits, particularly in movement disorders (103).

The idiopathic parkinsonian movement disorders are a group of distinct neurodegenerative diseases, including idiopathic Parkinson's disease (PD), and atypical parkinsonian disorders (APD), comprising multiple system atrophy (MSA), progressive supranuclear palsy (PSP) and corticobasal degeneration (CBD). In the early stages of disease, the differential diagnosis between PD and APD remains a clinical problem, with APD comprising up to 20% of patients presenting with parkinsonism (18). Although conventional magnetic resonance imaging (MR) can demonstrate changes in APD, these are essentially present in advanced stages of disease and have low specificity and sensitivity in the differential diagnosis (104).

The potential of DTI combined with DTT for the differential diagnosis and evaluation of the neurodegeneration of specific pathways in parkinsonian disorders has highlighted DTI as a potential useful tool in the clinical routine (105,106).

We reviewed DTI imaging of the normal brainstem and cerebellar white matter and the characteristic DTI patterns in the more frequent movement disorders. A retrospective review of the DTI studies performed in patients evaluated in Hospital de Santa Maria (Lisbon) with parkinsonian movement disorders was made, trying to ascertain the results obtained and correlating them with the published literature.

Methods

Retrospective review of structural MR imaging and DTI/DTT of brainstem and cerebellar white matter in healthy volunteers and patients with clinically proven parkinsonian

movement disorders including idiopathic Parkinson's disease (PD), multisystem atrophy (MSA), corticobasal degeneration (CBD), spinocerebellar ataxia (SCA), and Progressive Supra-nuclear palsy (PSP), evaluated in Hospital de Santa Maria - Lisbon with DTI studies in the last two years.

Subjects

Two healthy volunteers aged 42 and 54 years, and thirteen patients with early/advanced stage MSA, PSP, CBD, SCA, and PD. The diagnosis was made clinically, using established criteria (18). Control and patient data are summarized in Table 1.

Imaging protocol

All the studies that we reviewed, were performed in a 3.0-T Philips® MR scanner, using an eight channel head coil. DTI was performed with 5mm thickness using a single-shot EPI sequence. The diffusion encoding used in the studies varied between 15 or 24 directions (b values 0 - 800 s/mm2). In all the studies reviewed a T1-weighted and a T2-weighted axial scan have also been acquired.

Post-processing

DTI data were analysed using DTI Studio® or the PRIDE fibre-tracking tool supplied by Philips Medical Systems®. In all cases FA maps with grey-scale and colour coding were generated. The colour-coding was assigned as: red - left to right, blue – craniocaudal, green – rostral-dorsal directions.

Using the same post-processing tools both single and multiple regions of interest (ROIs) were selected for tractography in the pons, midbrain or any particular anatomical structure. The tracts were visualized by setting the tractography colour algorithm to show the principal anisotropy and direction with a threshold FA of less than 0.2.

Results

Conventional Imaging data

No anatomical or signal intensity abnormalities were seen in T1- and T2-weighted images in controls, patients with early MSA and PSP, the patient with PD or SCA1.

In the advanced MSA-C patients a significant atrophy of the pons and cerebellum was seen as well as T2 hyperintensity of the middle cerebellum peduncles and pontine cruciform signal. Small linear T2 hypointensity of the putamen was identified in patients with MSA-P and the "eye-of the tiger signal" and asymmetrical parietal atrophy in the CBD patients. Atrophy of the mesencephalon was seen in advanced PSP.

DTI/DTT

Controls

Transverse fibers of the vermis were apparent in red and are visible in all sections (Fig. 1-3). On parasagittal color maps the main tracts have a green color, with anteroposterior direction, connecting the cerebellar cortex and the emboliform and dentate nuclei (Fig. 3). The inferior cerebellar peduncle (ICP) can be identified in coronal sections, with blue color, lateral to the medial lemniscus (Fig.4). The middle cerebellar peduncle (MCP) projects to pontine nuclei and appears as a large symmetric green area, clearly visible in all planes, intermingling with fibers of the dentate nucleus (Fig. 1-3, 5-6). The superior cerebellar peduncles (SCP) were easily identified in axial and sagittal planes (Fig.3, 6), and the decussation of the SCP was visible in red color on horizontal sections (Fig.7) at the level of the midbrain.

Patients

DTI imaging with FA and colour coded maps in MSA cases of the cerebellar type (MSA-C) showed a significant decreased in fractional anisotropy (FA) in the TPF and MCP, with preservation of the pyramidal tract and medial lemniscus (Fig.8), similar to the previous reported cases (107). In sagittal images of the brain stem, atrophy and severe degeneration of both the MCP and TPF could be seen in all patients with advanced MSA, which was not seen in any of the controls or other patient groups. In MSA of the parkinsonian type (MSA-P) there was a decrease in FA of the MCP with only a slight decrease in the pontocerebellar fibers (Fig.9).

In PSP, we found a decreased FA in the SCP (significant in advanced cases and less prominent in early disease progression), as well as blue color decrease in the SCP and loss of the normal red color of the SCP decussation in the advanced case (Fig. 10); contrary to MSA cases there was relative integrity of TPF and MCP (108).

In the corticobasal degeneration patient we found only a slight FA decrease in the MCP, with no identifiable changes in the color coded map and no significant FA changes in the TPF or SCP.

In SCA changes are reported as variable, not allowing the differentiation between the different subtypes (109) but differing from healthy controls. Some studies in SCA type 1 and 2 have shown loss of cerebellar hemispheric fibers and decrease FA in the cerebellar peduncles and TPF (110), similar to what we found in a genetically confirmed SCA type 1 case (Fig. 11).

In Idiopathic Parkinson's Disease (PD) we found FA reduction in the substancia nigra compared with one of the controls (Table 2), with a lateral to medial gradient, similar to the one found by Vaillancourt (93).

Discussion

Many studies have been published in the last 10 years investigating MR imaging in the differential diagnosis of parkinsonian disorders especially PD from the atypical disorders as MSA and PSP. Several morphological changes have been described as characteristic of MSA or PSP but, in general, these conventional MR signs have a low sensitivity for the diagnosis (104,111). Recently some studies using DTI/DTT have shown a greater sensitivity of this technique in the differential diagnosis of parkinsonian disorders compared to conventional MR, rendering it attractive not only for future research but introducing it into the clinical practice (105, 109).

The results of our review, with a small number of patients, are in accordance with previous DTI data. In patients with late stage MSA we found the characteristic morphology changes especially prominent pontine/cerebellar atrophy, pontine cruciform sign and MCP signal changes (111). DTI data showed marked changes in the MCP and TPF in advanced cases but also FA and MCP/TPF color reduction in the early stages of the disease, similar to published studies (112), indicating that DTI data might be important in the distinction of MSA from controls as well as from PSP and Parkinson's disease (113).

The characteristic morphological MR changes of PSP were identified only on late stages of the disease, with prominent atrophy of the midbrain and SCP (114). Similar to previous studies (108) in our patient with advanced disease we found a decreased FA in the SCP and loss of the normal red color of the SCP decussation with relative integrity of the TPF

and MCP, enabling a differential diagnosis of this patient not only with controls but also with PD and MSA cases.

Corticobasal degeneration (CBD) has a distinctive clinical picture in late stages of the disease, but diagnosis is often uncertain at disease onset (115), with studies showing incorrect clinical diagnoses as well as pathologic overlap with other neurodegenerative diseases, namely PSP (116). In late stages CBD has characteristic asymmetric frontoparietal atrophy with less consistent putaminal signal changes on MR studies (117), as was found in our patient. On DTI there was only a slight FA decrease in the MCP but there were no significant changes in the TPF or SCP as seen in late stages MSA or PSP.

Conventional imaging differentiation of the different subtypes of SCAs is difficult and structural imaging can be normal in the early stages of the disease (109) with atrophy and signal changes of the brainstem and cerebellum appearing late in the disease (118). DTI studies in SCA have not enabled differentiation between SCA subtypes, namely SCA 1 and SCA2 but have shown strong differences with controls as was found in our case and correlating with clinical scores (109).

PD is known for its paucity of abnormal findings on MRI (103). The DTI study of Vaillancourt (93) found changes in the substancia nigra (SN) in PD patients with a lateral to medial gradient that was also found in our only patient with recent onset PD.

Diffusion tensor tractography is an excellent tool for imaging individual white matter tracts of the brainstem (112,119), however the technical limitations of this method need to be considered, especially the problems with concerning fiber crossing, delineation of tracts using manually drawn ROIs (120), distortion of axonal and neuronal architecture in neurodegenerative diseases, making it more difficult for the tracking algorithm to follow the fibres over longer distances or changes in direction. Tractography has also been less used in the study of movement disorders because data often require extensive manual postprocessing work, lacks standardization, are not easily reproducible for comparison.

Our work was just a retrospective review with a very small number of patients, based only on clinical diagnosis with no neuropathology confirmation, intended to evaluate the protocols used, the applicability, feasibility and relevance in clinical cases of the results obtained with DTI and DTT as part of the MR investigation in the differential diagnosis of parkinsonian disorders. We found DTI changes in advanced as well as early cases that had normal morphological imaging; these changes enabled patient differentiation from

controls and MSA patients from PSP. However, there is the need for prospective studies with a significant number of patients trying to evaluate the sensitivity and specificity o DTI imaging in the diagnosis of parkinsonian movement disorders, especially in early stages of disease.

In the majority of previous DTI studies field strengths of 1.5 T and fewer directions have mostly been used (112,119). In this review all the studies were performed in a 3.0T field strength, using 15 or 24 independent diffusion encoding directions in order to increase the directional resolution as well as being tolerable for the patient and less susceptible to movement artifacts. The limited data of our review do not enable us to draw any conclusions as to the number of optimal directions to be used.

The DTI protocols we reviewed are easy to implement in a clinical setting, offering the possibility to study, in vivo, the major connections of the brainstem-cerebellum in healthy individuals as well as offering a unique possibility to study pathological changes unidentifiable in conventional MR sequences. In the cases we reviewed, DTI data (colour mapping and DTT) supplemented routine T1- weighted, T2-weighted and FLAIR images in the differential diagnosis of parkinsonian disorders.

Although DTI/DTT have not yet become a routine procedure in the clinical setting, DTI/DTT protocols can be easily implemented and yield clinically relevant information. The different DTI pattern in movement disorders appears to be complementary to conventional structural MR (106), and in the future can be a useful tool for specific movement disorders identification in the clinical practice.

Furthermore, quantitative data on the diffusion properties of specific white matter tracts can be elicited, which might be of use in future studies of disease progression and effects of treatment in future research.

Conclusion

DTI imaging is very useful in identifying the normal brainstem and cerebellar white matter. White matter water-molecule disturbance in the brain-stem and cerebellar fibers in different types of movement disorders can be identified by DTI and provide a functional evaluation of the impaired extra-pyramidal circuits. Our results are concordant with other series demonstrating that DTI is a useful tool in the evaluation of the status of white matter fibers and some gray matter structures, and in combination with structural

imaging may have diagnostic value in patients with movement disorders. Our limited review indicates that DTI with DTT may add qualitative information that together with conventional MRI aids in the differential diagnosis of parkinsonian movement disorders.

Table1. Summary of patient data (*NA* not applicable; ↓ decreased)

Final clinical diagnosis	Age (years)	Sex (M/F)	Clinical information prior to DTI	Disease duration (early/long)	T1/T2-weighted MR changes	DTI
Control	42	M	NA	NA	Normal	Normal
Control	54	F	NA	NA	Normal	Normal
MSA-C	62	M	MSA	long	- pontine-cerebellar atrophy - T2 hyperintensity MCP - pontine cruciform signal	- ↓ ↓↓FA MCP and TPF - MCP atrophy/green color lost - TPF red color lost
MSA-C	69	F	Ataxia	long	- pontine-cerebellar atrophy - T2 hyperintensity MCP - pontine cruciform signal	- ↓ ↓↓FA MCP and TPF - MCP atrophy/green color lost - TPF red color lost
MSA-C	59	F	Ataxia	short	- pontine-cerebellar atrophy	- ↓ FA MCP and TPF - ↓MCP green color
MSA-C	63	M	Ataxia	short	Normal	- ↓ FA MCP and TPF - ↓MCP green color
MSA-C	72	F	Ataxia	short	Normal	↓ FA MCP and TPF - ↓MCP green color
MSA-P	71	M	Atypical parkinsonism	long	Atrophy and T2/T2* hypointensity putamen	- ↓ FA MCP
MSA-P	63	M	Atypical parkinsonism	short	Normal	- ↓ FA MCP
MSA-P	70	F	Atypical parkinsonism	short	Normal (basal ganglia T2 hypointensity normal for age group)	- ↓ FA MCP
PSP	64	M	Atypical parkinsonism	long	Midbrain atrophy	- ↓ FA SCP - SCP blue color lost - absence SCP decussation red color - normal MCP and TPF
PSP	68	M	Atypical parkinsonism	short	Normal	- ↓ FA SCP - SCP blue color reduction - SCP decussation red color reduction - normal MCP and TPF
CBD	70	F	Atypical parkinsonism Language changes	long	- asymmetric parietal atrophy (left> right) - "eye of tiger" signal - T2 hyposignal external putamen	- ↓ FA MCP - normal TPF and SCP
SCA1	56	M	Ataxia	long	- pontine cerebellar atrophy	- ↓ cerebellar hemispheric fibers - ↓FA MCP and TPF
PD	62	M	Parkinsomism	short	Normal	- SN FA changes

Table 2. Fraccional anisotropy values in ROIs placed in the SN (rostral, middle and caudal portions) in a healthy control and PD patient. In PD patient reduced FA was greater in the caudal compared with the rostral ROI.

	FA values	
ROIs SN	PD	Control
rostral	0,49	0,56
middle	0,40	0,54
caudal	0,42	0,60

Figures

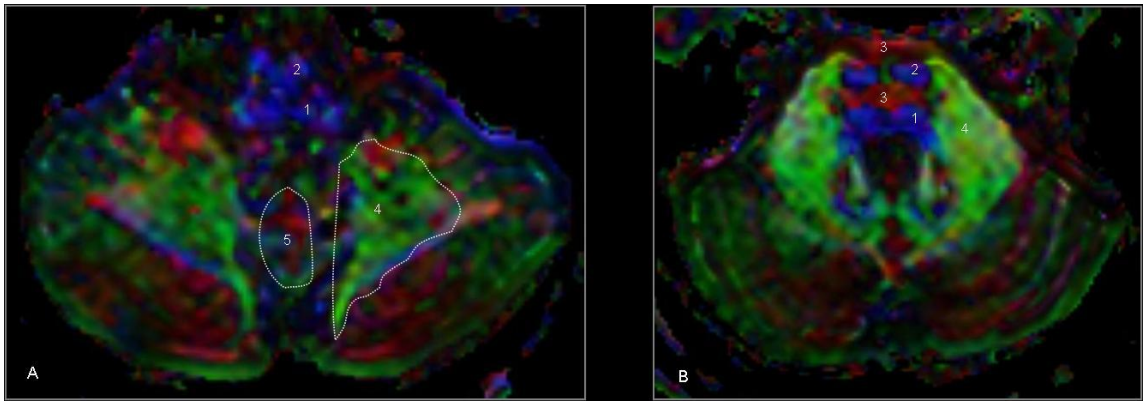

Figure 1. DTI on horizontal sections: at the level of upper medulla (A) the main cerebellar tracts, bellow the level of the dentate are visible by their green color. At the level of the mid part of the pons (B) the ascending fibers of the medial lemniscus and corticospinal tract can be followed easily; laterally the two middle cerebellar peduncles are outlined by their green color, around the dentate nucleus.1-middle leminscus. 2-pyramidal tract. 3-transverse pontine fibers. 4-middle cerebellar peduncle. 5-vermian transverse fibers.

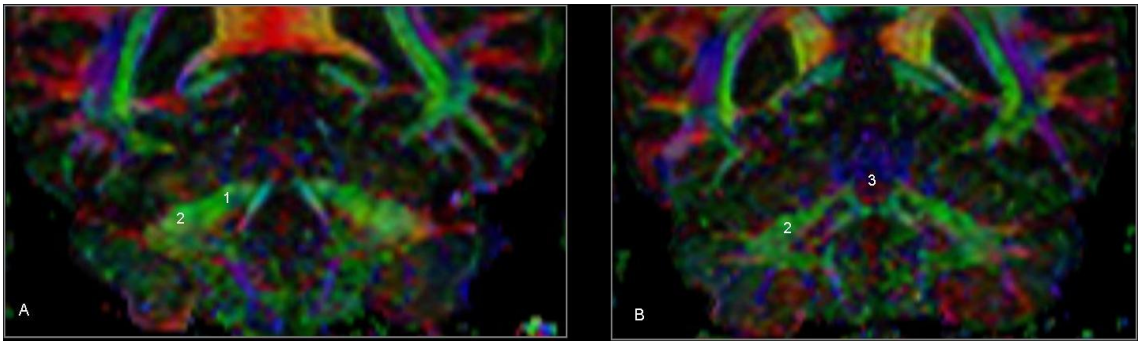

Figure 2. DTI coronal sections of the cerebellum behind the floor of the IV ventricle (A) and more posterior, at the level of the dentate nucleus (B). The afferent fibers of the middle cerebellar peduncle and the fibers to the dentate are clearly visible. The afferent fibers of the dentate are visible on section B, located more posteriorly. 1-dentate fibers. 2-middle cerebellar peduncle. 3-vermian transverse fibers.

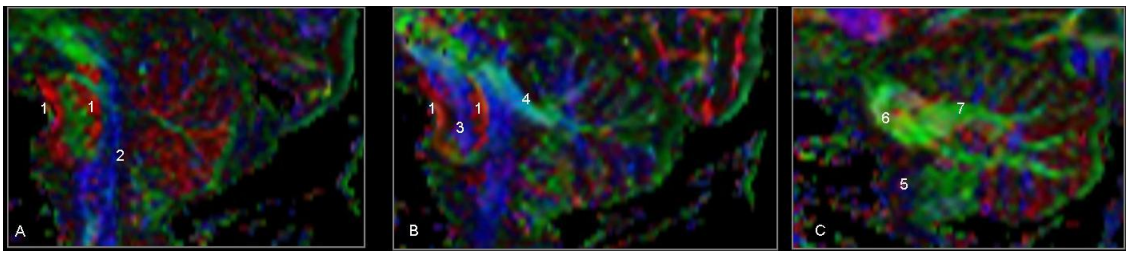

Figure 3. DTI sagittal sections of the brainstem and cerebellum on the midline (A), 5mm (B) and 10mm (C) from the midline. In the midline section almost all the vermian cerebellar surface corresponds to transverse fibers. More laterally the main fibers are directed from the cerebellar hemispheres to the main cerebellar nuclei. Above the level of the lateral part of the IV ventricle the superior cerebellar peduncle is well outlined. The two components of transverse pontine fibers are clearly visible by their red color. 1- transverse pontine fibers. 2-medial lemniscus 3-pyramidal tract.4-superior cerebellar peduncle. 5-inferior cerebellar peduncle. 6-middle cerebellar peduncle. 7-hemispheric cortical fibers to dentate and emboliform nuclei.

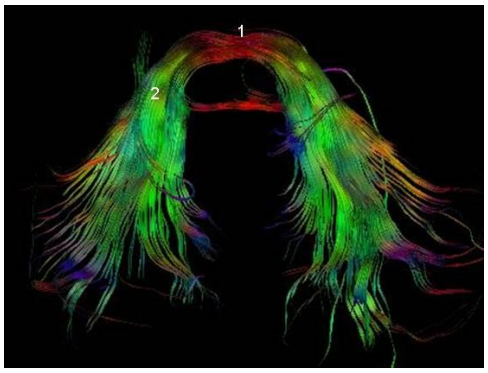

Figure 4. Selective tracking of the middle cerebellar peduncle on axial projection (ROI in the mid portion of the middle cerebelar peduncles bilaterally).1- transverse pontine fibers. 2-middle cerebellar peduncle.

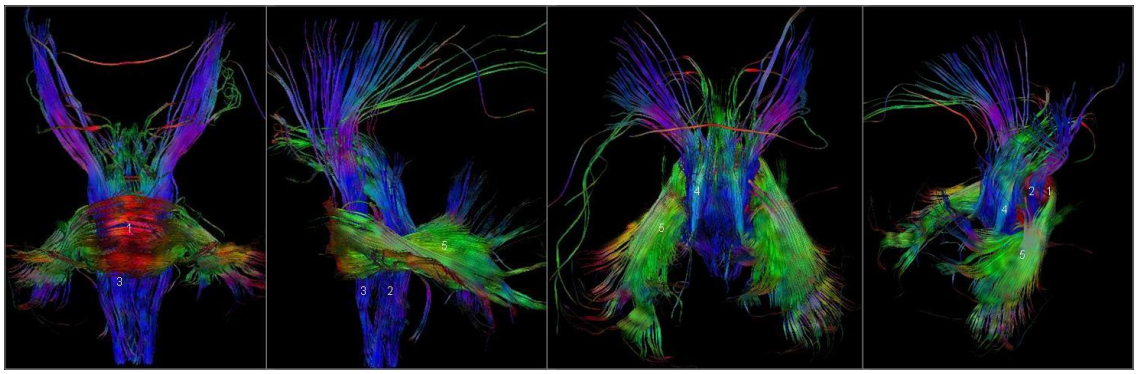

Figure 5. Selective tracking of the middle and superior cerebellar peduncle (ROI in the mid pons).1-transverse pontine fibers. 2-medial lemniscus 3-pyramidal tract.4-superior cerebellar peduncle. 5-middle cerebellar peduncle.

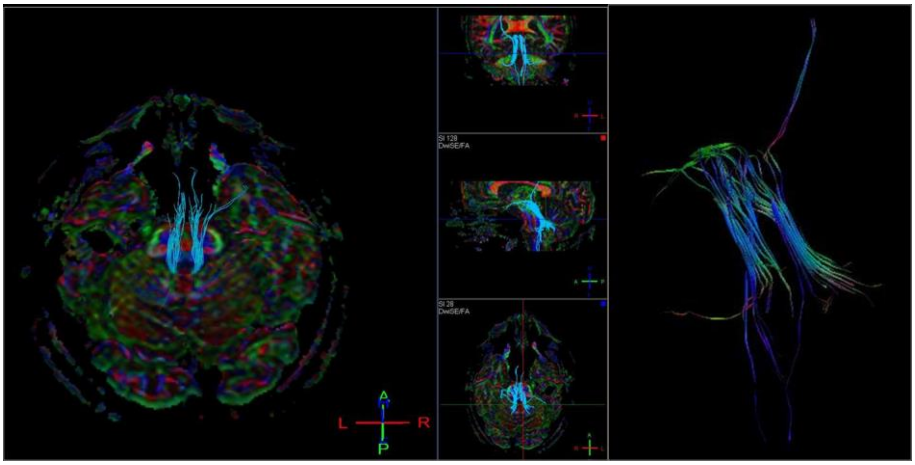

Figure 6. Selective tracking of the superior cerebellar peduncle (ROI in the superior cerebellar peduncle).

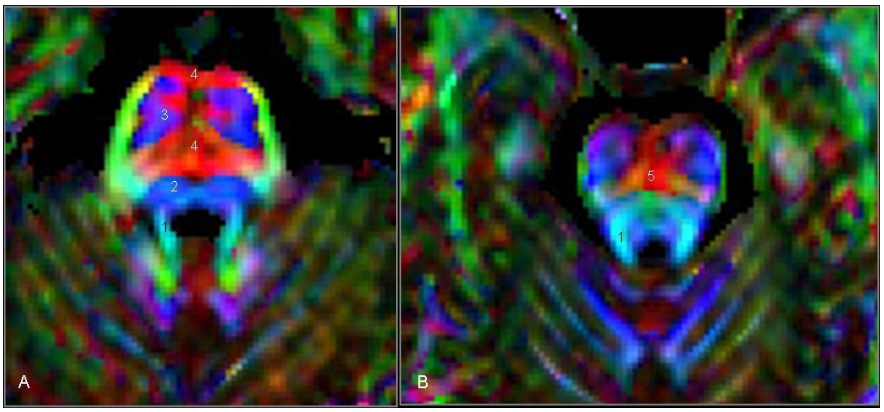

Figure 7. DTI on horizontal sections of the superior pons (A) and midbrain (B). 1-superior cerebelar peduncle (SCP). 2-middle leminscus. 3-pyramidal tract. 4-transverse pontine fibers. 5-SCP decussation.

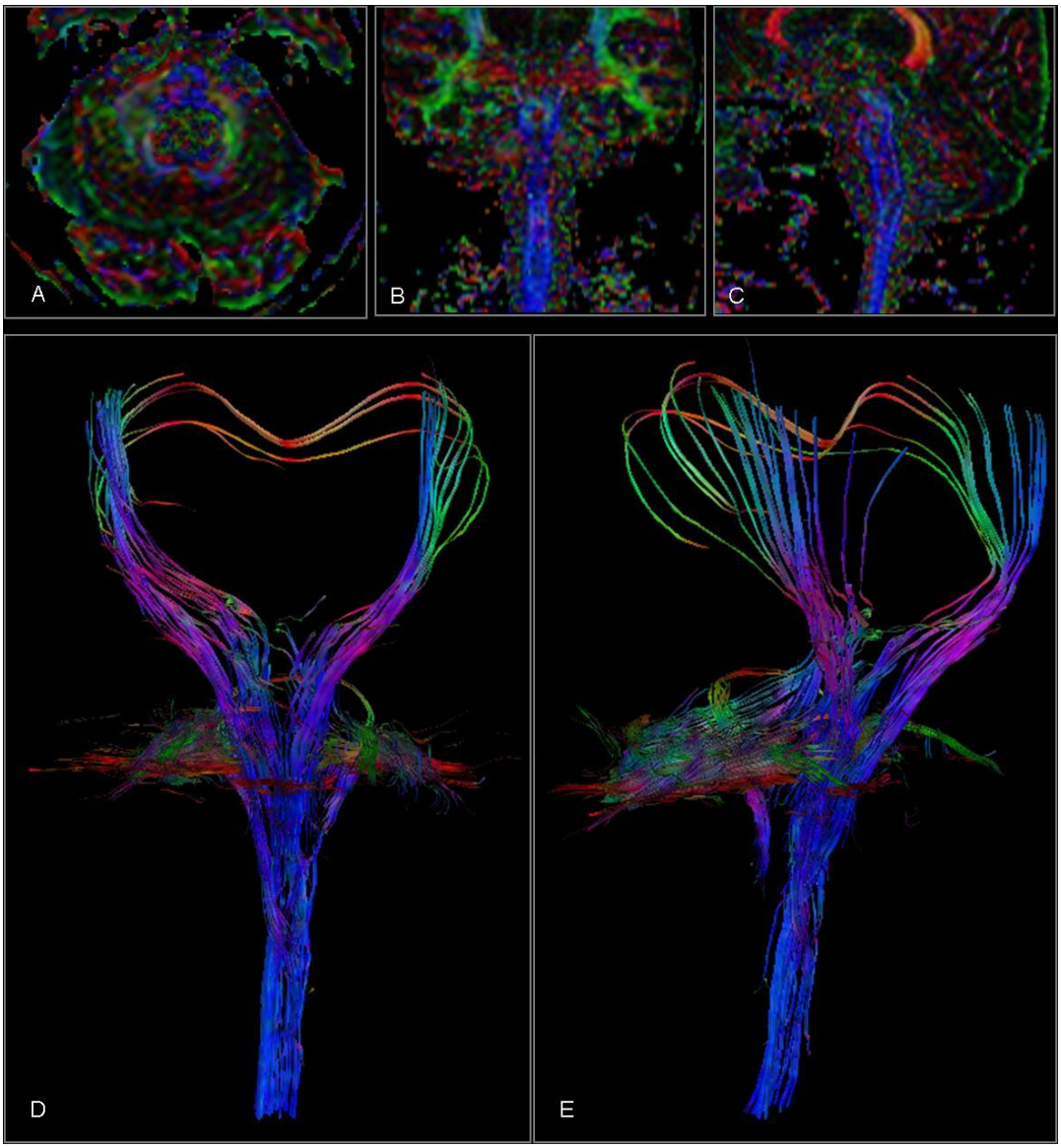

Figure 8. DTI horizontal section of the mid pons (A), coronal section of anterior pons (B), midline sagittal section (C) and tractography (D,E) in a patient with **MSA-C** showing significant decrease of the pontocerebellar fibers and transverse pontine fibers, with atrophy of the middle cerebellar peduncle. Relative integrity of pyramidal tract and medial lemniscus.

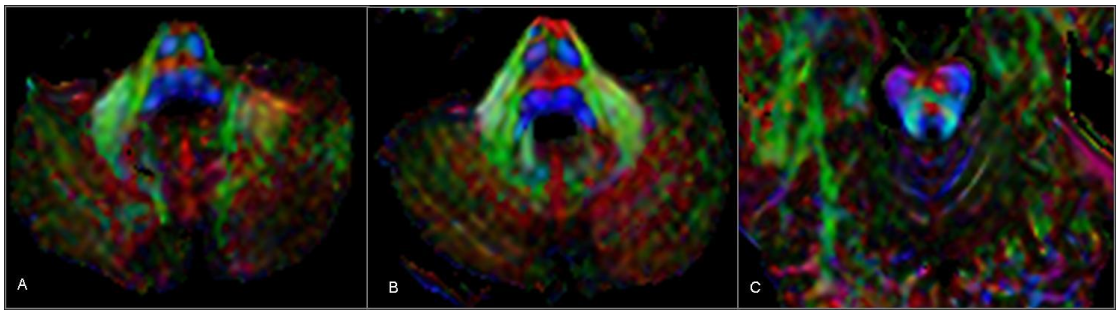

Figure 9. DTI on horizontal sections of the inferior (A), mid pons (B) and midbrain (C) in a patient with **MSA-P**, showing slight decrease of pontocerebellar fibers, with decrease in FA of the middle cerebellar peduncle. Integrity of pyramidal tract, medial lemniscus and superior cerebellar peduncle decussation.

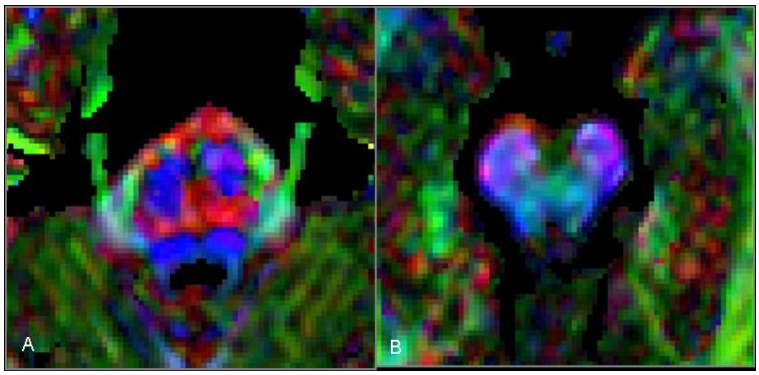

Figure 10. DTI on horizontal sections of the mid pons (A) and midbrain (B) in a patient with **PSP**, showing a thin superior cerebellar peduncle with no identifiable red color at the superior cerebellar peduncle decussation level. Integrity transverse pontine fibers and middle cerebellar peduncle.

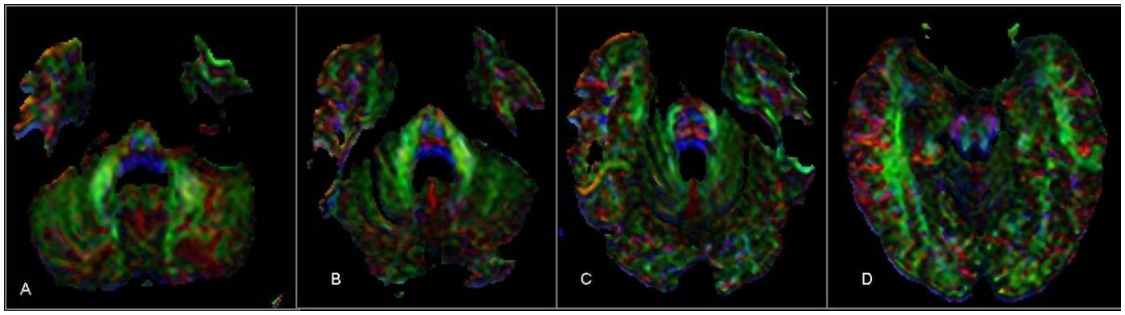

Figure 11. DTI horizontal sections of the medulla (A), mid (B), superior pons (C), midbrain (D) and tractography (E) in a patient with **SCA 1**, showing decrease of transverse pontine fibers. Integrity of middle cerebellar peduncle, pyramidal tract, medial lemniscus and superior cerebellar peduncle decussation.

1.3. Multimodal imaging

Integrating different imaging MR techniques might enhance diagnostic accuracy, as proposed by Péran and colleagues (121) in a study that combined information from volumetric analysis, iron content measured with R2* relaxometry, mean diffusivity and FA values in the SN to evaluate PD.

The investigation of imaging biomarkers in PD assumes in our view a preponderant role, in view of the growing ability of MR studies to enable an *in vivo* access to the morphology and microstructure of the brain parenchyma. The conjoint use of multiple sequences might to allow a wide evaluation of different pathophysiological aspects, studying their interaction and the impact in the improvement of precocious disease diagnosis.

2. MR IMAGING FOR THE DIAGNOSIS OF PARKINSON'S DISEASE

2.1. Substantia nigra neuromelanin magnetic resonance imaging in "de novo" Parkinson's disease patients

Reimão S, Pita Lobo P, Neutel D, Correia Guedes L, Coelho M, Rosa MM, Ferreira J, Abreu D, Gonçalves N, Morgado C, Nunes RG, Campos J, Ferreira JJ.

European Journal of Neurology (Eur J Neurol) 2015 Mar;22(3):540-6.

Published online 22 Dec 2014

doi:10.1111/ene.12613

Substantia nigra neuromelanin magnetic resonance imaging in "de novo" Parkinson's disease patients

Sofia Reimão, M.D.[1,4]*, Patrícia Pita Lobo, M.D.[2,4], Dulce Neutel, M.D.[2,4], Leonor Correia Guedes, M.D.[2,4], Miguel Coelho, M.D.[2,4], Mario M Rosa, M.D.[2,4,5], Joana Ferreira, MSc [3], Daisy Abreu, MSc[4], Nilza Gonçalves, MSc[4], Carlos Morgado, M.D.[1], Rita G Nunes, Ph.D.[3], Jorge Campos, Ph.D.[1], Joaquim J Ferreira, Ph.D.[4,2, 5]

[1] Neurological Imaging Department, Hospital de Santa Maria - Centro Hospitalar Lisboa Norte, Portugal

[2] Neurology Department, Hospital de Santa Maria - Centro Hospitalar Lisboa Norte, Portugal

[3] Institute of Biophysics and Biomedical Engineering, Faculty of Sciences, University of Lisbon, Portugal

[4] Clinical Pharmacology Unit, Instituto de Medicina Molecular, Portugal

[5] Laboratory of Clinical Pharmacology and Therapeutics, Faculty of Medicine, University of Lisbon, Portugal

Abstract

Background: Depigmentation of the *substantia nigra* (SN) and *locus coeruleus* (LC) is a conspicuous pathological feature of Parkinson's Disease (PD) and is related to the loss of neuromelanin, whose paramagnetic properties result in high signal on specific T1-weighted MRI. Recent studies have suggested that neuromelanin decrease in the SN and LC of PD patients may emerge as a possible diagnostic biomarker. We studied the SN neuromelanin signal in "de novo" and early stage PD patients to assess its diagnostic accuracy. This is the first study based on a semi-automated MRI analysis of the neuromelanin signal in "de novo" PD patients.

Methods: The inclusion criteria were untreated "de novo" PD and a 2 – 5 year disease duration; in addition, age matched healthy controls were enrolled. These were studied with a high-resolution T1-weighted MR imaging sequence at 3 Tesla to visualize neuromelanin. The primary outcome was SN high signal area, length and neuromelanin/midbrain ratio obtained with semi-automated methods.

Results: A total of 12 "de novo" PD patients and 10 PD patients with a 2 – 5 year disease duration were evaluated. The area, length of the SN T1 high signal and the SN neuromelanin/midbrain ratio were markedly decreased in the PD groups compared with age-matched controls, with a substantial overlap between the two PD groups.

Conclusions: Neuromelanin-sensitive MRI techniques can discriminate PD patients from healthy individuals with high sensitivity and specificity. Our findings are consistent with recent findings showing that PD neuromelanin changes remain stable during the course of the disease.

1. Introduction

Parkinson's disease (PD) is a neurodegenerative condition characterized by depletion of dopaminergic neurons in the *substantia nigra* (SN) *pars compacta* (SNpc) and noradrenergic neurons in the *locus coeruleus* (LC) (11). Pathological changes in the LC and SN occur early in the course of PD and have been described in preclinical stages (9). Depigmentation of the SN and LC is a conspicuous pathological feature of PD and is related to the loss of a melanin pigment known as neuromelanin.

Neuromelanin is a by-product of dopamine and noradrenaline metabolism and is thought to protect neurons from oxidative stress mediated by free metals or free radicals (35). This pigment has paramagnetic properties resulting in high signal on specific T1-weighted magnetic resonance imaging (MRI), enabling its identification *in vivo* (61,62). Recent studies have described a reduction in MRI neuromelanin-generated signal in the SN and LC in patients with PD (61,63).

We examined neuromelanin-sensitive MR imaging in "de novo" untreated PD patients and in PD patients with a 2 – 5 year disease duration to study the diagnostic accuracy of this MRI sequence at clinical presentation and to determine whether it was possible to obtain objective measurements of SN T1 high signal area and length using semi-automated methods that would discriminate PD patients from controls.

To our knowledge, this is the first study based on neuromelanin semi-automated MR imaging in "de novo" untreated PD patients.

2. Patients and methods

2.1. Patients and control subjects

The study was a cross-sectional case-control analysis (prospective follow-up ongoing) that included 32 subjects: 12 "de novo" patients with PD, 10 PD patients with a 2 to 5 year disease duration and 10 healthy subjects. Patients were recruited from the Movement Disorders Unit of the University Hospital of Santa Maria-Lisbon. "De novo" PD patients were included at the time of clinical diagnosis if they were not on antiparkinson medications, and all had less than 6 months since the beginning of clinical symptoms. PD patients with 2 to 5 year disease duration since clinical medical diagnosis were receiving

optimal pharmacotherapy with levodopa or dopamine agonists. All patients were diagnosed with PD by a movement disorders specialist according to the UK Brain Bank criteria (19) and were rated using the Unified Parkinson's Disease Rating Scale (UPDRS). The healthy control subjects were recruited from local hospital staff and relatives. Dementia, psychiatric illness or contraindications to an MRI were the exclusion criteria.
The examinations were performed with the understanding and written consent of each subject, with approval from the local ethics committee, and in compliance with national legislation and the Declaration of Helsinki guidelines.

2.2. MRI protocol

2.2.1. Imaging protocol

All data were acquired with a 3.0-Tesla Phillips scanner (Phillips Achieva®). The following pulse sequence was used as previously described by Sasaki and colleagues (61): T1-weighted FSE: repetition time/effective echo time, 633/10; echo train length, 3; number of slices, 20; slice thickness, 2.5 mm; intersection gaps, 0 mm; matrix size, 548 x 474; field of view, 220 mm (pixel size: .40 x .40 mm); and acquisition time, 8 min. The sections were carefully set in the oblique axial plane perpendicular to the fourth ventricle floor with coverage from the posterior commissure to the inferior border of the pons.
T1- and T2-weighted images of the entire brain were additionally obtained in all subjects and evaluated by an experienced neuroradiologist to exclude other pathological imaging findings, namely, changes in the parkinsonian index and other atypical parkinsonian syndrome changes, and lesions in the LC and SN areas that might interfere with further assessment.

2.2.2. Imaging analysis

Images were transferred to a Linux workstation for analysis, and an edge preserving filter (122) was applied using Matlab (R2012a, The Math Works, Natick. Massachusetts, USA) to reduce image noise. This is an adaptive mean filter, where the intensity of each pixel in the filtered image $\hat{u}(i)$ is determined from the neighbourhood V_i of each pixel i (8

neighbours in 2D). The weight *w(i,j)* given to each neighbouring pixel depends on the intensity difference between *i* and its neighbour *j*:

$\hat{u}(i) = \frac{\sum_{j \in V_i} w(i,j)\, u(j)}{\sum_{j \in V_i} w(i,j)}$ where $w(i,j) = 1 - \frac{|u(j)-u(i)|}{3\times255}$ and $w(i,i) = 0$.

In this way pixels with similar intensity levels are given a higher weight, reducing blurring across different anatomical structures.

To account for subject-dependent signal fluctuations, a circular region of interest (ROI) was drawn in the central part of the *crus cerebri* of each neuromelanin-sensitive image, which was then normalized by the mean signal intensity within this ROI. T1 high signal in the SN region was visible in 3 slices, and the middle slice corresponding to the greatest SN volume was selected.

A rectangular region containing the mesencephalon was then selected in this slice, and two symmetrical seed points were manually defined on the most medial part of the high-intensity area in the SN. A region growing algorithm (123) was used for segmentation starting from each seed point, and the area of interest (AOI) was automatically drawn. Pixels with a signal intensity within the interval $I_{seed} \pm 0.035\times(I_{max}-I_{min})$ were labeled as belonging to the AOI, where I_{seed} is the intensity at the seed point, and I_{max} and I_{min} the maximum and minimum signal intensities within the rectangular mesencephalon ROI. The threshold used to delimit the AOI was chosen following a preliminary optimization study where the threshold was varied using a batch process with tests performed on several example images; the final value of 3.5% was selected as it was the one that provided a better visual fit to the anatomical area. The area of interest (AOI) was automatically drawn, and the maximal length was then calculated.

We additionally calculated the global midbrain area and the ratio of SN neuromelanin T1 high-signal area to total midbrain area (neuromelanin ratio). Images were transferred to a PACS system and the slice were the neuromelanin area measurements were made was selected; in this slice the midbrain contours were manually drawn and the global area was calculated. Using this measure we then calculated the SN neuromelanin ratio for each patient.

2.3. Statistical analysis

The area, length and SN neuromelanin ratio obtained for each group were compared using non parametric analysis. Kruskal-Wallis tests, with pairwise comparisons in which the resulting p-values were corrected according to Bonferroni method, and Mann-Whitney U tests were used as appropriate.

A p-value of 0.05 was considered significant. Statistical analysis was performed with R 2.15.2.

Receiver operation characteristics (ROC) curve analysis was conducted for the comparison between PD patients and normal subjects, and the specificity and sensitivity of the tests and the optimal cutoff point as well as the area under the curve (AUC) were also assessed.

Differences in the clinical characteristics among these groups were assessed. Differences in the sex distribution among groups were evaluated with χ^2-test. The Kruskal-Wallis test was performed for comparison of the median age between groups as well as for UPDRS total score and UPDRS part III.

3. Results

MR imaging was performed on all subjects, and the image quality allowed the clear identification of the high signal area in the SN region (Fig 1). Automated analysis was possible on all subjects except one patient in the 2 to 5 year disease duration group whose MRI had significant artifacts and had to be excluded. Therefore, 12 patients with "de novo" PD, 9 patients with 2 to 5 year disease duration and 10 healthy controls were eligible for further analysis. The clinical characteristics of these subjects are shown in Table 1. No significant differences were observed in age and sex among the 3 groups, and there were also no significant differences in H&Y stage and UPDRS scores between the "de novo" and the 2 to 5 years disease duration PD patients.

The median area and length obtained for "de novo" PD patients was 19.88 mm^2 and 33.41 mm, respectively. For the 2-5 year PD group, the median area was 12.58 mm^2 and the median length was 23.14 mm; for healthy controls, an area of 25.40 mm^2 and a length of 52.75 mm were observed.

The area and maximal length were markedly decreased in “de novo” and the 2-5 year PD groups compared with the healthy control group (Fig 1) with a *p*-value of 0.003 and a *p*-value of 0.002, respectively for area and length in “de novo” patients compared to controls and a *p*-value <0.001 for area and length in the 2-5 year PD group compared to controls (Fig 2). However, substantial overlaps were observed between the “de novo” and the 2-5 year disease duration groups (Fig 2), with no significant difference observed between the two groups (*p*-value of 0.22 for area and *p*-value of 0.62 for length), although the median area and length of the “de novo” PD group tended to be slightly higher than that of the 2-5 year PD group.

We found no significant differences in the global midbrain area between the three groups (*p*- value > 0.205). The ratio of SN neuromelanin ratio was markedly decreased in the in “de novo” and the 2-5 year PD groups compared with the healthy control group (*p*-value of 0.014 and of <0.001, respectively) (Table 2). The ratio also had a substantial overlap between the “de novo” and the 2-5 year disease duration groups with no significant difference observed between the two groups (*p*-value of 0.141).

ROC analyses for the area showed an AUC of 0.73 in patients with “de novo” PD, whereas it was 0.85 in patients with 2-5 year disease duration. AUC values obtained for length were 0.79 for “de novo” PD and 0.82 for the 2-5 year PD group.

Among these, the sensitivity and specificity of the SN high signal area for discriminating the “de novo” PD group from the healthy control group was 70% and 65%, respectively, when the cut-off value for the area was set at 23 mm^2. The sensitivity and specificity for discriminating the 2-5 year PD group from the control group was 60% and 100%, respectively, with an area cut-off value of 21 mm^2. The sensitivity and specificity for the maximal length of the SN high signal for discriminating the “de novo” PD group from the control group was 83.3% and 70%, respectively, for a length cut-off value of 45.73 mm. For discriminating the 2-5 year PD group from the control group, the sensitivity and specificity was 83% and 70%, respectively, with a length cut-off value of 45.6 mm (Table 3 and Fig 3).

4. Discussion

In the present study, with semi-automated MRI measures, we were able to detect significant changes in the area and length of the T1-high signal area of the SN

corresponding to the neuromelanin in early stage PD compared with healthy individuals. Clinical symptoms of PD are generally apparent when a substantial part of the dopaminergic neurons of the SN are lost (14,124) and therefore it is expected that even in early disease stages, a substantial loss of neuromelanin-containing neurons would be detectable by MRI-sensitive sequences. It is also known from pathological studies that the neuronal loss in PD is more pronounced in the ventrolateral region of the SNpc with relative preservation of the dorsal region (14) and so we studied both the area and length of the SN T1-high signal region because the maximal length gives a measure of the longitudinal extension additional to the global area.

In the present study, both the area and the maximal length of the SN T1-high signal region were significantly reduced, suggesting neuronal depletion in patients with early PD compared with healthy individuals. Moreover, we obtained high sensitivity and specificity of the values of both of our measurements when differentiating patients with early PD from controls. The sensitivity and specificity of the maximal length are higher that the sensitivity and specificity obtained for the area measurements for discriminating the “de novo” PD group from the healthy controls. This finding supports the longitudinally expected difference of the SN with greater ventrolateral neuronal loss in early stage PD.

To evaluate the possible impact of midbrain volume reduction in PD patients that might influence neuromelanin measurements we calculated the ratio of SN neuromelanin T1 high-signal area to total midbrain area for each group. As expected the midbrain area was similar between the groups and the calculated ratios showed a significant reduction of SN neuromelanin in “de novo” and 2-5 year PD patients, demonstrating that the individual midbrain area does not influence the detection of neuromelanin changes in PD.

In our study, we did not observe significant differences in the area or length of the SN neuromelanin between the groups with “de novo” and 2-5 year disease duration PD. These findings, using semi-automated methods, are consistent with recent findings in a study that investigated signal intensity changes in SN neuromelanin (125), which also found no difference between untreated and advanced stage (H&Y 3-5) PD patients. Interestingly, these findings are also consistent with transcranial sonography studies in PD demonstrating that the ultrasound signal does not change in the course of the disease (126). We studied the area and length of the SN T1 high signal region, and these measures

are similar to the signal intensity changes recently reported in the SNpc (125), providing two different measures of the reduction of SN neuromelanin in early PD.

Our sensitivity and specificity results are consistent with previous reports (125,127). The semi-automated method used in our study is less operator dependent and less time consuming that the manual SN segmentation for neuromelanin estimation (125). The use of a region growing algorithm for SN segmentation increases accuracy and reduces the time required for image analysis. To improve signal-to-noise ratio (SNR) of this algorithm a previous group performed image smoothing applying a Gaussian filter on a 3D sequence (127). As Gaussian filters lead to edge blurring we used an alternative filtering approach that gives more accurate area estimations and enabled semi-automated measurements of SN T1-high signal on 2D images with only a few required operator dependent steps (signal normalization and definition of seed points).

The correlation of neuromelanin decrease with the known pathological changes associated with disease duration and progression of clinical severity (14) needs to be investigated. The different imaging and measurement methods in previous studies might explain the inconsistent findings in neuromelanin patterns in relation to disease duration (63,128). Additionally, the correlation of iron load with the SN neuromelanin-sensitive MRI needs further analysis, as it is known that iron content in the SN increases in PD and during its progression (129). Neuromelanin exhibits paramagnetic properties when bound to iron that result in the acceleration of T1 relaxation (130,131), and therefore, the increased iron load in SN in PD patients might enhance neuromelanin-related contrast. Variations in the neuromelanin-related signal of the SNpc related to the iron content are currently being investigated by our group with a direct correlation of the neuromelanin signal with iron quantification with a relaxometry sequence.

However, our study has several limitations, namely the small number of patients in each group and the absence of pathological confirmation because the PD diagnosis was only clinical. Another aspect is related to the disadvantages of the imaging technique, including the long acquisition time, the relatively low spatial resolution and the existence of in-plane signal inhomogeneity. In addition, the region-growing post-processing technique used in this study for semi-automated measurement of volumes requires the determination of seed points and normalization of signal intensity that could not be completely automated. The total imaging analysis is relatively time consuming and

requires the implementation of post-processing software that is not widely available. However, only two operator-dependent steps are required, and the rest of the analysis is automated and operator independent. Motion artifacts were not a problem in our early stage patients, with few involuntary movements, but advanced-stage patients might have problems that will need to be addressed.

Further prospective studies are required to address all of these issues.

5. Conclusions

MR neuromelanin-sensitive images were sufficient for detecting significant changes in the SN at the time of clinical diagnosis of PD. Our findings suggest that the neuromelanin changes remain stable with disease progression, consistent with previous findings based on sonography. MRI neuromelanin-sensitive techniques might become a useful diagnostic tool with high sensitivity and specificity for the diagnosis of PD.

Tables and legends

Table 1: Demographics for Parkinson's and control subjects

	"de novo" PD	**2-5 years PD**	**Controls**	***p*-value**
No. (female/male)	12 (7/5)	9 (2/7)	10 (4/6)	0.186
Age, years (mean±SD)	63.23(± 11.9)	67.22(±6.7)	61.2(±7.3)	0.289
H&Y (mean±SD)	2(2-2)	2(2-2)	-	-
Total UPDRS (mean±SD)	44.46(±26.0)	49.86 (±14.0)	-	0.149
UPDRS-III motor score (mean±SD)	29.08(±14,2)	27.43(±10.4)	-	0.498

PD: Parkinson's Disease; No: number; SD: standard deviation.

Table 2: SN neuromelanin T1 high-signal and midbrain measurements

	"de novo" PD	**2-5 years PD**	**Controls**	***p*-value***
SN neuromelanin area (mm^2) – median (range)	19.88 (4.78-47.84)	12.58 (1.85-28.86)	25.4 (14.51-51.55)	<0.001
SN neuromelanin length (mm) – median (range)	33.41 (7.40-67.89)	23.14 (4.70-63.07)	52.75 (25.53-92.76)	<0.001
Midbrain area (mm^2) – median (range)	60.30 (51.88-72.19)	63.20 (56.96-70.42)	59.30 (56.55-66.84)	0.205
SN neuromelanin ratio – median (range)	0.36 (0.08-0.85)	0.19 (0.03-0.53)	0.42 (0.24-0.83)	<0.001

*Comparisons using Kruskal-Wallis test

PD: Parkinson's Disease; SN neuromelanin ratio = SN T1-high signal area/midbrain area

Table 3: ROC analysis of neuromelanin-sensitive MRI for discriminating patients with "de novo" PD and 2-5 years PD duration from healthy subjects

	"de novo" PD vs. control			
	Cutoff value	Sensitivity (%)	Specificity (%)	AUC
Area	23.0mm^2	70	65	0.73
Length	45.8mm	83.3	70	0.79
	2 - 5 years PD duration vs. control			
	Cutoff value	Sensitivity (%)	Specificity (%)	AUC
Area	21.1mm^2	60	100	0.85
Length	45.6mm	83	70	0.82

PD: Parkinson's Disease; AUC: area under the curve

Figures and legends

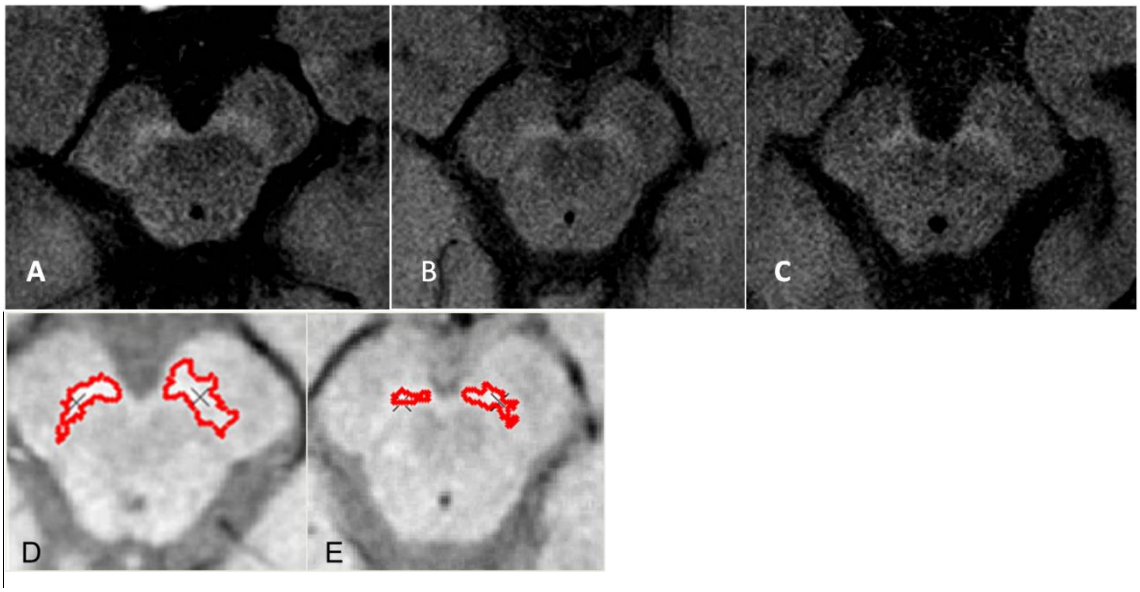

Fig. 1. Neuromelanin-sensitive MRI images of the SN of a healthy control (A), a "de novo" PD patient (B) and of a 2-5 years PD patient (C) and segmented images of a healthy control (D) and of a 2-5 year PD patient (E), showing diminished size of the T1 high intensity area of the SN in PD patients as compared with that in controls.

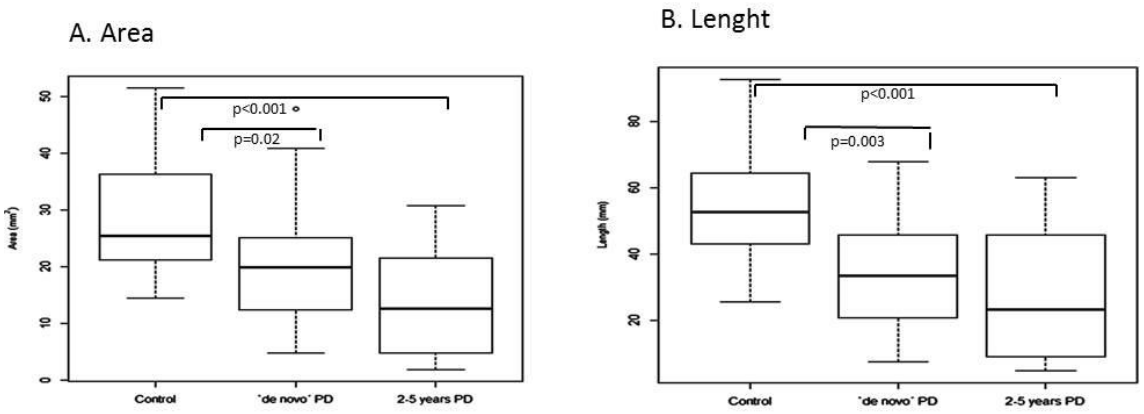

Fig. 2. Areas (A) and maximal length (B) of the SN high intensity region on neuromelanin-sensitive MR images in patients with "de novo" and 2-5 year PD and healthy controls *p*-values, Mann-Whitney *U*-test.

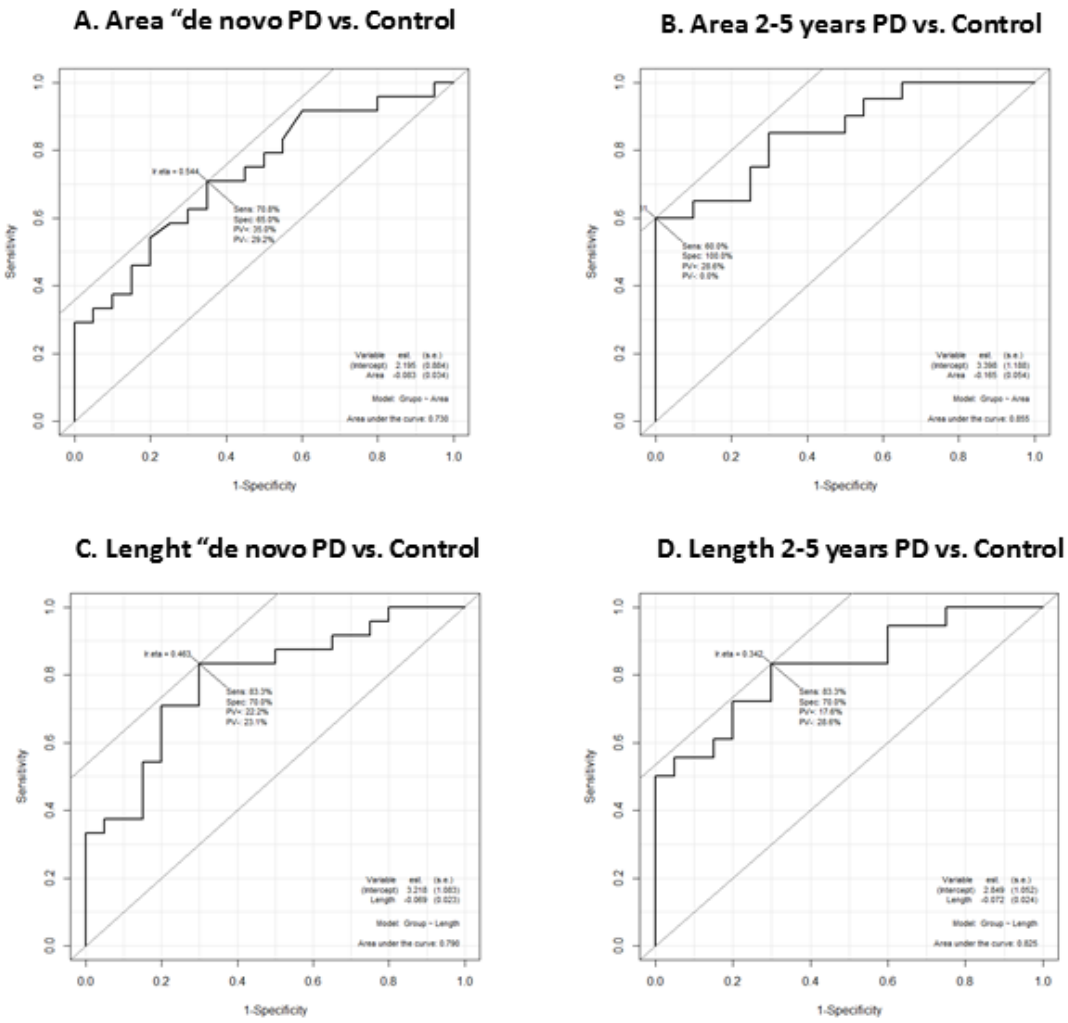

Fig. 3. ROC curves of the area for differentiating between "de novo" PD and healthy subjects (A) and between 2-5 years PD patients and healthy controls (B); ROC curves of the length to differentiate between "de novo" PD and healthy subjects (C) and between 2-5 years PD patients and healthy controls (D).

2.2. Quantitative analysis versus visual assessment of neuromelanin MR imaging for the diagnosis of Parkinson's disease.

Reimão S, Pita Lobo P, Neutel D, Correia Guedes L, Coelho M, Rosa MM, Ferreira J, Abreu D, Gonçalves N, Morgado C, Nunes RG, Campos J, Ferreira JJ.

Journal of Parkinson's Disease – accepted for publication

Quantitative analysis versus visual assessment of neuromelanin MR imaging for the diagnosis of Parkinson's disease

Sofia Reimão[1,4], Patrícia Pita Lobo[2,4], Dulce Neutel[2,4], Leonor Correia Guedes[2,4], Miguel Coelho[2,4], Mario M Rosa[2,4], Joana Ferreira[3], Daisy Abreu[4], Nilza Gonçalves[4], Carlos Morgado[1], Rita G Nunes[3], Jorge Campos[1], Joaquim J Ferreira[4,5]*

[1] Neurological Imaging Department, Hospital de Santa Maria - Centro Hospitalar Lisboa Norte, Portugal

[2] Neurology Department, Hospital de Santa Maria - Centro Hospitalar Lisboa Norte, Portugal

[3] Instituto de Biofísica e Engenharia Biomédica, Faculdade de Ciências, Universidade de Lisboa, Portugal

[4] Clinical Pharmacology Unit, Instituto de Medicina Molecular, University of Lisbon, Portugal

[5] Laboratory of Clinical Pharmacology and Therapeutics, Faculty of Medicine, University of Lisbon, Portugal

Abstract

Purpose: Specific MR sequences have been able to identify the loss of neuromelanin in the *substantia nigra* (SN) of early stage Parkinson's disease (PD) patients. Since this technique may have a significant impact in clinical patient management, easy and widely available imaging analysis is needed for routine use. In this study we compared a quantitative analysis with a visual assessment of SN neuromelanin-sensitive MR images in early stage PD patients, in terms of pattern changes recognition and diagnostic accuracy.

Methods: The inclusion criteria were untreated "de novo" PD patients or a 2 – 5 year PD duration; in addition, age matched controls were enrolled. These were studied with a high-resolution T1-weighted MR imaging sequence at 3.0 Tesla to visualize neuromelanin. The primary outcome was the comparison of quantitative width measurement with visual assessment by experienced neuroradiologists of SN neuromelanin sensitive MR images for PD diagnosis.

Results: A total of 12 "de novo" PD patients, 10 PD patients with 2 - 5 year disease duration and 10 healthy controls were evaluated. We obtained a good accuracy in discriminating early-stage PD patients from controls using either a quantitative width measurement of the T1 high signal or a simple visual image inspection of the SN region.

Conclusions: Visual inspection of neuromelanin-sensitive MR images by experienced neuroradiologists provides comparable results to quantitative width measurement in the detection of early stage PD SN changes and may become a useful tool in clinical practice.

1. Introduction

Recent MR studies have described a reduction of neuromelanin signal in the *substantia nigra* (SN) of Parkinson's disease (PD) patients (61,63,132) with high diagnostic accuracy even in early disease stages (125,127). These findings reflect the known pathological features of PD with dopaminergic neuronal loss in the SN *pars compacta* and consequent reduction of neuromelanin content (9). This neuronal loss occurs asymmetrically and primarily in the ventrolateral and caudal region of the SN with relative preservation of the dorsal and rostral region (14), and MR-sensitive neuromelanin studies have been able to identity these specific disease changes (133).

PD diagnosis in the early disease stage can be challenging but has important therapeutic and prognostic consequences (18). For this reason, neuromelanine sensitive-MR imaging may have the potential to become an alternative to the more expensive and risky nuclear medicine techniques (134) currently used in the diagnostic evaluation of early stage PD.

Previous neuromelanin MR studies have used automated post-processing (127) or manual ROI tracing of the SN region (125,133) but these methods are time consuming or need additional post-processing software. Since this technique may have a significant impact on clinical patient management, an easy and widely available mechanism for image analysis is needed to enable the routine use of these MR images.

In this study we examined neuromelanin-sensitive MR imaging in "de novo" untreated PD patients and in PD patients with a 2 – 5 year disease duration, comparing quantitative width measurement with visual image assessment by experienced neuroradiologists to ascertain their ability to detect SN neuromelanin changes and to differentiate between PD early-stage patients and controls.

To the best of our knowledge this is the first study in early stage PD patients comparing different neuromelanin MR imaging evaluation methods, in particular using visual assessment or manual width measurements.

2. Patients and methods

2.1. Patients and control subjects

The study was a cross-sectional case-control (prospective follow-up ongoing) that included 32 subjects: 12 "de novo" patients with PD, 10 PD patients with 2 - 5 year disease duration and 10 healthy subjects. Patients were recruited from the Movement Disorders Unit of the University Hospital of Santa Maria-Lisbon. "De novo" PD patients were included at the time of clinical diagnosis if they were not on antiparkinson medications. PD patients with 2 - 5 year disease duration were receiving optimal pharmacotherapy with levodopa or dopamine agonists. All patients were diagnosed with PD by a movement disorders specialist according to the UK Brain Bank criteria (19) and were rated using the Unified Parkinson's Disease Rating Scale (UPDRS). The healthy control subjects were recruited from local hospital staff and relatives. Dementia, psychiatric illness or contraindications to an MRI were the exclusion criteria.

All the examinations were performed with the understanding and written consent of each subject, with approval from the local ethics committee, and in compliance with national legislation and Declaration of Helsinki guidelines.

2.2. MRI protocol

2.2.1. Imaging protocol

All data were acquired with a 3.0-Tesla Phillips scanner (Phillips Achieva®). The following pulse sequence was used as previously described by Sasaki and colleagues (61): T1-weighted FSE: repetition time/effective echo time, 633/10ms; echo train length, 3; number of slices, 20; slice thickness, 2.5 mm; intersection gaps, 0 mm; matrix size, 548 x 474; field of view, 220x220 mm^2 (pixel size: .40 x .40 mm^2); and acquisition time of 8 min. The sections were carefully set in the oblique axial plane perpendicular to the fourth ventricle floor with coverage from the posterior commissure to the inferior border of the pons.

Additionally, T1- and T2-weighted images of the entire brain were obtained in all subjects and evaluated by an experienced neuroradiologist to exclude other pathological imaging findings that could interfere with further assessment.

2.2.2. Imaging analysis

Images were transferred to a PACS workstation for analysis. T1 high signal in the SN region was visible in 3 slices, and the middle slice corresponding to the greatest SN volume was selected. In this slice, a line was defined following the maximal longitudinal length of the SN area and was divided into three equal segments to define the lateral, central and medial SN parts. One of the authors (a neuroradiologist), blinded to the subject information, performed manual measurements of the maximal width of the T1 high signal area perpendicular to the length line for the three SN parts, as shown in Fig 1d. Measurements were performed on both sides.

In addition, visual assessment of the neuromelanin SN T1 high signal was performed by two neuroradiologists (R.S. and M.C.) who have more than 10 years experience, were blinded to the clinical status of the subjects and did not know each other's evaluation nor the results of the width measurements. SN T1 high signal area was visible on three slices and the middle slice was selected for analysis, similar to the quantitative method. The SN T1 signal was then evaluated according to symmetry and size/signal intensity (rated as normal/reduced). Where applicable, the SN part of T1 high signal greatest size/signal intensity reduction was identified (medial/central/lateral). According to these parameters the subjects were then classified into 4 groups: "probable PD", if the SN T1 high signal area was markedly reduced in size/intensity and markedly asymmetrical; "possible PD" was used for reduced size/signal intensity and asymmetrical T1 high signal SN areas and "not PD" if the SN T1 high signal area was normal in size/intensity and symmetrical. All other cases were rated "uncertain".

4.3. Statistical analysis

The SN T1 high signal width obtained for each group was compared using non parametric analysis. Kruskal-Wallis tests, with pairwise comparisons in which the resulting *p*-values were corrected according to Bonferroni method, and Mann-Whitney U tests were used as appropriate. Receiver operation characteristics (ROC) curve analysis was conducted for the comparison between PD patients groups and normal subjects, and the specificity and sensitivity of the tests and the optimal cutoff points as well as the area under the curve (AUC) were also assessed. Differences in the sex distribution among groups were

evaluated with χ^2-test. The Kruskal-Wallis test was performed for comparison of the median age between groups as well as for UPDRS total score and UPDRS part III.

A *p*-value of 0.05 was considered significant. Statistical analysis was performed with R 2.15.2.

5. Results

MR imaging quality allowed the identification of the SN high signal area and width measurements on all subjects. We analyzed 12 patients with "de novo" PD, 10 patients with 2 - 5 year disease duration and 10 healthy controls whose clinical characteristics are shown in Table 1. No significant differences were observed in age and sex among the 3 groups, and there were also no significant differences in H&Y stage and UPDRS scores between the "de novo" and 2 - 5 years disease duration PD patients. All PD patients had mild disease severity with H & Y of 1-2 and mean UPDRS motor score of 29.12(±12.92). Symptoms at onset were predominantly unilateral with half of the "de novo" PD patients presenting criteria for asymmetric disease on UPDRS part III (135).

Quantitative width measurements of SN T1 high signal are shown on Table 2. The median global averaged width of the T1 high signal in the SN was significantly decreased in both PD groups when compared with healthy controls with a *p*-value <0.001 and 0.002 respectively (Fig 2). This pattern of width differences between the groups was more pronounced in the lateral, rather than the central, SN segments (Table 2 and Fig 2) and the medial SN width was only decreased significantly when comparing the 2-5 year PD group with the controls (*p*-value=0.002). We found no significant differences between left and right SN width for all the segments (*p*-value = 0.714). A substantial overlap was observed between the "de novo" and the 2-5 year PD groups, with no significant differences in the width measurements.

ROC analysis is detailed in Table 3 and indicated good area under the curve (AUC) values for the lateral segment width in both PD patients groups. The sensitivity and specificity of the width measurement in the lateral part of the SN was 88% and 65% respectively, when the cut-off value for SN width was set at 1.86mm for discriminating the "de novo" PD group vs. controls and were both 75%, with a width cut-off value of 1.97mm, for discriminating between the 2-5 year PD group and controls (Table 3).

The visual assessment results of the SN high signal area for the two raters are shown in Table 3. The neuromelanin size/signal was decreased in the vast majority of PD patients (only rated as normal in 2 PD "de novo" patients). Marked asymmetry was found in almost all the 2-5 year PD patient's but only in half of the "de novo" PD group. Raters independently classified as "probable/possible PD" 17/22 of PD patients (rater 1) and 20/22 (rater 2); 6/10 and 8/10 of the controls were rated as "not PD". No PD patient was classified as "not PD" and no healthy control was classified as "probable PD".

6. Discussion

Visual assessment of neuromelanin-sensitive MR images by experienced neuroradiologists was able to detect changes in the SN of early-stage PD patients with a discrimination power similar to that of a quantitative measurement of T1 high signal width. The sensitivity, specificity and AUC of the SN neuromelanin width measurements for the distinction of early stage PD patients from healthy controls were comparable to the PD patient's identification rates obtained by visual assessment.

Neuroradiologists were also able to detect a greater reduction of neuromelanin in the lateral part of the SN in PD patients and a less pronounced change in the central and medial segments, in accordance with the quantitative width measurements and reflecting the known pathological gradient of neuronal depletion in PD (11).

Although the quantitative width measurements were not significantly different between the "de novo" and the 2-5 year PD groups, on visual inspection the 2-5 year PD patients were classified with greater certainty as "probable PD" that the "de novo" PD patients. We think that these findings may reflect the more global analysis provided by visual inspection as it takes into account several parameters such as size, signal and morphological data, allowing the identification of a disease pattern. These data are in agreement with neuropathology findings in PD which correlate the decrease of SN neuromelanin with clinical severity (14). However this decrease was not reflected in our quantitative measurements which were similar to previous reports of SN neuromelanin signal intensity changes (125) and transcranial sonography (126) in PD suggesting a stability of the neuromelanin content with disease duration. The different imaging and post-processing methods used in these studies may explain the inconsistent findings in

neuromelanin patterns with disease duration (63,128) and additional research on neuromelanin MRI signal changes throughout PD evolution is needed.

PD motor symptoms are usually asymmetric at the time of clinical presentation and throughout the course of the disease (19,135,136). We were not able to find a significant asymmetry in the SN neuromelanin nor a correlation with the clinically most affected side in our PD patients either with visual inspection or with quantitative analysis. This may be due to the small number of subjects in our samples which limits the power of the study.

Previous neuromelanin MR studies have used quantitative measurements with automated analysis or manual ROI tracing (125,127,133). These post-processing techniques are time consuming or need post-processing software which limits clinical implementation of neuromelanin imaging. In our study, visual inspection was able to identify a pattern of SN neuromelanin that allowed a good discrimination between PD patients and controls with high agreement with quantitative measurements. Additionally, the sensitivity and specificity obtained for these MRI neuromelanin studies are only slightly lower than those obtained in [^{123}I]- FP-CIT SPECT studies in identifying PD patients (134,137). Finally, neuromelanin sensitive MRI has a relatively low cost compared with PET or SPECT imaging and can be applied to all compliant patients with few involuntary movements and no MRI contraindications, unlike transcranial sonography where up to 18% of individuals have insufficient temporal acoustic windows (138).

Our study has several limitations, mainly the small number of patients. The imaging technique requires a 3.0Tesla MR machine which has an impact on availability and the neuromelanin sequence has a long acquisition time, a relatively low spatial resolution and is prone to in-plane signal inhomogeneity. In addition, we used a fully manual, operator dependent image analysis technique that can have a high variability.

However, we obtained a good agreement in visual assessment between the two raters and the findings are consistent with quantitative data and with previous studies using different methods and techniques (63,125,127).

Motion artifacts were not a problem for visual inspection or width measurement in our PD patients groups, but these were early stage H&Y 1-2, with few involuntary movements. Image artifacts may be an issue in advanced-stage PD patients interfering with image evaluation.

Using a fast, easy, highly available assessment of SN neuromelanin with visual inspection or width measurement, we were able to detect a disease pattern change in early stage PD patients. Visual inspection of MR sensitive neuromelanin imaging of the SN may become an attractive tool in clinical practice for PD diagnosis, but additional studies are needed to validate this method and to determine how this imaging technique can affect the management of PD patients.

5. Conclusion

Visual inspection of neuromelanin-sensitive MRI techniques has similar results compared to a quantitative width analysis of SN changes in early-stage PD, allowing the identification of a specific disease pattern and a good distinction of PD patient's from healthy controls. These findings can have an impact on a wider use of neuromelanin MR imaging in clinical practice for PD patients evaluation.

Table 1: Demographics for Parkinson's disease patients and control subjects

	"de novo" PD	**2-5 years PD**	**Controls**	***p*-value**
No. (female/male)	12 (7/5)	10 (2/8)	10 (4/6)	0.186
Age, years (mean±SD)	63.23(± 11.9)	66.9(±6.4)	61.2(±7.3)	0.289
H&Y (mean±SD)	2(2-2)	2(2-2)	-	-
Total UPDRS (mean±SD)	44.46(±26.0)	46.75(15.6)	-	0.149
UPDRS-III motor score (mean±SD)	29.08(±14.2)	25.88(±11.3)	-	0.498

PD: Parkinson's Disease; No: number; SD: standard deviation.

Table 2: SN neuromelanin T1 high-signal width measurements

	"de novo" PD	**2-5 years PD**	**Controls**	***p*-value***
SN global average width (mm) – median (range)	2.48 (0 - 0.539)	2.32 (0 - 4.33)	3.25 (0 - 0.597)	<0.002
SN lateral width (mm) – median (range)	1.54 (0 - 0.264)	1.24 (0 - 0.387)	2.25 (0 - 0.399)	<0.002
SN central width (mm) – median (range)	2.60 (0.138 - 0.457)	2.32 (0.000 - 0.417)	3.34 (0.231 - 0.536)	0.019
SN medial width (mm) – median (range)	3.39 (0.214 - 0.539)	3.30 (0.163 - 0.433)	3.91 (0.307 - 0.597)	0.005

*Comparisons using Kruskal-Wallis test

PD: Parkinson's Disease

Table 3: Visual assessment of the SN T1 high signal

	Rater 1				Rater 2			
	SN T1 high signal area			Subject's classification	SN T1 high signal area			Subject's classification
	Size/signal intensity (↓/normal)	SN part of greatest reduction	Symmetry (A/S)		Size/signal intensity (↓/normal)	SN part of greatest reduction	Symmetry (A/S)	
"de novo" PD	11/1	7 lateral	6/6	5 probable PD	10/2	11 lateral	11/1	6 probable PD
		0 central		3 possible PD		0 central		4 possible PD
		0 medial		4 uncertain		0 medial		2 uncertain
		4 global		0 not PD		0 global		0 not PD
2-5 year PD	10/0	8 lateral	8/2	9 probable PD	10/0	10 lateral	10/0	10 probable PD
		0 central		1 possible PD		0 central		0 possible PD
		0 medial		0 uncertain		0 medial		0 uncertain
		2 global		0 not PD		0 global		0 not PD
Controls	4/6	2 lateral	2/8	0 probable PD	1/9	3 lateral	3/7	0 probable PD
		0 central		4 possible PD		0 central		0 possible PD
		0 medial		0 uncertain		0 medial		2 uncertain
		2 global		6 not PD		0 global		8 not PD

PD: Parkinson's disease; ↓: reduced; A/S: asymmetric/symmetric

Table 4: ROC analysis of neuromelanin signal width for discriminating patients with "de novo" PD and 2-5 year PD duration from controls.

	"de novo" PD vs. controls			
	Cutoff value	Sensitivity (%)	Specificity (%)	AUC
SN lateral part	0.1860000	88,5	65	0,806
SN central	0.3130000	69,2	85	0,748
SN medial part	0.3370000	30,8	100	0,652
	2 - 5 years PD vs. controls			
	Cutoff value	Sensitivity (%)	Specificity (%)	AUC
SN lateral part	0.1970000	75	75	0,77
SN central	0.3130000	65	85	0,739
SN medial part	0.3670000	55	95	0,792

Figures

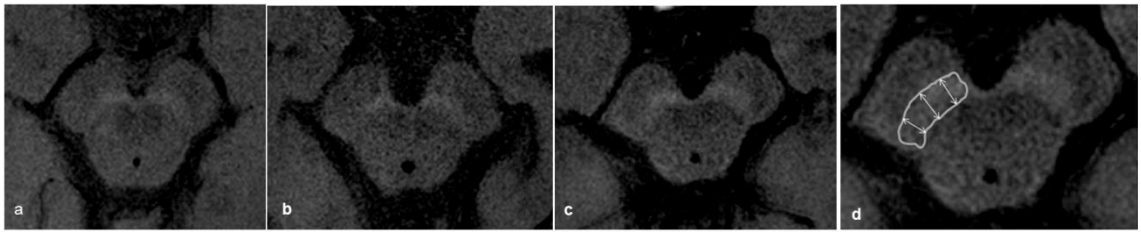

Fig 1. SN neuromelanin-MRI of a "de novo" PD patient (a), a 2-5 year PD patient (b) and a control subject (c); width measurement example (d) in a control subject.

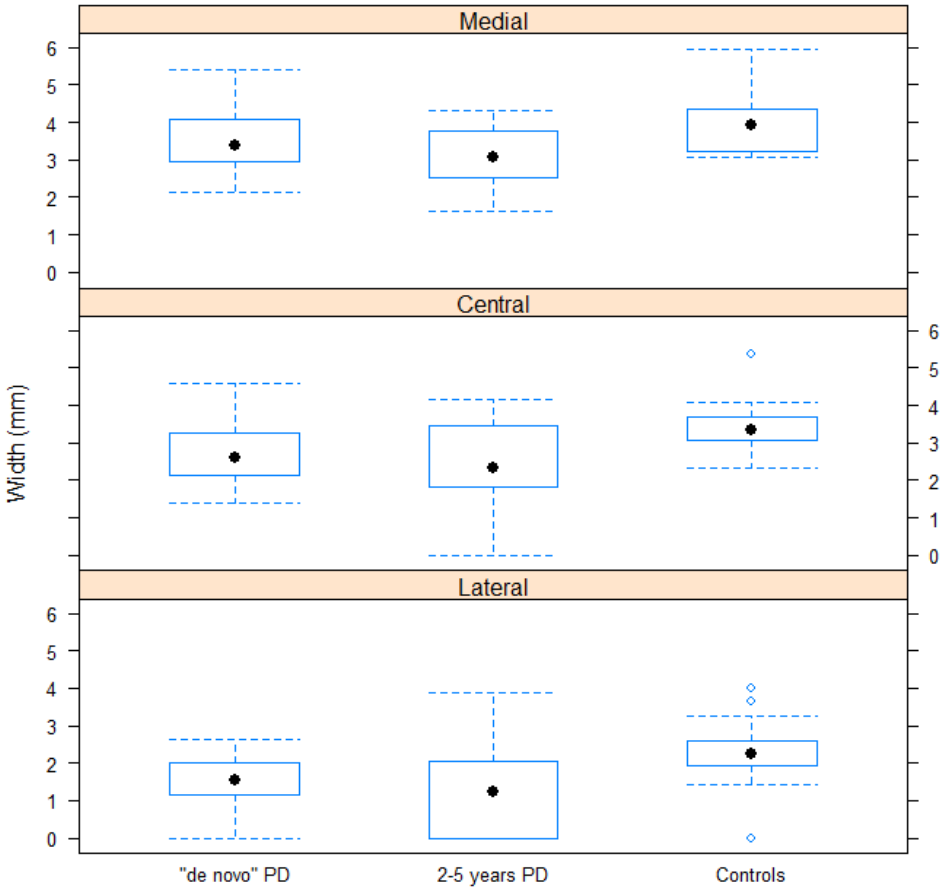

Fig 2. Width of the SN high-intensity region on neuromelanin-sensitive MR images in patients with "de novo" PD, 2-5 year PD and healthy controls; Mann-Whitney *U*-test.

2.3. MRI correlation of iron content with neuromelanin in the Substantia nigra of early stage Parkinson's disease

Reimão S, Ferreira S, Nunes RG, Pita Lobo P, Neutel D, Abreu D, Gonçalves N, Campos J, Ferreira JJ

Submitted for publication

MR correlation of iron content with neuromelanin in the *Substantia nigra* of early stage Parkinson's disease

Sofia Reimão[1,4], Sara Ferreira[2], Rita G Nunes[2], Patrícia Pita Lobo[3,4,6], Dulce Neutel[3,4], Daisy Abreu[4], Nilza Gonçalves[4], Jorge Campos[1], Joaquim J Ferreira[3,4,5,6]

[1] Neurological Imaging Department, Hospital de Santa Maria - Centro Hospitalar Lisboa Norte, Portugal
[2] Instituto de Biofísica e Engenharia Biomédica, Faculdade de Ciências, Universidade de Lisboa, Portugal
[3] Neurology Department, Hospital de Santa Maria - Centro Hospitalar Lisboa Norte, Portugal
[4] Clinical Pharmacology Unit, Instituto de Medicina Molecular, Faculty of Medicine, University of Lisbon, Portugal
[5] Laboratory of Clinical Pharmacology and Therapeutics, Faculty of Medicine, University of Lisbon, Portugal;
[6]CNS – Campus Neurológico Sénior, Torres Vedras, Portugal

Abstract

Background: Magnetic resonance studies have demonstrated a significant reduction of neuromelanin in the *substantia nigra* (SN) of Parkinson's disease (PD) patients with high accuracy for differential diagnosis compared to non-PD controls and Essential Tremor. However, studies state not knowing how paramagnetic effects of iron influence neuromelanin signal as a limitation. In this study we combined a neuromelanin-sensitive MR sequence with T2*-relaxometry iron quantification analysis to study the SN of early-stage PD patients to investigate the correlation between these parameters.

Methods: The inclusion criteria were untreated "de novo" PD patients and a 2 – 5 year disease duration (early PD); in addition, age matched controls were enrolled. These were studied at 3.0 Tesla with a high-resolution T1-weighted MR sequence to visualize neuromelanin and a relaxometry sequence for iron quantification. The primary outcome was the correlation of the width of the neuromelanin high signal region and the T2* values in the lateral, central and medial segments of the SN.

Results: We found very weak correlations of T2* values with neuromelanin width, positive for global and negative for the medial and lateral SN segments in both PD groups and control subjects. The SN neuromelanin width was markedly reduced in the "de novo" and early PD groups compared with controls in all SN segments, but no significant difference in T2* values was found between the groups.

Conclusions: SN neuromelanin signal does not have a significant correlation with iron content in PD patients or controls. The neuromelanin MR signal reduction in PD does not seem to be significantly influenced by paramagnetic iron effects.

1. Introduction

Recent magnetic resonance (MR) studies have described a reduction of neuromelanin in the *substantia nigra* (SN) and *locus coeruleus* (LC) of Parkinson's disease (PD) patients (61-63,125,139), with a very high diagnostic sensitivity and specificity for disease diagnosis even in early disease stages (125,139). These *in vivo* MR imaging findings seem to reproduce the known pathological pattern of greater pigmentation loss in the lateral SN of PD patients (125) and so this imaging technique may become a valuable tool for disease investigation.

However, all previously published MR neuromelanin studies refer not being able to ascertain how the local iron content in the SN could influence the neuromelanin-sensitive MR signal changes in PD as a significant limitation (62,63).

It is known that iron content in the SN is increased in PD at the time of diagnosis and seems to increase with disease progression (69,70,129). Dopaminergic neurons of the SN *pars compacta* (SNpc) and noradrenergic neurons of the LC contain significant amounts of iron sequestered in neuromelanin granules (65) with approximately 20% of SN iron bonded to neuromelanin in its ferric form (66) and the remainder stored as ferritin and hemosiderin (67,68).

In PD, as evidenced by post mortem studies, individual neuromelanin granules of the SN have higher iron levels (71), but the loss of functional nigral neurons early in the course of the disease results in a general decrease in the number of neuromelanin granules, with iron being sequestered in SNpc neurons Lewy bodies (72) and an increased loading of ferritin with iron (73).

Paramagnetic substances such as iron increase proton transverse relaxation rate (R_2), but the MR signal changes are dependent on several factors (74) that result from tissue composition with multiple interactions (75). Different MR imaging sequences have been used to study iron distribution in PD, yielding inconsistent results but recent studies report a difference in magnetic susceptibility (82) and R_2* values in the lateral SN of PD patients (80). However, the influence of iron paramagnetic effects on T1-weighted neuromelanin-sensitive MR signal changes in PD patients is unknown.

To investigate the correlation and the possible contribution of the iron content in the different segments of the SN to the neuromelanin signal changes in PD, we combined a

specific neuromelanin-sensitive MR sequence with an iron quantification analysis using T2*-relaxometry at 3.0T to study early-stage PD patients. To the best of our knowledge this is the first MR study analyzing the correlation of SN neuromelanin and iron in PD.

2. Patients and methods

2.1. Patients and control subjects

The study was a cross-sectional case-control (prospective follow-up ongoing) that included 32 subjects: 12 "de novo" patients with PD, 10 PD patients with a 2 - 5 year disease duration (early PD) and 10 healthy subjects. Patients were recruited from the Movement Disorders Unit of the University Hospital of Santa Maria-Lisbon. "De novo" PD patients were included at the time of clinical diagnosis if they were not on antiparkinson medications. PD patients with 2 - 5 year disease duration were receiving optimal pharmacotherapy with levodopa or dopamine agonists. All patients were diagnosed with PD by a movement disorders specialist according to the UK Brain Bank criteria (19) and were rated using the Unified Parkinson's Disease Rating Scale (UPDRS). "De novo PD" patients were drug naïve and early PD patients were imaged and clinically evaluated on-medication. The healthy control subjects were recruited from local hospital staff and relatives. Dementia, psychiatric illness or contraindications to an MRI were the exclusion criteria.

All the examinations were performed with the understanding and written consent of each subject, with approval from the local ethics committee, and in compliance with national legislation and Declaration of Helsinki guidelines.

2.2. MRI protocol

2.2.1. Imaging protocol

A combined neuromelanin and iron quantification MR protocol was performed simultaneously in a 3.0-Tesla Phillips scanner (Philips Achieva; Philips Medical Systems, Best, Netherlands). The neuromelanin-sensitive pulse sequence parameters were similar to the previously described by Sasaki and colleagues (61): T1-weighted FSE: repetition time/effective echo time, 633/10 ms; echo train length, 3; number of slices, 20; slice

thickness, 2.5 mm; intersection gaps, 0 mm; matrix size, 548 x 474; field of view, 220 x 190 mm^2 (pixel size: .40 x .40 mm^2); and acquisition time, 8 min). The intersection gap was set to 0 mm and not to 1mm as in previous studies (61) to ensure full coverage of the SN; to avoid cross-talk effects related to overlapping slice profiles, an interleave slice order was used, maximizing the time between excitation of adjacent slices. The sections were carefully set in the oblique axial plane perpendicular to the fourth ventricle floor with coverage from the posterior commissure to the inferior border of the pons.

The T2* relaxation data were acquired with a multiecho FFE sequence with 7 equally spaced echoes with a spacing of 4.7 ms, starting from 13.8 ms; repetition time 1406 ms, flip angle 18°; 28 slices; slice thickness 4mm, gaps, 1mm; matrix size, 288 x 160, field of view, 240 x 180 mm^2; and acquisition time 4 min. Images were acquired in axial orientation parallel to the commissures line and covering the whole brain.

In addition, T1- and T2-weighted images of the entire brain were obtained in all subjects and evaluated by an experienced neuroradiologist to exclude other pathological imaging findings, namely, changes in the parkinsonian index and other atypical parkinsonian syndrome changes, and lesions in the SN area that could interfere with further assessment.

2.2.2. Imaging analysis

Images were transferred to a PACS workstation for analysis, which was performed blinded to patient's diagnosis.

T1 high signal in the SN region was visible in 3 slices, and the middle slice, corresponding to the greatest SN volume, was selected. In this slice, a line was defined following the maximal longitudinal length of the SN area and was divided into three equal segments defining the lateral, central and medial SN parts. One of the authors (a neuroradiologist), blinded to the subject information, performed manual measurements of the maximal width of the T1 high signal area perpendicular to the length line for the three SN parts (Fig 1 A), as previously reported (139). Measurements were performed on both sides.

T2* maps (T2* = 1/R2*) were calculated using an in-house tool developed in Matlab (version 7.11; The Mathworks, Natick, MA, USA) blinded to the neuromelanin measurements. Prior to fitting, the logarithm of the signal in each voxel was calculated. A voxel-by-voxel linear least squares fitting of the log-signal $\ln[S(TE)]$ was performed using

the data for all 7 echo-times as described by the equation, where S_0 would be the signal measured at zero *TE*:

$$\ln[S(TE)] = \ln[S_0] - \exp\left[-\frac{TE}{T2^*}\right]$$

To minimize the impact of potential image outliers, the Matlab *robustfit* function was used to perform linear regression while automatically adjusting the weighting factor given to each time point (140).

Regions of interest (ROIs) were manually drawn for each individual in the FFE image corresponding to the shortest TE, blinded to the neuromelanin measurements. The slice immediately inferior to the red nucleus was selected, corresponding to the greatest SN volume. The maximal longitudinal length of the SN area was divided in three equal segments defining SN lateral, central and medial parts, similar to the neuromelanin measurements. We then drew ROIs in the center of each SN segment, with no overlap (Fig 1 B and C) with an equal diameter (each with four voxels - voxel size 0.43mm - providing an ROI area of 2.3mm^2). ROIs were drawn bilaterally and the mean T2* values were extracted. The mean value across the left and right ROIs in the SN was used for statistical analysis.

6.3. Statistical analysis

Differences in the clinical characteristics among these groups were assessed using χ^2-test and Kruskal-Wallis test. For each SN ROI we assessed neuromelanin and T2* differences between groups using non parametric analysis. For Kruskal-Wallis tests, with pairwise comparisons, the resulting *p*-values were corrected according to the Bonferroni method.

Spearman correlation was assessed for each SN segment between neuromelanin width and the T2* quantitative value.

A *p*-value of 0.05 was considered significant. Statistical analysis was performed with R 2.15.2 (R Foundation for Statistical Computing, Vienna, Austria).

7. Results

The identification of the SN neuromelanin high signal area and the acquisition of T2* maps was feasible in all subjects. We analyzed 12 patients with “de novo” PD, 10 early PD

patients with 2 - 5 year disease duration and 10 healthy controls whose clinical characteristics are shown in Table 1. No significant differences were observed in age and sex among the 3 groups, and there were also no significant differences in H&Y stage and UPDRS scores between the "de novo" and the early PD patients. Symptoms at onset were predominantly unilateral with half of the patients presenting criteria for asymmetric disease on UPDRS part III (141).

To study the correlation of the neuromelanin width measurements with the T2* values we analyzed the SN globally, with an average of the measures of the 3 segments, and then considered the different segments separately. For the global SN we found only a very weak positive correlation of T2* values with the neuromelanin width (value of 0.15) (Table 2). For the different SN segments analyzed separately, in the medial and lateral SN segment we found a negative correlation of these measurements for all groups; in the central area a negative correlation was found only for the early PD group (Table 2). Combining both PD groups and analyzing them as a whole, the correlation value was 0.25, positive but very weak (*p*-value 0.004) regardless of the SN position. We found a weak correlation between the measured parameters with regards to sides (right and left) for each group [early PD : 0.205 (*p*-value: 0.414), "de novo" PD: 0.12 (*p*-value: 0.609), Control group: -0.014 (*p*-value: 0.94)].

The SN neuromelanin manual width measurements were markedly reduced in the "de novo" and early PD groups compared with controls in all SN segments with *p*-values <0.001 (Table 2). The greatest reduction was evident at the lateral and central SN segments with *p*-values of <0.001 and 0.005, respectively. There was no significant difference between "de novo" and early PD groups for the neuromelanin measurements on all the segments (Table 3), although the values of the former were slightly lower than the latter. No significant differences were found in neuromelanin measurements between right and left sides for either group (*p*-value for controls of 0.53, *p*-value for early PD patients of 0.782 and *p*-value for "de novo" patients of 0.631).

We found no statistically significant difference in T2* values between the "de novo" PD, early PD and control groups in either of the SN segments (*p*-values of 0.16, 0.52 and 0.88 for the medial, lateral and central SN, respectively) (Table 4), although the median T2* values were lower in both PD patients groups than in the control group.

For each group there were significant differences between the T2* values between the three SN segments (*p*-value of 0.01 for the Controls, a *p*-value of 0.01for the early PD group and a *p*-value of 0.001 for "de novo" PD patients group) (Table 4), with lower values in the medial segment and higher in the lateral. For the three groups significant differences were found between the lateral and medial segment, and for the "de novo" group there were also significant differences between central and medial segment.

No significant differences were found between the right and the left side T2* measurements either globally (*p*-value of 0.78) or with respect to group (controls *p*-value = 0.88, "de novo" PD *p*-value = 0.63 and early PD *p*-value = 0.78).

4. Discussion

The combined analysis of the SN neuromelanin and T2* values did not find a significant correlation between the two parameters. There was only a very weak correlation between T2* values and neuromelanin width with a positive value for the global measurements and a negative value for the medial and lateral segments.

Neuromelanin is thought to protect neurons from oxidative stress mediated by free metals or free radicals (35,142,143), sequestering iron in the SN and LC neurons (144). However the reduction of nigral neurons in the early stage of PD diminishes the number of neuromelanin granules with a consequent reduction of regional iron load of the granules. We hypothesize that this reduction in the percentage of iron that is stored bound to neuromelanin with a possible increase of the proportion of iron stored as ferritin, hemosiderin and in Lewy bodies might explain the very low and even absence of correlation we found between neuromelanin measurements and iron levels in the SN of early stage PD patients. Another possibility is that these parameters reflect different pathophysiological processes with separate mechanisms involved in SN neuronal neuromelanin loss compared to the causes of increased iron accumulation. The significance of the different associations (positive/negative) among groups and SN segments (Table 2) is hard to interpret due to the limited number of patients and the weak correlation values; future studies are needed to clarify these data.

As expected the SN neuromelanin was significantly decreased in our early stage PD patients groups compared to controls, in agreement with previous studies using different

imaging analysis methods (61-63,125). We used manual width measurements of the SN T1 high signal region to study the pattern changes in its different segments and were able to detect a greater lateral reduction of neuromelanin signal, as expected (61,125,140). However, we found no significant differences in the SN T2* measurements of PD patients compared to controls, although the values of the controls tend to be higher than the PD groups for all the segments.

The T2* values of the medial SN are lower than the central or the lateral segments for all groups, which reproduces the expected rostral-caudal gradient in susceptibility in PD patients and controls (82).

These MR relaxometry findings do not reproduce the results of some of the previous MR studies using R2* or SWI which reported differences in the lateral (but not medial) SN of PD patients suggesting a relative increase of iron (82,80). The very early disease stages of our patients or the small sample size limits the power of our findings. However, in the literature there is a wide variability of results regarding iron MR changes in PD (121,145,146), possibly due to methodology differences in the estimation of brain iron, the anatomical variability or the individual variations of the SN size and shape, the evaluated disease stages and lack of reproducibility studies, yielding inconsistent results.

In brain tissue multiple iron interactions occur, possibly explaining the poor correlation between T2 times and direct measures of iron and ferritin, with factors other than iron having a role in determining the transverse relaxation parameters (75,147). Shortened T2 values in the SN and striatum have been reported in PD, but with small changes, apparently unrelated to disease duration, and with a substantial overlap between patients and controls (148,149). T2* imaging methods have shown a correlation between increased SN iron-related contrast and clinical severity (150), and T2' an increased iron content in the SN (129) that correlated with motor features (151). We used a quantitative T2*-relaxometry to measure brain iron because this appears to be the most sensitive parameter to study iron concentration *in vivo* (78).

Previous studies in healthy subjects found no significant changes in the SN iron content with increasing age (147) and in our study there was no significant age differences between PD patients and healthy controls; so the obtained T2* values do not seem to be influenced by the age interval of the studied subjects.

In spite of the clinical asymmetrical presentation in most of our PD patients, we found no significant differences between the left and the right SN neuromelanin or T2* values. Previous studies of chemical analysis in healthy subjects found higher iron concentrations on the left hemisphere compared to the right which was thought to be related to motor lateralization and location of dopaminergic neurons (152). However, these data were not reproducible in a posterior study that found no parallel hemispheric differences in the relaxation rates (78), similar to our findings in PD and control subjects.

"De novo" PD patients have high UPDRS part III scores, but contrary to the early PD group, they were evaluated before medication was initiated, and the values have a wide range (15-64 years) at the expense of the high value of 3 patients that had a wide interval from the beginning of symptoms until PD diagnosis.

Our study has several limitations, namely the small number of patients in each group and the absence of pathological confirmation. Further complications are due to disadvantages of the imaging technique, including the long acquisition time of the neuromelanin-sensitive sequence with additional relatively low spatial resolution and in-plane signal inhomogeneity. However, we used a fully manual, operator dependent image analysis, that did not need post-processing software which makes it a widely available method. Our manual approach has the additional advantage of identifying individual variations of SN size and shape, significantly improving anatomical precision in width measurements and ROI placement. On the other hand, due to wider areas of SN in the selected slice, the sub-thalamic nucleus may not have been completely excluded from the ROIs.

Motion artifacts were not a problem for neuromelanin width measurement or the elaboration of T2* maps in either of our PD patients groups, but these were early stage H&Y 1-2, with few involuntary movements. Image artifact may be an issue in advanced-stage PD patients and will need to be addressed.

The within-subject and inter-rater reproducibility of these measurements has not been fully established, further studies are required to address this issue and allow a wider implementation of this multimodal MR imaging analysis.

5. Conclusion

The iron content in the SN of early stage PD patients does not have a significant correlation with neuromelanin MR signal changes. The SN signal changes in PD patients can be attributed to a pigment reduction and are not directly related to local iron concentration. Iron accumulation and neuromelanin reduction in PD may be independent processes whose contribution to PD pathophysiology needs to be studied.

Tables and legends

Table 1: Demographics for Parkinson's disease patients and control subjects

	"de novo" PD	**Early PD**	**Controls**	***p*-value**
No. (female/male)	12 (7/5)	10 (2/8)	10 (4/6)	0.18
Age, years (mean±SD)	63.2(± 11.9)	66.9(±6.4)	61.2(±7.3)	0.28
H&Y (mean±SD)	2(2-2)	2(2-2)	-	-
Total UPDRS (mean±SD)	44.4(±26.0)	46.7(15.6)	-	0.14
UPDRS-III motor score (mean±SD)	29.0(±14.2)	25.8(±11.3)	-	0.49

PD: Parkinson's Disease; No: number; SD: standard deviation.

Table 2: Spearman Correlation between SN T2* and neuromelanin width

	Spearman Correlation between SN T2*and neuromelanin width (*p*-value)			
	Regardless position	Considering position		
		SN lateral	SN medial	SN central
Total	0.248 (0.001)	NA	NA	NA
"de novo" PD	0.317 (0.013)	-0.024 (0.917)	-0.085 (0.719)	0.054 (0.821)
Early PD	-0.002 (0.989)	-0.104 (0.699)	-0.436 (0.091)	-0.557 (0.024)
Controls	0.304 (0.025)	-0.203(0.418)	-0.082(0.1578)	0.260(0.297)

SN: *substantia nigra*; PD: Parkinson's disease; NA: Not applicable

Table 3: SN neuromelanin T1 high-signal width measurements

	"de novo" PD	**Early PD**	**Controls**	***p*-value***
SN global average width (mm) – median (range)	2.48 (0 – 5.39)	2.32 (0 - 4.33)	3.25 (0 – 5.97)	<0.002
SN lateral width (mm) – median (range)	1.54 (0 – 2.64)	1.24 (0 – 3.87)	2.25 (0 – 3.99)	<0.002
SN central width (mm) – median (range)	2.60 (1.38 – 4.57)	2.32 (0 – 4.17)	3.34 (2.31 – 5.36)	0.019
SN medial width (mm) – median (range)	3.39 (2.14 – 5.39)	3.30 (1.63 – 4.33)	3.91 (3.07 – 5.97)	0.005

*Comparisons using Kruskal-Wallis test

PD: Parkinson's Disease; SN: *substantia nigra*

Table 4: T2* values in the SN segments

	T2* (sec) (Median ±range)			
	Controls	Early PD	"de novo" PD	*p*-value between groups
SN global	25.35 (12.5-53.8)	21.05 (9.8-48.2)	21.05 (10.5-41.5)	0.11
SN lateral	29 (20.2-42.9)	27.15 (9.8- 45.6)	25.7 (13.7-41.1)	0.52
SN central	24.9 (16.7-42.2)	23.65 (10-48.2)	26.35 (10.5-41.5)	0.88
SN medial	19.9 (12.5-53.8)	18.7 (10.8 -28.7)	17.1 (12 -31.8)	0.16
p-value between segments	0.01	0.01	0.001	

Comparisons using Kruskal-Wallis test

PD: Parkinson's Disease

Figures and legends

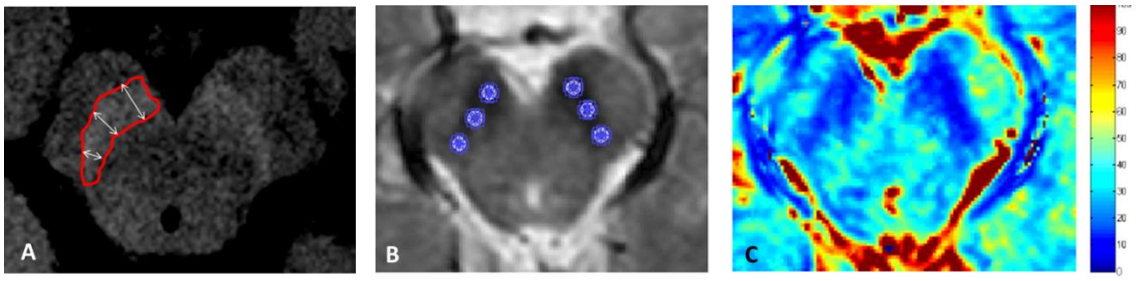

Fig.1. Analysis of the SN neuromelanin and FFE MR imaging. Neuromelanin width measurements in the SN segments in a healthy control (A); MR FFE image with the shortest TE with drawn ROIs in the medial, central and lateral SN segments (B) and corresponding T2* map (C).

2.4. Reproducibility of diffusion tensor imaging (measurements) in early stage Parkinson's disease

Reimão S, Morgado A, Nunes RG, Pita Lobo P, Neutel D, Abreu D, Gonçalves N, Campos J, Ferreira JJ.

Submitted for publication

Reproducibility of *substantia nigra* diffusion tensor imaging measurements in early stage Parkinson's disease

Sofia Reimão MD[1,4], Ana Morgado MS[2], Rita G Nunes PhD [2], Patrícia Pita Lobo MD [3,4,6], Dulce Neutel MD [3,4], Daisy Abreu MS [4], Nilza Gonçalves MS [4], Jorge Campos PhD [1], Joaquim J Ferreira PhD [3,4,5,6]

[1] Neurological Imaging Department, Hospital de Santa Maria - Centro Hospitalar Lisboa Norte, Portugal

[2] Instituto de Biofísica e Engenharia Biomédica, Faculdade de Ciências, Universidade de Lisboa, Portugal

[3] Neurology Department, Hospital de Santa Maria - Centro Hospitalar Lisboa Norte, Portugal

[4] Clinical Pharmacology Unit, Instituto de Medicina Molecular, Faculty of Medicine, University of Lisbon, Portugal

[5] Laboratory of Clinical Pharmacology and Therapeutics, Faculty of Medicine, University of Lisbon, Portugal

[6]CNS – Campus Neurológico Sénior, Torres Vedras, Portugal

Abstract

Purpose: Recent diffusion tensor imaging (DTI) studies have suggested that microstructural abnormalities in the *substantia nigra* (SN) of early stage Parkinson's disease (PD) patients may emerge as a possible diagnostic biomarker. We sought to establish the reproducibility of DTI measurements in early stage PD patients as well as in controls, since several factors can increase signal variability of diffusion-weighted images influencing DTI metrics in the SN.

Material and Methods: The inclusion criteria were untreated "de novo" PD or a 2 – 5 year disease duration; age matched healthy controls were also enrolled. These were studied with a DTI sequence at 3 Tesla with 3 acquisitions: a baseline scan, a repetition within the same session and a third acquisition 15 days later. Reproducibility of fractional anisotropy (FA) and mean diffusivity (MD) were assessed using a region-of-interest (ROI)-based approach in the SN and quantified using the intraclass correlation coefficient (ICC).

Results: A total of 7 "de novo" PD patients, 7 PD patients with a 2 – 5 year disease duration and 6 controls were evaluated. We obtained high ICCs indicating a good level of reliability for all diffusion metrics (FA and MD) in the SN for both PD patients groups and control subjects.

Conclusions: SN DTI measurements are reliable and reproducible in PD patients and so can be used in further studies, namely longitudinal evaluation, to investigate small changes, since the within-subject variability of this imaging technique is low.

1. Introduction

Diffusion tensor imaging (DTI) has been widely used in the last few years to study neurodegenerative diseases, since it can reflect changes in the microstructural properties of the brain parenchyma. Recently a large number of DTI studies have focused on Parkinson's disease (PD), not only investigating white matter changes (99,98), but also looking at grey matter alterations in specific anatomical locations related to this disease's pathophysiology, especially the *substantia nigra* (SN)(93,153). The potential of this imaging technique to detect early neuropathological changes in PD makes it an attractive tool and a possible imaging diagnostic biomarker and research tool for improving knowledge on the mechanisms of the disease. The evaluation at multiple time points with DTI may also become very useful to enable the study of disease progression in PD.

Compared to conventional MR sequences, diffusion-weighted images suffer from higher levels of image ghosting, susceptibility artifacts, eddy-currents and geometric distortions (154). Additionally, these sequences are very sensitive to motion effects, which are more frequent in movement disorders such as PD (155), with greater signal loss compared to T1- or T2-weigted images. This may lead to a bias when comparing images obtained in patients and controls, since the latter should suffer from fewer motion artifacts. All these factors can increase signal variability in diffusion-weighted images and so it is important to demonstrate the reproducibility of DTI measurements if they are going to be used as a tool to accurately quantify microstructural changes and progressive alterations.

The reliability of DTI metrics has been previously studied (155-160), including in some movement disorders such as Huntington's disease (161,162) that share some of the same imaging problems as PD. These studies have, however, presented widely variable estimates of the reliability of DTI measurements. These results can be related to several factors namely differences in imaging acquisition parameters, scanner characteristics (e.g. field strength), post-processing methodology (regions of interest (ROI) versus voxel-based) and brain area specificity (158,163,164), making comparisons difficult.

Recent studies suggested that DTI changes in the SN of early stage PD patients can have a very high diagnostic accuracy (93,153). These data however need further investigation, namely concerning the within-subject variability (i.e. scan-rescan variability), because if

this is large relative to the between-subject variability, then sensitivity for meaningful measurement alterations will be compromised.

Our study thus investigated the reliability of DTI measurements in the SN of early-stage PD patients and compared it with that observed in healthy controls, through within-scanner and test-retest studies. We quantified DTI metrics variability using the intraclass correlation coefficient (ICC) and investigated possible disease-related group changes that could influence DTI reliability.

2. Patients and methods

2.1. Patients and control subjects

This study was a cross-sectional case-control analysis (prospective follow-up ongoing) that included 20 subjects: 7 “de novo” patients with PD, 7 PD patients with a 2 to 5 year disease duration and 6 healthy subjects. Patients were recruited from the Movement Disorders Unit of the University Hospital of Santa Maria-Lisbon. “De novo” PD patients were included at the time of clinical diagnosis if they were not on antiparkinson medications, provided less than 6 months had passed since the beginning of reported clinical symptoms. The PD patients who had been diagnosed 2 to 5 years prior to the study were receiving optimal pharmacotherapy with levodopa or dopamine agonists. All patients were diagnosed with PD by a movement disorders specialist according to the UK Brain Bank criteria (19) and were rated using the Unified Parkinson’s Disease Rating Scale (UPDRS). The healthy control subjects were recruited from local hospital staff and relatives. Dementia, psychiatric illness or contraindications to an MRI were the exclusion criteria.

The examinations were performed with the understanding and written consent of each subject, with approval from the local ethics committee, and in compliance with national legislation and the Declaration of Helsinki guidelines.

2.2. MRI protocol

2.2.1. Imaging protocol

All data was acquired with a 3 T MRI system (Achieva 3.0, Philips Medical Systems, Best, Netherlands). For each participant three DTI scans were acquired: a first baseline scan (scan 1), an *inside scanner* repetition (scan 2), for which the patient remained inside the scanner, the head repositioned and a new survey was acquired for imaging planning, followed by a third acquisition, 15 days later (scan 3). The three DTI image acquisitions used the same imaging parameters. The "de novo" patients only initiated antiparkinson medication after the completion of the third scan.

All images were acquired with an 8-channel phased-array head coil. DTI was performed using a single shot, spin-echo planar imaging (EPI) pulse sequence with the following acquisition parameters: repetition time(TR)/effective echo time (TE), 15755/55ms; b values 0, 1000 s/mm^2; 32 diffusion gradient directions; flip angle, 90°; field of view (FOV), 224mm $\times$ 240mm; reconstruction matrix, 268 $\times$ 288; 1 average; slice thickness of 2mm with no gap; 80 slices and 10 min acquisition time.

In addition, T1- and T2-weighted images of the entire brain were obtained in all subjects and evaluated by an experienced neuroradiologist to exclude other pathological imaging findings.

2.2.2. Imaging analysis

Each subject's images from the different scans were randomly numbered and analyzed as independent studies to ensure that no effect of acquisition order would influence the results.

Images were transferred to a Linux workstation for analysis and DTI image processing was performed using FSL (FMRIB, Oxford, UK, version 4.0.1)(165,166).

Square ROIs with a predetermined size were manually drawn for each subject, with the researcher blinded to the subject identity and scan number. We used the same regions-of-interest (ROI) method as described by Vaillancourt et al (93), each SN ROI with four voxels (voxel size 0.836$\times$0.836 mm^2), were placed in the medial, central and lateral SN (Fig 1 A-C). All ROIs were placed bilaterally.

Both fractional anisotropy (FA) and mean diffusivity (MD) were extracted from all the ROIs for each subject. The mean FA and MD across the left and right ROIs were calculated and used in statistical analysis.

7.3. Statistical analysis

Differences in the clinical characteristics among these groups were assessed. Differences in the sex distribution among the groups were evaluated with the χ^2-test. The Kruskal-Wallis test was performed for comparison of the median age between groups as well as for the total UPDRS score and for part III of the UPDRS evaluation.

The intraclass correlation coefficient (ICC) was used to assess the reliability of DTI measures and was calculated for PD groups and control subjects separately for each region. Confidence intervals (CI) at 95% were obtained for ICC values using the delta method. Measurement reproducibility was assessed by using the Bland-Altman method (167) to define the agreement between the measurements, without differentiating between PD and control data.

All statistical analysis was performed with R 2.15.2. (R Foundation for Statistical Computing, Vienna, Austria) and a *p*-value of 0.05 was considered significant.

8. Results

MR imaging and DTI metrics calculation was feasible in all subjects. We analyzed data from 7 patients with “de novo” PD, 7 patients with 2-5 year disease duration and 6 healthy controls (clinical characteristics shown in Table 1). No significant differences were observed in age and sex among the 3 groups, and there were also no significant differences in H&Y stage and UPDRS scores between the untreated “de novo” and the 2-5 year disease duration PD patients.

FA and MD values for the three DTI scans are summarized in Table 2. No significant differences were found in FA or MD values either between PD patients and healthy controls or between “de novo” and 2-5 year PD patients (Table 2).

The ICCs, CIs and variance for the FA and MD values are shown in Table 3. We obtained high ICC (>0.6) for both metrics in the SN ROIs for both PD groups and controls and also when considering the values irrespective of group. For FA values, the ICC was above 0.9

with a very narrow confidence interval for all ROIs. The ICCs for MD values were above 0.6 with wider confidence intervals.

Between-subject variance was larger in the PD groups than in controls but the within-subject variances in PD patients groups and controls were similar, varying between 0.048 and 0.078 for FA, and between 0.020 and 0.029 for MD (Table 3).

The analysis with Bland-Altman plots for FA and MD showed a good agreement between the scans with differences lying within a small range (Fig 2). Satisfactory precision parameters were found for the SN in all scans.

9. Discussion

We obtained high ICC (>0.96) and a very narrow confidence interval for FA diffusion tensor metrics in the SN, indicating a good level of reliability of this parameter for within-scanner and test-retest evaluations. For FA values, the analysis of within-scanner and test-retest data reproducibility demonstrated high levels of reliability with a similar distribution of variability between the PD groups and controls. MD values had a higher variability compared to FA with lower ICCs (above 0.6) and a wider confidence interval.

The ICC values for DTI metrics obtained here are in agreement with previously published studies, namely on Huntington's disease (161,162), using test-retest (163,168) or between scanners (157,158,169) methodology. However, contrary to previous DTI reproducibility studies (161,163) the ICCs for FA metrics in our study were lower that the ICCs for MD in the SN in both patients and control groups. MD includes averaging across the tensor elements (the eigenvalues) that would be expected to increase the signal-to-noise ratio and lead to reduced variability compared to FA. Nevertheless, our data shows that FA, although primarily suited for the evaluation of white matter microstructure, can also be used to more accurately evaluate grey matter structures even in small size anatomical locations such as the SN.

Contrary to the initial study of Vaillancourt et al (93), we found no significant differences in the SN's FA or MD values between PD patients and controls. However our results are in consonance with other posterior studies that also found no difference in the DTI metrics in the SN area (23). Future studies with a significantly larger number of patients are needed to clarify DTI changes in the SN of PD patients.

We obtained high within-subject agreement for both DTI metrics in the SN for all the groups (Table 3), in agreement with previous studies (170,171). However the levels of within-subject (i.e. scan-rescan) variability were higher relative to between-subject variability for both FA and MD which could compromise sensitivity when attempting to detect pathological meaningful changes.

Between-subject variance was larger in the PD groups than in controls (Table 3), as would be expected, with reasonably similar within-subject variances in PD patients groups and controls. This implies that ICC differences observed between controls and PD are related to between-subject variations, and consistent with the scanning technique being equally reliable in both groups.

The evaluated areas were selected because they are key anatomical locations in PD pathophysiology and targeted in most MR DTI studies. We used ROI manual delineation, despite it being time consuming and operator dependent, as it ensures a good anatomical correlation, taking into account the anatomical variability. It has also been previously demonstrated that ROI measurements seem to be more accurate than voxelwise analysis (161) that requires inter-subject registration and smoothing, which may be a source of errors when comparing the estimated FA values.

Acquisitions at 3.0T and higher magnetic fields are more prone to susceptibility effects, which vary depending on the orientation relative to the main field (156). For this reason, the high level of iron in the *substantia nigra* could have led to more variable results at 3.0T, but these did not seem to significantly influence the diffusion signal and our DTI metrics.

As there was repositioning of the subjects, the position of the head within the magnetic field changed between the scans and there was additionally a long time interval (two weeks) between scans 2 and 3. The high reliability of DTI metrics found in our study indicates that in longitudinal studies the consistency of head position seems to be of less importance when using ROI methods that compensate for the variations in the subtle differences in orientation and slice positioning (160).

Our study has some limitations, namely the relatively small sample size for each group, even though the number is consistent with most of the published DTI studies in PD (93,121,172,173) and it is not expected that the degree of variability changes significantly with an increase in the number of subjects.

Additionally, we only analyzed grey matter structures, which have a very different FA compared with white matter, but previous studies had found similar variability in grey and white matter DTI parameters (161).

Although the reliability of DTI has already been demonstrated across scanners (174), we used a 3.0T MR scanner and our results may not directly apply to lower magnetic fields. Reliability of DTI metrics can be affected by a number of factors either extrinsic (motion artifacts, acquisition resolution, positioning, alignment), intrinsic (MR scanner performance, field homogeneity, coil and gradient features) or related to post-processing (analysis software, data processing strategy) (156,170,171,175), so our results cannot be extrapolated to every DTI sequence or equipment as these inevitably influence the reproducibility of DTI metrics. This variability still restricts the determination of standard data in the study of PD with DTI metrics.

We did not investigate inter-rater or intra-rater agreement because these issues have already been addressed in previous studies with satisfactory to very good results for most anatomic locations (156,170,175). However, these may still be problematic when interpreting FA and MD maps with an ROI analysis where the variability is mainly related to the anatomical training of the observer in the correct selection of the location to analyze (175). It would be beneficial, therefore, to have more than two observers analyzing every ROI and to evaluate additional locations, although it should be safe to assume that our findings can be extrapolated to other grey matter brain areas.

In diseases such as PD, where the expected differences between patients and controls may be quite subtle, it is important to characterize the regional variation of the studied metrics to ensure a correct interpretation of group comparisons (163). Our data indicate that in the studied grey-matter ROIs, relevant for PD pathology investigation, DTI FA metrics can be reliably used in future studies since variability of repeated measurements have no significant influence on the results. We found no evidence of group bias that could have influenced reliability.

In conclusion, the low *within scanner* and *scan-rescan* variability, as well as the homogeneity among the anatomical sites in terms of DTI metrics reliability gives support to the further use of these imaging parameters for the detection of brain structural changes in PD.

5. Conclusions

We obtained high ICC for MD and especially FA diffusion tensor metrics, indicating a good level of reliability of these parameters. These findings give support to the use of these measurements in further studies, namely longitudinal within-subject evaluation, and cross-sectional comparisons.

Tables and legends

Table 1: Demographics for Parkinson's and control subjects

	Untreated "de novo" PD	2-5 years PD	Controls	*p*-value
No. (female/male)	7 (5/2)	7 (2/5)	6 (2/4)	0.2852
Age, years (mean±SD)	67(52-82)	68(62-78)	61(49-72)	0.3451
H&Y (mean±SD)	2(2-2)	2(2-2)	-	-
Total UPDRS (mean±SD)	32(26-82)	46.5(39-67)	-	0.3518
UPDRS-III motor score (mean±SD)	24(15-50)	26.5(17-	-	0.8301

PD: Parkinson's Disease; No: number; SD: standard deviation.

Table 2: Diffusion tensor metrics in PD patients and control subjects

	FA median (range)			***p*-value***		
	"de novo" PD	**2-5 y PD**	**Controls**	**Controls vs 2-5y PD**	**Controls vs "de novo" PD**	**2-5y PD vs "de novo" PD**
RM 1	0.53 (0.16)	0.50 (0.21)	0.53 (0.13)	1.00	1.00	1.00
RM *In scanner*	0.53 (0.14)	0.52 (0.17)	0.53 (0.12)	1.00	1.00	1.00
RM 15 days	0.56 (0.18)	0.53 (0.16)	0.54 (0.13)	1.00	1.00	1.00
	MD median (range)			***p*-value***		
	"de novo" PD	**2-5 y PD**	**Controls**	**Controls vs 2-5y PD**	**Controls vs "de novo" PD**	**2-5y PD vs "de novo" PD**
RM 1	0.78 (0.14)	0.81 (0.09)	0.78 (0.08)	0.45	1.00	1.00
RM *In scanner*	0.83 (0.11)	0.76 (0.24)	0.76 (0.13)	1.00	0.16	0.10
RM 15 days	0.81 (0.13)	0.77 (0.14)	0.76 (0.09)	1.00	1.00	0.61

*Comparisons using Kruskal-Wallis test
PD: Parkinson's Disease; y: year

Table 3: Intraclass correlation coefficient (ICC) for mean FA and MD values

	"de novo" PD			2-5 year PD			Controls			Not considering groups		
	Between subject σ^2	Within subject σ^2	ICC (CI)	Between subject σ^2	Within subject σ^2	ICC (CI)	Between subject σ^2	Within subject σ^2	ICC (CI)	Between subject σ^2	Within subject σ^2	ICC (CI)
FA	0.0008	0.053	0.96 (0.87; 0.99)	0.001	0.078	0.97 (0.90; 1.00)	0.0001	0.048	1.00 (0.99; 1.00)	0.00181	0.1803	0.974 (0.942;0.989)
MD	0.008	0.029	0.79 (0.22; 0.96)	0.031	0.005	0.60 (0.40; 0.92)	0.0001	0.020	0.86 (0.35; 0.98)	0.00373	0.09693	0.739 (0.458;0.888)

ICC: intraclass correlation coefficient, 95% CI: confidence interval, σ^2: variance.

Figures

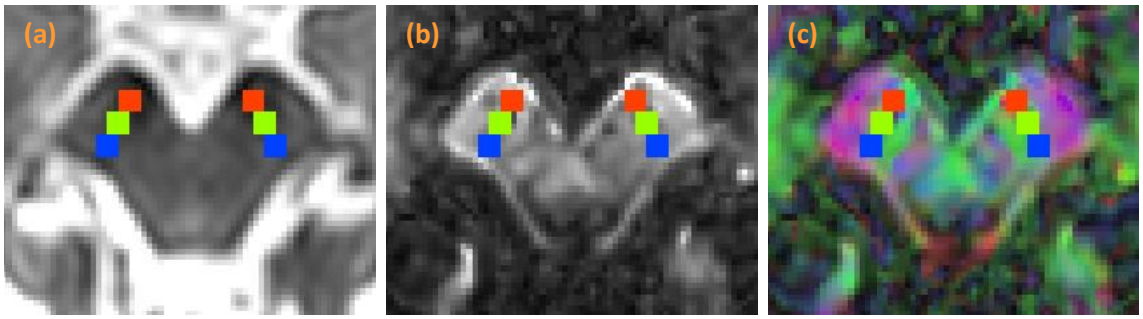

Fig 1. ROI manual tracing

Manual tracing of SN ROIs in the b0 image (a) correspondent FA (b) and color coded map (c).

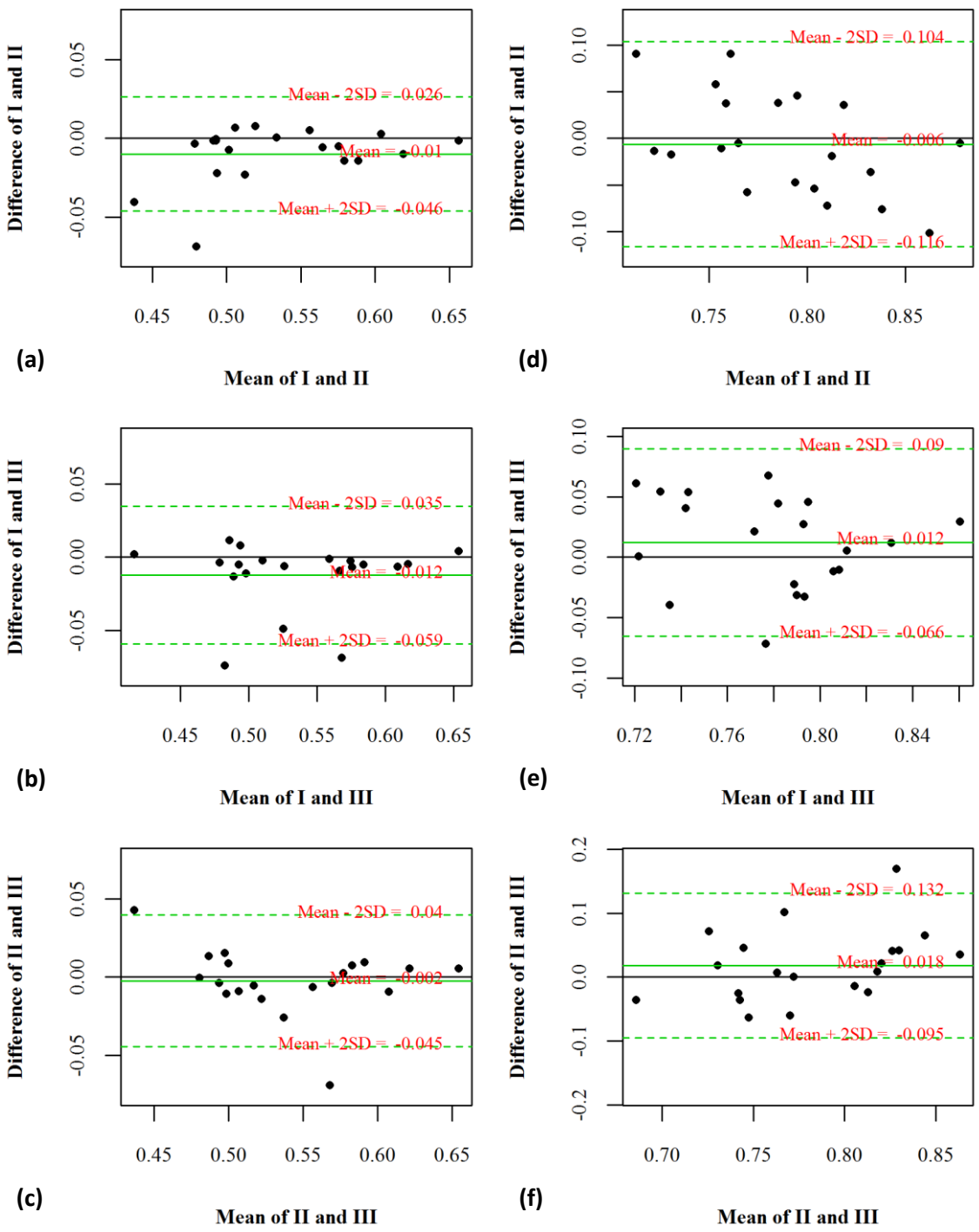

Fig. 2. Bland-Altman plot for SN FA values

Agreement systematic bias and proportional bias analysis of fractional anisotropy (FA) (a-c) and mean diffusivity (MD) (d-f) values between the three scans for the SN ROIs.

3. MR IMAGING FOR THE DIFFERENTIAL DIAGNOSIS OF PARKINSON'S DISEASE

The differential diagnosis of PD with Essential tremor (ET) and atypical parkinsonian syndromes (APS), including multiple-system atrophy (MSA), supra-nuclear palsy (PSP) and cortico-basal degeneration (CBD) can be challenging. So far, much of the interest on imaging approaches in this context has focused on nuclear medicine techniques with specific metabolites, in particular ^{123}I-ioflupano (DaTSCAN®), since they allowed an evaluation of dopaminergic function and the detection of nigro-striatal disfunction with high sensitivity and specificity for PD diagnosis (176). However the high cost, low availability and exposure to ionizing radiation (177) limit the clinical application of these methods that also have an overlap with normal subjects in PD early stages (178), in spite of the high accuracy values, and do not allow the distinction between PD and APS such as MSA or PSP (176).

MR imaging studies have an increasing relevance in the differential diagnosis of PD with APS and ET, through the analysis of morphological, functional and microstructural information in specific anatomic areas.

Essential tremor (ET) is one of the most prevalent neurological disorders and the most frequent cause of tremor (179). Clinically, ET shares important features with neurodegenerative disorders but the pathophysiology of the disease remains unknown (180). The differential diagnosis of ET from PD assumes a great importance not only in establishing the adequate therapy but also in defining prognosis. However, the clinical differentiation between these conditions can be challenging in the early stages of the disease (181,182) and so additional studies might significantly help to increase diagnostic accuracy.

A significant number of imaging studies have focused on ET, using morphological and functional information (183-185) trying to investigate specific disease changes that might help to understand the pathophysiological mechanisms of the disease and to differentiate ET from other tremor conditions.

A T2* relaxometry study in 3.0Tesla MR has shown an increased iron deposition in the globus pallidum, SN and right dentate nucleus of ET patients, raising new hypothesis as to the pathophysiology of this disease and the motor pathways involved in tremor genesis (186). Also DTI studies found specific disease microstructural pattern changes in ET that are different from other tremor conditions (187, 188).

These studies suggested that the SN might have pathological changes in ET patients, sharing some similarity with PD. Neuromelanin sensitive MR imaging in PD had found disease specific changes but the SN neuromelanin had not yet been studied in ET. So we evaluated the SN neuromelanin MR signal in ET patients, analyzing the possible detection of an imaging pattern that allowed the differential diagnosis with PD.

3.1. Substantia nigra neuromelanin-MR imaging differentiates Essential tremor from Parkinson's disease.

Reimão S, Pita Lobo P, Neutel D, Correia Guedes L, Coelho M, Rosa MM, Azevedo P, Ferreira J, Abreu D, Gonçalves N, Nunes RG, Campos J, Ferreira JJ.

Movement Disorders 2015

Mar 11. doi:10.1002/mds.26182

[Epub ahead of print]

Substantia nigra neuromelanin-MR imaging differentiates Essential tremor from Parkinson's disease

Sofia Reimão[1,4], Patrícia Pita Lobo[2,4,6], Dulce Neutel[2,4], Leonor C Guedes[2,4,6], Miguel Coelho[2,4], Mário M Rosa[2,4,5], Pedro Azevedo[3], Joana Ferreira[3], Daisy Abreu[4], Nilza Gonçalves[4], Rita G Nunes[3], Jorge Campos[1], Joaquim J Ferreira[4,2,5,6]

[1] Neurological Imaging Department, Hospital de Santa Maria - Centro Hospitalar Lisboa Norte, Portugal
[2] Neurology Department, Hospital de Santa Maria - Centro Hospitalar Lisboa Norte, Portugal
[3] Instituto de Biofísica e Engenharia Biomédica, Faculdade de Ciências, Universidade de Lisboa, Portugal
[4] Clinical Pharmacology Unit, Instituto de Medicina Molecular, Faculty of Medicine, University of Lisbon, Portugal
[5] Laboratory of Clinical Pharmacology and Therapeutics, Faculty of Medicine, University of Lisbon, Portugal
[6]CNS – Campus Neurológico Sénior, Torres Vedras, Portugal

Abstract

Background: Essential tremor (ET) is a very common movement disorder that has no diagnostic markers. The differentiation with Parkinson's disease (PD) can be clinically challenging in some cases, and there is a high rate of misdiagnosis. MRI studies have been able to identify neuromelanin changes in the *substantia nigra* of PD patients, but they have thus far not been investigated in ET. In this study, we aimed to characterize neuromelanin-MR signal changes in ET and evaluate its diagnostic accuracy in the differential diagnosis with PD.

Methods: The inclusion criteria were patients with ET and untreated "de novo" PD patients; in addition, age matched controls were enrolled. These were studied with a high-resolution T1-weighted MR imaging sequence at 3.0 Tesla to visualize neuromelanin. The primary outcomes were the area and width of the SN region with high signal.

Results: A total of 15 ET patients and 12 "de novo" PD patients were evaluated. The area and width of the T1 high-signal in the SN region were markedly decreased in the PD group compared with the ET and age-matched controls, and there was a greater decrease in the ventrolateral segment. The neuromelanin measures in the ET group although slightly lower were not significantly different from the healthy control group. We obtained a sensitivity of 66.7% and a specificity of 93.3% in discriminating ET from early stage PD.

Conclusions: Neuromelanin-sensitive MRI techniques can discriminate ET from early stage tremor-dominant PD and can be a useful clinical tool in the evaluation of tremor disorders.

1. Introduction

Essential tremor (ET) is a very common neurological disorder (189-192), that has an estimated prevalence of approximately 5% in the population over 65 years of age (179,193). ET is clinically characterized by a symmetric 4- to 8Hz action tremor that most frequently affects the hands and arms, but it can also involve the head (194). Typical ET cases can be easily diagnosed and distinguished from Parkinson's disease (PD), which is characterized by an asymmetrical 3- to 5-Hz resting tremor (181). However, the clinical differentiation between these conditions can be challenging, and there is a considerable overlap in the clinical features, particularly in the early stages of the disease (181,182). This differentiation is very important in defining prognosis and treatment decisions and in identifying patients for research, but a high rate of ET misdiagnosis has been described in several studies (195-198), emphasizing the need for additional diagnostic evaluation.

The etiology of ET is unknown, and its pathophysiology is still poorly understood. Several MRI studies have investigated the morphological and functional brain alterations in ET patients (187,199,200), and some pathological studies have recently shown evidence of structural brain changes in this disease that might be associated with neurodegeneration (201).

Recent imaging studies have reported changes in the SN of ET patients with an increased echogenicity in sonography studies (202,203) and MR T2*-relaxometry signal reduction (186), suggesting the involvement of the SN and nigrostriatal degeneration as in Parkinson's disease (PD).

PD is characterized by depigmentation of the *substantia nigra pars compacta* (SNpc) and of the *locus coeruleus* (LC), which is related to the loss of neuromelanin (35). Over the few last years, new MRI sequences have been able to detect a significant reduction in the SN neuromelanin signal in PD (61-63,132), and these changes have a high diagnostic sensitivity and specificity for PD diagnosis, even in the very early clinical stages.

Despite the identified SN changes in ET, the SN neuromelanin changes in ET have not previously been studied. In this study, we analyzed the neuromelanin MR signal pattern in ET and the accuracy of this imaging technique in the differential diagnosis with early stage PD. To the best of our knowledge, this is the first study of MR neuromelanin imaging in ET.

2. Patients and methods

2.1. Patients and control subjects

The study had a cross-sectional case-control design that included 37 subjects, 15 patients had ET, 12 patients had "de novo" PD, and 10 were control subjects. Patients were recruited from the Movement Disorders Unit of the University Hospital of Santa Maria-Lisbon. The PD patients were included at the time of clinical diagnosis if they were not on antiparkinson medications. All patients were diagnosed by a movement disorders specialist and fulfilled the ET criteria of the Movement Disorder Society on Tremor (204) or the PD UK Brain Bank criteria (19). The healthy control subjects were recruited from local hospital staff and relatives. Dementia, psychiatric illness or contraindications to an MRI were the exclusion criteria.

All examinations were performed with the understanding of and written consent from each subject, with approval from the local ethics committee, and in compliance with national legislation and the Declaration of Helsinki guidelines.

2.2. MRI protocol

2.2.1. Imaging protocol

All data were acquired using a 3.0 -Tesla Phillips scanner (Phillips Achieva®). The following neuromelanin-sensitive pulse sequence was used as previously described by Sasaki and colleagues (61): T1-weighted FSE: repetition time/effective echo time, 633/10 ms; echo train length, 3; number of slices, 20; slice thickness, 2.5 mm; intersection gaps, 0 mm; matrix size, 548 x 474; field of view, 220 x 190 mm^2 (pixel size: .40 x .40 mm^2); and acquisition time, 8 min. The sections were carefully set in the oblique axial plane perpendicular to the fourth ventricle floor, with coverage from the posterior commissure to the inferior border of the pons.

T1- and T2-weighted images of the entire brain were additionally obtained in all subjects and evaluated by an experienced neuroradiologist to exclude other pathological imaging findings, namely, changes in the parkinsonian index and other atypical parkinsonian syndrome changes as well as lesions in the LC and SN areas that could interfere with further assessment.

2.2.2. Imaging analysis

Images were transferred to a Linux workstation for analysis, and an edge preserving filter (122) was applied using Matlab (R2012a, The Math Works, Natick, MA, USA) to reduce the image noise. T1 high signal in the SN region was visible in 3 slices, and the middle slice corresponding to the greatest SN volume was selected (Fig 1 A-C). A rectangular region was then selected in this slice, and two symmetrical seed points were manually defined on the most medial part of the high-intensity area in the SN. A region growing algorithm (123) was used for segmentation starting from each seed point, and the area of interest (AOI) was automatically drawn. Pixels with a signal intensity within the interval $I_{seed} \pm 0.035 \times (I_{max}-I_{min})$ were labeled as belonging to the AOI, where I_{seed} is the intensity at the seed point, and I_{max} and I_{min} are the maximum and minimum signal intensities, respectively, within the rectangular mesencephalon ROI. The threshold used to delimit the AOI was chosen after a preliminary optimization study using healthy controls and PD patients (139) in which the threshold was varied using a batch process; the final value of 3.5% was selected since it provided a better visual fit to the anatomical area. The optimal threshold value depends on the contrast and signal-to-noise ratio of the input images, and so it should be adjusted for each specific set of acquisition conditions – imaging sequence, and coils used for signal reception. The area of interest (AOI) was automatically calculated (Fig 1D-F). As there were no significant differences regarding side for the SN area measurements, the median value was obtained from an average between the left and right neuromelanin area obtained for each subject.

Additional manual measures were performed in the same slice used for the automatic measurements. The high signal region was selected in this slice, and a line was defined following the maximal longitudinal length of the SN area. This line was divided into three equal segments defining the lateral, central and medial SN parts. One of the authors (R.S.), who was blinded to the subject information, performed manual measurements of the maximal width of the T1 high signal area perpendicular to the length line for the three SN parts, as shown in Fig 1G. Measurements were performed on both sides and as there were no significant differences between the left and the right side the averaged value was used.

9.3. Statistical analysis

The SN high signal area and width obtained for each group were compared using non-parametric analysis. Kruskal-Wallis tests, with pairwise comparisons in which the resulting *p*-values were corrected according to Bonferroni method, and Mann-Whitney U tests were used as appropriate. A *p*-value below 0.05 was considered significant. Receiver operation characteristics (ROC) curve analysis was conducted to assess the discrimination capacity of the measures, SN area and width, for ET and PD as well as PD patients and controls; additionally, the specificity and sensitivity values were obtained. Optimal cutoff points were assessed through a method that simultaneously maximized the sensitivity and specificity. The area under the curve (AUC) was also assessed. All statistical analysis was performed with R 2.15.2.

10. Results

The obtained MR imaging quality allowed for the clear identification of the high-signal area in the SN region in all subjects. The automated analysis and manual width measurements were possible on all acquired images. We analyzed 15 patients with ET, 12 patients with “de novo” PD, and 10 controls. The clinical characteristics of these subjects are shown in Table 1. The ET patients were older than the “de novo” PD patients and controls; no significant differences were observed in sex among the 3 groups (*p*-value = 0.925). ET patients had a median disease duration of 10 years (3-21 years). PD patients had a mild disease severity with H & Y of 2 and a mean UPDRS motor score of 29.08. Tremor of the hands was the presenting symptom in 11 of the 12 PD patients with only one patient presenting with an akinetic-rigid form. Symptoms at onset were predominantly unilateral with half of the patients presenting criteria for asymmetric disease on UPDRS part III (141).

Using an automated analysis of the SN high signal, we obtained a median area of 19.76 mm^2 for the “de novo” PD patient group, 25.77 mm^2 for the ET group, and 27.78 mm^2 for the controls. We found no significant differences between left and right SN areas (*p*-value = 0.630).

In the lateral part of the SN, the manually measured median width of the T1 high signal was 1.5 mm, 2.0 mm and 2.4 mm in the PD, ET and healthy control groups, respectively. In the central part, the median width was 2.5 mm, 3.2 mm and 3.3 mm in the PD, ET and

healthy control groups, respectively. In the medial segment, the median widths were 3.4 mm, 3.8 mm and 3.8 mm in the PD, ET and healthy control groups, respectively. If we considered all of the SN segments, the average width of the manually measured T1 high signal was 2.5 mm in the "de novo" PD patients, 3.2 mm in ET group and 3.2 mm in the healthy control group.

The measured area of the SN T1-high signal was only slightly reduced in the ET patients compared to controls with a *p*-value >0.05, but it was markedly decreased in the PD group compared with the ET and healthy control groups; the *p*-value was <0.001 for both comparisons (Fig 2).

In the ET group we identified 2 outliers whose SN area was above the superior level of the control group (Fig 2). To see how the outlying observations could influence the results we removed them and performed a sensitivity analysis. Excluding the outliers the SN neuromelanin median area in ET patients was 25.54 mm^2 and the group comparisons yielded similar results with a significant reduction in the neuromelanin SN high-signal area in PD patients compared with ET and controls (*p*-value <0.001) and no significant differences between the ET patients compared with controls (*p*-value = 0.909). The SN neuromelanin manual width measurements were reduced in the PD group compared with ET and controls with *p*-values of 0.002 and <0.001, respectively. The greatest reduction was evident at the lateral and central SN segments with *p*-values of <0.001 and =0.005, respectively (Fig 3). Two outliers were identified in the lateral SN segment (1 control and 1 ET patient) (Fig 3), with measured width close to zero. We reviewed these images and the lateral midbrain region had reduced image quality which might have influenced the visual identification of the T1 high signal area image and the manual measurement. We did not find any significant differences between the ET and control groups for the neuromelanin SN measurements (*p*-value = 0.261), using either method, although the median measurements of the ET group tended to be slightly lower than the controls (Fig 2 and 3).

The sensitivity and specificity of the SN high signal area for discriminating the ET patients from the PD patients were 66.7% and 93.3%, respectively, when the cut-off value for the area was set at 24.08 mm^2.

The sensitivity and specificity for discriminating the "de novo" PD group from the control group were 70.8% and 80%, respectively, with an area cut-off value of 24.08 mm^2 (Fig 4).

11. Discussion

In the present MRI study, we were able to detect significant differences in the neuromelanin SN pattern of ET compared with PD. In ET, the neuromelanin in the SN was not significantly reduced compared with the healthy control group, but the PD patients, even at the time of clinical diagnosis, exhibited a significant reduction in the SN T1-high signal, which was more pronounced laterally in accordance with the known pathological changes (141). Using different SN neuromelanin signal measurement methods, i.e., manual and semi-automated, we obtained similar findings for the T1-high signal area and width, enabling the differentiation of ET patients from the “de novo” PD group with very high sensitivity and specificity.

It is known from pathological studies that the neuronal loss in PD occurs asymmetrically and early in the course of PD or even in preclinical stages (9), and that it is more pronounced in the ventrolateral region of the SNpc with relative preservation of the dorsal region (14). We used manual width measurements additionally to the automated global area to study the pattern changes in the different segments of the SN T1 high signal region. In agreement with previous neuromelanin studies (61-63,125), our neuromelanin data reproduce the SN pathological findings in PD, suggesting SN neuromelanin neuronal depletion in patients with early PD that is absent in ET or healthy individuals. We were not able to find a significant asymmetry in the SN area nor a correlation with the clinically most affected side in our PD patients. This may be due to the small number of subjects in our samples that limits our power.

Considering the reported sonography changes of the SN in ET (202,203), our data show that, contrary to the findings in PD, the increased echogenicity of the SN in ET is not related to a reduced SN neuromelanin content. These sonography changes might only be related to the increased tissue iron content in ET, which has been recently documented in an MR quantitative study (186). Our results corroborate the hypothesis that iron deposition and neuromelanin loss might be separate processes that are related to different pathological processes and variable clinical manifestations, such as specific tremor characteristics. The correlation of neuromelanin and the iron content of the SN requires further investigation and the determination of the different disease pathological patterns that affect the SN in ET and PD and result in different clinical characteristics.

Although the clinical diagnosis of ET in typical cases requires no further diagnostic investigation, in the subset of patients with atypical signs and symptoms, particularly in the early disease stages, there can be a significant benefit from further diagnostic evaluation because the distinction with PD has important therapeutic and prognostic consequences. In this study, the obtained moderate sensitivity and high specificity for MRI neuromelanin studies are only slightly lower than those obtained in [^{123}I]- FP-CIT SPECT studies in discriminating ET from PD (134,137,198). This MRI technique is safe and widely available; as a result, it might have the potential to become an alternative to the more expensive nuclear medicine techniques that have additional risks (134) in the diagnostic evaluation of tremor disorders.

However, our study has several limitations, including the small number of patients in each group and the absence of pathological confirmation. The small sample size of our study groups limits the precision of the obtained estimates of sensitivity and specificity, and so further studies are needed to strengthen the performance characteristics of this imaging method in the distinction between PD and ET patients.

Another aspect is related to the disadvantages of the imaging technique, including the long acquisition time, the relatively low spatial resolution and the existence of in-plane signal inhomogeneity. Slice positioning and partial voluming may be confounding factors in surface-based measurements, which could potentially be improved by using a three-dimensional acquisition (127).

Additionally, the region-growing post-processing technique used in this study for the semi-automated measurement of areas requires the determination of seed points and normalization of signal intensity that could not be completely automated. Although the same criteria were followed for the placement of the seed points on each image, in the future the impact of varying their position on the estimated neuromelanin SN area should be investigated so as to determine the reproducibility of this method.

The total imaging analysis is relatively time consuming and requires the implementation of post-processing software that is not widely available. However, the manual analysis yields very similar results, and, although it is operator-dependent, it is very fast and widely available without the need for post-processing software. The within-subject and inter-rater reproducibility of MR neuromelanin measurements has not been fully established, and so the reproducibility of these parameters needs to be addressed in

further studies, especially concerning the manual analysis, in order to allow a wider implementation of this imaging technique.

Motion artifacts were not a problem in either the ET or PD groups, but these were early stage patients. Advanced-stage patients with exuberant tremor might have artifact problems that will require further adjustments.

Two outliers (1 control and 1 ET patient) had neuromelanin lateral SN widths close to zero which could be related to the poor image quality in the lateral midbrain region. A possible source of subject-dependent contrast variation is the effective B1 field which is determined by the electrical properties of the tissue (its conductivity and permittivity). In the future, the acquisition protocol should be further optimized, so as to improve image contrast and consistently enable good visualization of the SN.

The number of patients in our study did not allow statistical correlation with clinical severity or age group correction of the SN neuromelanin measurements. However a previous neuromelanin MR study with 80 PD patients found no correlation between age and neuromelanin SN volumes in PD patients or control subjects (63) and so it is not likely that age would be an influencing factor in our results, although it is something we can not completely exclude. In the same study the authors found an inverse correlation between neuromelanin-sensitive SN volume and the Hoehn and Yahr stage and disease duration in PD patients.

Our small sample does not allow PD patient's stratification in clinical sub-types for further analysis but almost all our PD patients had tremor as the presenting symptom. It is known that akinetic-rigid and tremor-dominant subtypes of PD have different neuropathological patterns (205), with greater SN neuronal loss in akinetic-rigid patients (with ventrolateral predominance) compared with tremor-dominant patients (with medial predominance) (206). We found a significantly different SN neuromelanin pattern in ET versus PD patients, in agreement with the known absence of pathomorphological SN changes in ET, but further studies are needed to specifically investigate the difference in neuromelanin SN MRI changes in PD clinical subtypes. The obtained sensitivity for PD patient's discrimination was lower than the specificity which might be intrinsically related to SN neuromelanin changes in PD. The current understanding of the relationship between the extent of dopamine cell loss and the clinical manifestations of PD remains unclear and previous dopaminergic brain imaging studies have reported that some PD patients with

mild symptoms have no evidence of dopaminergic dysfunction (178). Also the SN neuromelanin volume may not directly reflect the dopaminergic function since degenerated nigral cells might still contain neuromelanin granules (14), influencing MRI signal measurements.

5. Conclusion

MR neuromelanin-sensitive images were able to accurately distinguish ET from tremor-dominant PD patients even at the time of PD clinical diagnosis. We detected significant neuromelanin changes, in the SN of PD patients that are not present in ET, highlighting the different pathological processes in the SN of these two tremor conditions. MRI neuromelanin-sensitive techniques might become a useful diagnostic tool for the differentiation of ET from PD in very early clinical stages.

Table and Figure legends

Table 1: Demographics for Essential tremor, Parkinson's disease and control subjects

	ET	**PD**	**Controls**	***p*-value**
No. (female/male)	15 (8/7)	12 (7/5)	10 (4/6)	0.925
Age, years (mean±SD)	70.5 (±12.5)	63.2(± 11.9)	61.2(±7.3)	0.036
UPDRS-III motor score (mean±SD)	-	29.1(±14.2)	-	-

ET: Essential tremor; PD: Parkinson's disease; No: number; SD: standard deviation.

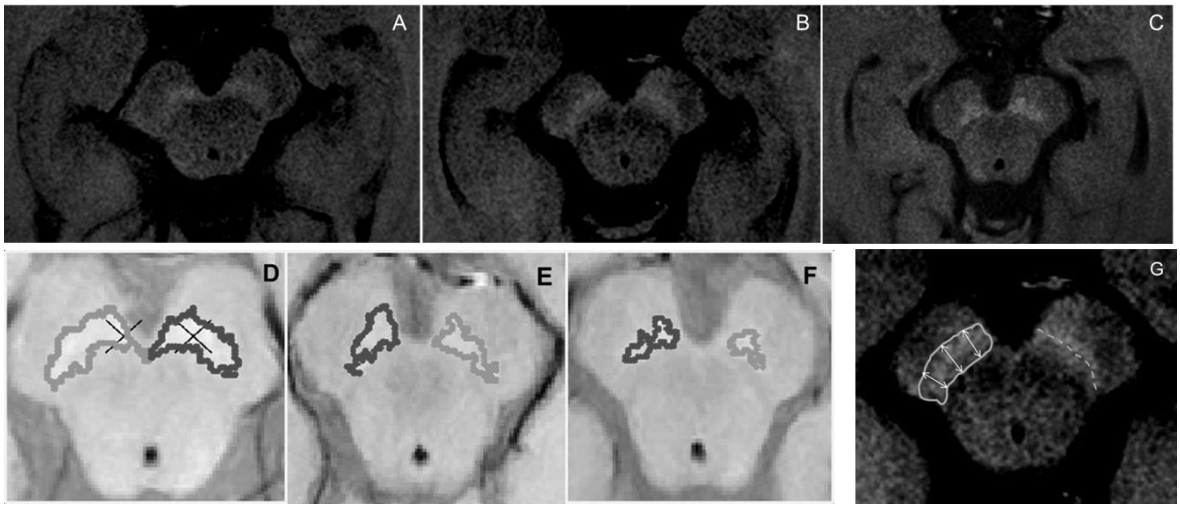

Fig. 1. SN neuromelanin-MRI of a control (A), an ET (B) and PD patients (C); segmented areas in the same groups: control (D), ET (E) and PD patients (F); the crosses in (D) represent the placement of the seed points in that specific subject; width measurement example (G) in an ET patient.

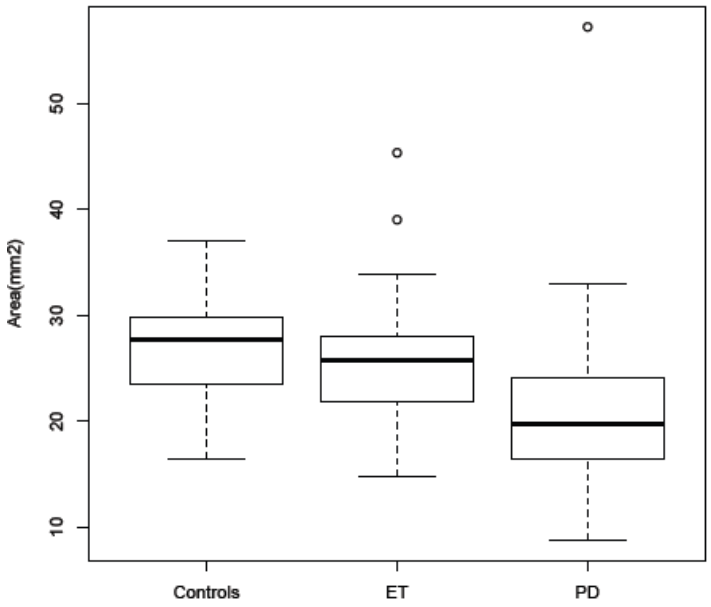

Fig. 2. Area of the SN high-intensity region on neuromelanin-sensitive MR images in patients with ET, "de novo" PD and controls; *p*-values, Mann-Whitney *U*-test.

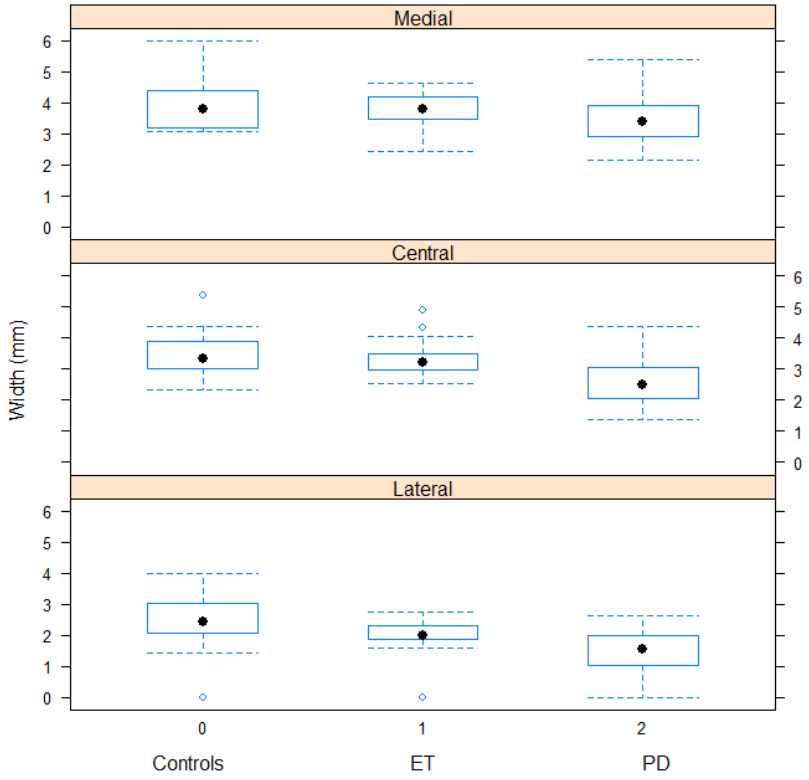

Fig. 3. Width of the SN high-intensity region on neuromelanin-sensitive MR images in patients with ET, "de novo" PD and healthy controls *p*-values, Mann-Whitney *U*-test.

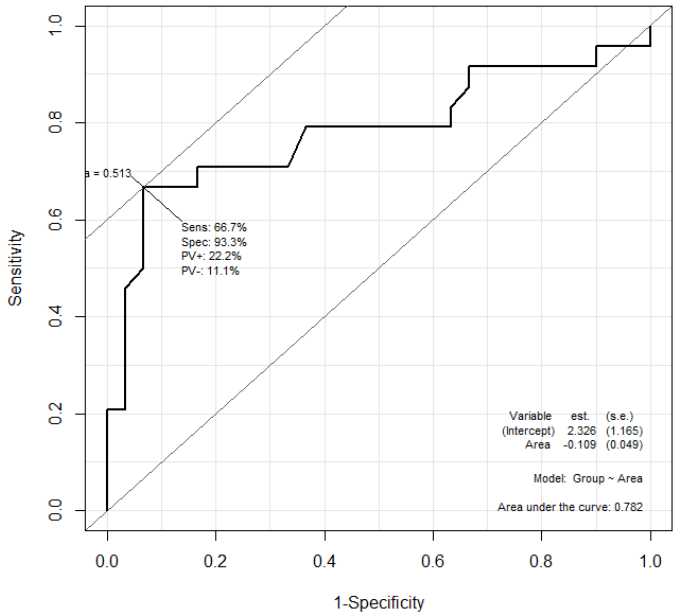

Fig. 4. ROC curve of the area for differentiating between ET and "de novo" PD patients.

DISCUSSION

PD diagnosis in early and even pre-motor stages is a particularly relevant topic, not only in view of the need of a precocious implementation of an adequate therapeutic plan but also in light of the possible development of disease modifying treatments.

For many years, neuroimaging studies in PD focused on the investigation of established disease, looking at specific disease alterations and trying to ascertain clinical correlations. However, even in very advanced disease stages, MR studies with conventional sequences were very discouraging, failing to depict disease changes, namely in the SN, that could influence the diagnosis or establish a correlation with disease progression (24).

The characteristic PD pathological changes, identified post-mortem in early and pre-clinical disease stages (9), were undetectable by neuroimaging studies *in vivo*. Particularly the characteristic depigmentation of the SN related to the loss of the pigment neuromelanin was undetectable by neuroimaging techniques. However, the development of advanced MR techniques in high field magnets opened new possibilities to study brain neurodegeneration. Finding valid imaging biomarkers has become an important field of research that might have a significant impact in clinical practice and even influence etiological and pathophysiological disease comprehension.

Our work had as a main objective the application of new MR imaging techniques to study the SN in PD, early in the disease course, mainly focusing on untreated patients at the time of clinical diagnosis. Early-stage PD, especially nonmedicated patients, were considered the best group to evaluate the impact of imaging methods in early disease identification and differential diagnosis. The imaging analysis sought a complementary multimodal evaluation to visualize the SN changes, with the neuromelanin sensitive sequences assuming a particular emphasis. Iron quantification and its interaction with neuromelanin and DTI microstructural changes were additional imaging parameters that allowed a complementary analysis of PD changes.

The performed MR imaging protocol was initially delineated and optimized to the PD population, focusing on some particular aspects that could interfere with image acquisition, especially movement artifacts from involuntary movements. The protocol was feasible and we find it easy to implement widely in a clinical setting with a high-field 3.0T machine. The developed imaging analysis tools, with easily usable interfaces, have

allowed an efficacious evaluation of the different studied parameters and may have a significant impact on the implementation of imaging analysis on the clinical practice.

The first line of our research focused on the **diagnosis of early-stage PD with MR imaging**. Neuromelanin sensitive MR imaging of early stage PD was initially evaluated with a semi-automated analysis to determine the area and length of the SN high signal area in early disease stages. The developed graphic post-processing user interface allowed a fast and easy visualization of the neuromelanin SN region and the extraction of measurements using a "region-growing" algorithm. Although not entirely automated, this analysis is very operator independent and widely usable. The imaging filters were additionally optimized for image analysis which allowed an improved reliability of the measurements.

Our study was innovative not only for analyzing the neuromelanin of PD patients but also for applying these imaging techniques to study "de novo" unmedicated patients with a post-processing imaging analysis not based on anatomical segmentation. This study allowed the detection of significant changes in the SN neuromelanin of PD patients compared with controls with a high sensitivity and specificity for the disease diagnosis. We were additionally able to reproduce *in vivo* the characteristic pathological disease pattern changes in the SN with a greater alteration in the ventrolateral SN and preservation of the dorsal segment (14).

In our analysis we did not find a significant difference in the neuromelanin measurements between "de novo" and 2 – 5 year disease patients. These data were in agreement with previous studies, not only MR neuromelanin analysis (125) but also transcranial sonography (126) in which the SN signal did not seem to change through the course of the disease.

Considering the clinical implementation of our results, easy and widely available imaging analysis without the need of a post-processing software was needed for current usage. So we compared quantitative methods with a simple visual analysis of the neuromelanin sensitive MR images in early stage PD patients to evaluate the feasibility and accuracy of these analyzing methods. The image visual inspection by experienced neuroradiologists had as good results as a quantitative width analysis of the SN neuromelanin area, which can favor a future implementation of this technique in the clinical practice.

As a whole, the neuromelanin sensitive MR imaging in early stage PD diagnosis was feasible using different imaging post-processing options, either quantitative or with simple visual inspection, using semi-automated or manually demarcated areas, and with all the approaches we were able to detect a significant reduction of the SN neuromelanin in PD patients compared to controls with a disease characteristic pattern that reproduces the known pathological changes (14). The different methodology used for imaging analysis in these studies further validates the findings.

The need for additional research of the neuromelanin correlation with disease progression and with the applied therapy aroused from our data analysis and motivated additional studies that are already in course.

The possible use of these imaging analysis in pre-clinical stages, namely in subjects with a familial history, asymptomatic genetic mutation carriers or in the investigation of disease risk factors such as exposure to pesticides, the relationship with the protective effect of tobacco smoke and the correlation of brain neuromelanin in melanoma patients are projects that we have already delineated and that we expect might contribute in the future to an additional understanding of the disease pathological processes.

All previously published MR neuromelanin studies referred as a significant limitation not being able to ascertain how the SN iron content in the SN influenced the neuromelanin-sensitive MR signal changes in PD (62,63). To investigate the correlation and the possible contribution of the iron content in the different segments of the SN to the neuromelanin signal changes in PD, we combined a specific neuromelanin-sensitive MR sequence with a iron quantification analysis using T2*-relaxometry at 3.0T to study early-stage PD patients.

We found very weak correlations of T2* values with neuromelanin width, positive for global and medial SN and negative for lateral and central segments. The SN neuromelanin width was markedly reduced in the “de novo” and 2-5 year PD groups compared with controls in all SN segments but no significant difference in T2* values was found between the groups.

Our data showed that iron content in the SN does not significantly influence neuromelanin signal changes in PD patients and is probably not a limiting factor in the evaluation of neuromelanin pattern changes. The identifiable reduction of neuromelanin

in the SN of early stage PD does not seem to be influenced by the local iron load, answering previous questions as to this would be a limitations in the interpretation of these imaging findings.

The evaluation of the iron brain content with MRI is a very important line of future research, with quantitative and qualitative analysis that needs to be reproducible across sites. The combined analysis of iron with other parameters namely diffusion tensor metrics may add new data to the comprehension of the multifaceted process of neurodegeneration in PD. The investigation of other brain areas other that the SN in terms of iron content may depict the global brain involvement by the disease, and we are already conducting studies to evaluate changes in the basal ganglia and motor cortex of PD patients. Additionally, the iron distribution patterns in other parkinsonian syndromes and ET, namely in the SN, basal ganglia and motor cortex may give an insight as to the differences in pathophysiology of the different syndromes. We have already developed a project to analyze quantitatively the differences between PD and ET in several brain areas.

MR DTI studies have recently focused on Parkinson's disease, looking at grey matter microstructural alterations in specific anatomical locations related to disease pathophysiology, especially the *substantia nigra* (93,153); the potential of this imaging technique to detect early neuropathological changes in PD made it an attractive tool emerging as a possible imaging diagnostic biomarker and a research tool for improving knowledge on the mechanisms of the disease. The evaluation at multiple time points with DTI may also become very useful in PD enabling the study of disease progression.

The reliability of DTI metrics has been previously studied (157,158), including in some movement disorders such as Huntington's disease (15,162) that share some imaging problems with PD, but these studies shown a widely variable estimate of the reliability of DTI measurements and so it was important to demonstrate the reproducibility of DTI measurements in PD patients if these were going to be used as a tool to accurately quantify microstructural changes and its progressive alterations.

Our study investigated the reliability of DTI measurements in the SN of early-stage PD patients and compared them with healthy controls, through within-scanner and test-

retest studies. We obtained high ICCs indicating a good level of reliability for all diffusion metrics (FA and MD) in the SN of both PD patients and control subjects.
The fact that SN DTI measurements are reliable and reproducible in PD patients validates it's usage in further studies, namely longitudinal evaluation, investigating small changes in this anatomical location.

The second line of our research focused on the **differential diagnosis of PD with ET with MR imaging**. The importance of a establishing a correct diagnosis at early disease stages is well recognized; compared to MR the currently used nuclear medicine techniques (134,137,198) are more expensive and have additional risks (134) which motivated our research in the MR diagnostic evaluation of tremor disorders.
We studied the SN neuromelanin MR imaging of ET patients, analyzing the high signal area and comparing it with PD patients and controls. In ET we found no identifiable change of the neuromelanin measurements compared to controls. Our data showed that contrary to PD patients, in ET the described sonography changes (202,203) are not related to a neuromelanin reduction but are probably associated with increased iron content, in agreement with a recent MR study that showed increased iron load in ET (186). So, our data seems to point to the hypothesis that iron deposition and neuromelanin loss might be separate processes related to distinct neuropathological processes and different clinical manifestations. This was the first study analyzing *in vivo* the neuromelanin in ET and our results have shown a high sensitivity and specificity of this imaging technique for the differential diagnosis with PD.

There are some overall limitations to our investigation that are common to the study design including the small sample size of our study groups and the absence of pathological confirmation of PD. However, all the subjects were evaluated by a Neurologist, specialist in movement disorders, and the established criteria for PD and ET diagnosis were fulfilled. The number of patients in our study groups also did not allow statistical correlation with clinical characteristics.
The acquisition protocol and the performed imaging analysis have additional limitations. The selected multi-modal imaging protocol has disadvantages intrinsic to the specific sequences and also related to a long acquisition time of the whole protocol; the total

imaging analysis is also relatively time consuming, the post-processing software used in these studies is not fully automated or widely available, which might preclude the full implementation of this imaging protocol on a daily basis. Our findings are specific to a high-field 3.0T MR scanner and are not directly applicable to 1.5T scanners, further limiting its application. Motion artifacts were not a problem in the studied groups, but these were early stage patients; some adjustments may have to be made when dealing with advanced-stage patients with exuberant tremor.

Further studies are needed to strengthen the performance characteristics of this imaging method for PD diagnosis and in the distinction between PD and ET patients, extending these findings even to lower field magnets, analyzing the correlation of the different parameters with clinical characteristics and studying disease progression.

Looking at the global work developed in this dissertation two developed domains were especially relevant to allow the concretization of the achieved results: the establishment of a collaborative research network and the implementation of a study group devoted to this area of investigation. Research networks are critically important tools for research concretization in the field of neurodegenerative diseases, namely PD, that share multi-disciplinary interactions; these are vital to the comprehension of the disease and to the development of the most adequate care of individual patients. The implementation of an effective study group that aggregates professionals from different areas, namely neurologists, neuroradiologists and physicists was the basis support platform to support the long term research needed to achieve meaningful results.

At the beginning of this work, two major research and development paths were defined: diagnosis of PD at early disease stages and differential diagnosis with ET with neuroimaging MR techniques. During the development and concretization of the different studies a multi-modal MR protocol was defined and optimized with a particular emphasis in the *in vivo* visualization of neuromelanin and this was found to have a significant impact in the diagnosis of early-stage PD and its differential diagnosis with ET. These findings opened a path for ongoing and future research that can change the neuroimaging investigation of PD at early disease stages and support new perspectives focused on the design and improvement of imaging tools to support decision making at a crucial stage of disease management.

The recognizable complexity of neurodegenerative processes in PD and its systemic involvement highlights the importance of obtaining data from a combination of neuroimaging evaluation tools, looking at different processes. A multi-modal MR evaluation may help to explore new questions related to disease pathophysiology and the interaction of different concurrent processes, namely concerning neuromelanin and iron, with a possible impact in future therapies.

Future lines of research soon emerged from are work, some of which are already being pursued, with particular emphasis on the neuromelanin sensitive-MR imaging, focusing on technical upgrading and validation issues, imaging analysis optimization, and a posterior extension to the evaluation of other PD groups particularly pre-manifest genetic PD mutation carriers and melanoma patients; the study of therapeutical effects and disease progression with clinical correlation using the same imaging protocol is already ongoing. We highlight that the use of standardized MR protocols may allow between sites comparisons and the definition of guidelines to patients management and this may allow future evaluation of therapeutical effects and aid the definition of clinical trials.

The developed imaging protocol is feasible and widely implementable without the need of sophisticated post processing tools or time consuming approaches.

The change of perspective concerning neuroimaging in PD, evolving from a simple exclusion of secondary causes to a true investigation of disease mechanisms and emergence of biomarkers with impact in disease diagnosis needs to be pursued and improved in order to make an impact in clinical practice and patient's management.

CONCLUSION

The present dissertation is the culminate result of an investigation project developed using MR imaging to study the SN in PD at early disease stages. The conducted work has allowed the implementation of a new imaging approach to study PD and the construction of a multi-disciplinary team focused on this area of research. It was possible to develop efficacious tools, of easy clinical application, with high sensitivity and specificity for PD diagnosis, even at the time of clinical diagnosis, which might significantly change the indications of MR imaging methods for the study of PD.

Our studies with neuromelanin sensitive MR imaging have shown a high sensitivity and specificity of these imaging methods for PD diagnosis and an apparent stability of this pigment with disease progression. This new imaging technique at 3.0T has also allowed the differential diagnosis with ET patients that were found to have no significant SN neuromelanin changes, with accuracy similar to the nuclear medicine methods. These findings may significantly impact the evaluation of tremor disorders.

The comprehension of the interaction of neuromelanin and iron has shown that the iron content in the SN of PD patients does not significantly influence the neuromelanin signal in this topography, strengthening the interpretation of neuromelanin-sensitive imaging and motivating the investigation of possible separate pathways of neurodegeneration in PD.

The reliability of DTI metrics in the SN of PD patient's, strengthens the future usage of these parameters to detect small microstructural changes in this area. The reproducibility of DTI metrics at the SN validate the usage of these imaging parameters in longitudinal evaluation, since the within-subject variability of this imaging technique is low.

Looking at the global work presented in this dissertation the developed studies were pioneer in PD imaging field and have set the grounds for a different approach to PD neuro-imaging investigation. The group interactions that were built opened new possibilities and are the basis for a long term path that we hope may bring a contribution to the imaging study of movement disorders. The developed multi-modal imaging protocol, the graphic user interfaces and the imaging-clinical cooperation, can make a difference when looking at PD diagnosis and differential diagnosis and possibly open new possibilities for future research that answer new questions and pursues lines of investigation, with a possible impact in disease management and comprehension.

REFERENCES

1. Twelves D, Perkins KS, Counsell C. Systematic review of incidence studies of Parkinson's disease. Mov Disord 2003;18:19–31.

2. Abdullah R, Basak I, Patil KS, et al. Parkinson's disease and age: the obvious but largely unexplored link. Exp Gerontol 2014 Sep 26. pii: S0531-5565(14)00271-X [Epub ahead of print].

3. Parkinson J. An essay on the shaking palsy. London: Whittingham & Rowland, 1817.

4. Calne DB. Parkinson's disease is not one disease. Parkinsonism Rel Dis 2000;17:3-7.

5. Lang AE, Lozano AM. Parkinson's disease. First of two parts. N Engl J Med 1998;339:1044–1053.

6. Lang AE, Lozano AM. Parkinson's disease. Second of two parts. N Engl J Med 1998;339:1130–1143

7. Chaudhuri, KR, Schapira. Non-motor symptoms of Parkinson's disease: dopaminergic pathophysiology and treatment. Lancet Neurol 2009;8(5):464-474.

8. Merello M. Non-motor disorders in Parkinson's disease. Rev Neurol 2008;47(5):261-270.

9. Braak H, Del Tredici K, Rub U, de Vos RA, Jansen Steur EN, Braak E. Staging of brain pathology related to sporadic Parkinson's disease. Neurobiol Aging. 2003;24:197–211.

10. Spillantini M, Schmidt ML, Lee VM et al. α-Synuclein in Lewy bodies. Nature 1997;388:839–840.

11. Mann DM, Yates PO. Pathological basis for neurotransmitter changes in Parkinson's disease. Neuropathol Appl Neurobiol 1983; 9: 3-19.

12. Damier P, Hirsch EC, Agid Y, Graybiel AM. The substantia nigra of the human brain. II. Patterns of loss of dopamine-containing neurons in Parkinson's disease. Brain. 1999;122:1437–1448.

13. Gibb WR, Lees AJ. Anatomy, pigmentation, ventral and dorsal subpopulations of the substantia nigra, and differential cell death in Parkinson's disease. J Neurol Neurosurg Psychiatry. 1991;54:388–396.

14. Fearnley JM, Lees AJ. Ageing and Parkinson's disease: substantia nigra regional selectivity. Brain. 1991;114:2283–2301.

15. Kish SJ, Shannak K, Hornykiewicz O. Uneven pattern of dopamine loss in the striatum of patients with idiopathic Parkinson's disease. Pathophysiologic and clinical implications. N Engl J Med. 1988; 318:876–880.

16. Koller WC. When does Parkinson's disease begin? Neurology 1992;42(Suppl 4):27–31.

17. Mackenzie I. The pathology of Parkinson's disease. BCMJ 2001;43(3):142-147.

18. Litvan I, Bhatia KP, Burn DJ, et al. Movement Disorders Society Scientific Issues Committee report: SIC Task Force appraisal of clinical diagnostic criteria for parkinsonian disorders. Mov Disord 2003;18:467–486.

19. Huges AJ, Daniel SE, Kilford L, Lees AJ. Accuracy of clinical diagnosis of idiopathic Parkinson's disease: a clinic-pathological study of 100 cases. J Neurol Neurosurg Psychiatry 1992; 55: 181-184.

20. Michell AW, Lewis SJ, Foltynie T, Barker RA. Biomarkers and Parkinson's disease. Brain 2004;127:1693–1705.

21. Hughes AJ, Daniel SE, Ben-Shlomo Y, Lees AJ. The accuracy of diagnosis of parkinsonian syndromes in a specialist movement disorder service. Brain 2002;125:861–870.

22. Marshall VL, Reininger CB, Marquardt M, et al. Parkinson's disease is overdiagnosed clinically at baseline in diagnostically uncertain cases: a 3-year European multicenter study with repeat [123I]FP-CIT SPECT. Mov Disord 2009;24(4):500-508.

23. Cochrane C, Ebmeier K. Diffusion tensor imaging in parkinsonian syndromes. A systematic review and meta-analysis. Neurology 2013;80:857-864.

24. Oikawa H, Sasaki M, Tamakawa Y, Ehara S, Tohyama K. The substantia nigra in Parkinson disease: proton density-weighted spin-echo and fast short inversion time inversion-recovery MR findings. AJNR Am J Neuroradiol 2002;23:1747–1756.

25. Hirsch WL, Kemp SS, Martinez AJ et al. Anatomy of the brainstem: correlation of in vitro MR images with histologic sections. AJNR Am J Neuroradiol 1989;10:923-928.

26. Hutchinson M, Raff U, Lebedev S. MRI correlates of pathology in parkinsonism: segmented inversion recovery ratio imaging (SIRRIM). Neuroimage 2003;20:1899–1902.

27. Minati L, Grisoli M, Carella F, De Simone T, Bruzzone MG, Savoiardo M. Imaging degeneration of the substantia nigra in Parkinson disease with inversion-recovery MR imaging. AJNR Am J Neuroradiol 2007;28:309–313.

28. Helms G, Draganski B, Frackowiak R, Ashburner J, Weiskopf N. Improved segmentation of deep brain grey matter structures using magnetization transfer (MT) parameter maps. Neuroimage 2009;47:194–198.

29. Seppi K, Poewe W. Brain magnetic resonance imaging techniques in the diagnosis of parkinsonian syndromes. Neuroimaging Clin N Am 2010;20:29–55.

30. Seppi K, Schocke MF. An update on conventional and advanced magnetic resonance imaging techniques in the differential diagnosis of neurodegenerative parkinsonism. Curr Opin Neurol 2005;18:370–375.

31. O'Neill J, Schuff N, Marks WJ,Jr.Feiwell R, Aminoff MJ, Weiner MW. Quantitative 1H magnetic resonance spectroscopy and MRI of Parkinson's disease. Mov Disord 2002;17:917–927.

32. Helmich RC, Janssen MJ, Oyen WJ, Bloem BR, Toni I. Pallidal dysfunction drives a cerebellothalamic circuit into Parkinson tremor. Ann Neurol 2011;69:269–281.

33. Huang C, Dyke J, Pan H, et al. Assessing network activity in Parkinson's disease with arterial spin labeling MRI. NeuroImage 2007;36:S111.

34. Zecca L, Zucca FA, Wilms H, Sulzer D. Neuromelanin of the substantia nigra: a neuronal black hole with protective and toxic characteristics. Trends Neurosci. 2003;26:578–580.

35. Double KL, Gerlach M, Schünemann V, *et al*. Iron-binding characteristics of neuromelanin of the human substantia nigra. Biochem Pharmacol 2003; 66: 489-494.

36. Zhang W, Philips K, Wielgus A et al. Neuromelanin activates microglia and induces degeneration of dopaminergic neurons: implications for progression of Parkinson's disease. Neurotox Res 2011; 19(1)**:**63–72.

37. Liu R, Gao X, Lu Y, Chen H. Meta-analysis of the relationship between Parkinson disease and melanoma. Neurology 2011; 76: 2002–2009.

38. Bertoni JM, Arlette JP, Fernandez HH, Fitzer-Attas C, Frei K, et al. Increased melanoma risk in Parkinson disease: a prospective clinicopathological study. Arch Neurol 2010; 67: 347–352.

39. Ferreira JJ, Neutel D, Mestre T, Coelho M, Rosa MM, et al. Skin cancer and Parkinson's disease. Mov Disord 2010; 25: 139–148.

40. Gao X, Simon KC, Han J, Schwarzschild MA, Ascherio A. Family history of melanoma and Parkinson disease risk. Neurology 2009; 73: 1286–1291.

41. Driver JA, Logroscino G, Buring JE, Gaziano JM, Kurth T. A prospective cohort study of cancer incidence following the diagnosis of Parkinson's disease. Cancer Epidemiol Biomarkers 2007; Prev 16: 1260–1265.

42. Olsen JH, Friis S, Frederiksen K. Malignant melanoma and other types of cancer preceding Parkinson disease. Epidemiology 2006;17:582–587.

43. Wright WA, Evanoff BA, Lian M, et al. Geographic and ethnic variation in Parkinson disease: a population-based study of US Medicare beneficiaries. Neuroepidemiology 2010; 34: 143–151.

44. Dahodwala N, Siderowf A, Xie M, Noll E, Stern M, et al. Racial differences in the diagnosis of Parkinson's disease. Mov Disord 2009;24: 1200–1205.

45. Elbaz A, Moisan F. Update in the epidemiology of Parkinson's disease. Curr Opin Neurol 2008;21: 454–460.

46. Dwyer T, Blizzard L, Ashbolt R, Plumb J, Berwick M, et al. Cutaneous melanin density measured by spectrophotometry and risk of malignant melanoma, basal cell carcinoma and squamous cell carcinoma of the skin. Am J Epidemiol 2002;155: 614–621.

47. Aitken JF, Elwood JM, Lowe JB, Firman DW, Balanda KP, et al. A randomised trial of population screening for melanoma. J Med Screen 2002; 9: 33–37.

48. Wirdefeldt K, Gatz M, Pawitan Y, Pedersen NL. Risk and protective factors for Parkinson's disease. A study in Swedish twins. Ann. Neurol 2005; 57:27–33.

49. Quik M. Smoking, nicotine and Parkinson's disease. Trends Neurosci 2004;27:561–568.

50. De Palma G, Dick FD, Calzetti S, et al. Geoparkinson Study Group. A case control study of Parkinson's disease and tobacco use: gene-tobacco interactions. Mov Disord 2010;25:912–19.

51. Yerger VB, Malone RE. Melanin and nicotine: a review of the literature. Nicotine Tob Res 2006;8:487–98.

52. Ikemura M, Saito Y, Sengoku R, Sakiyama Y, Hatsuta H, et al. Lewy body pathology involves cutaneous nerves. J Neuropathol Exp Neurol 2008; 67: 945–953.

53. Matsuo Y, Kamitani T. Parkinson's disease-related protein, alpha-Syn, in malignant melanoma. PLoS One 2010; 5: 10481.

54. Peng X, Tehranian R, Dietrich P, Stefanis L, Perez RG. Alpha-Syn activation of protein phosphatase 2A reduces tyrosine hydroxylase phosphorylation in dopaminergic cells. J Cell Sci 2005;118(Pt 15): 3523–3530.

55. Ando H, Kondoh H, Ichihashi M, Hearing VJ. Approaches to identify inhibitors of melanin biosynthesis via the quality control of tyrosinase. J Invest Dermatol 2007; 127: 751–761.

56. Pan T, Zhu J, Hwu W, Jankovic J. The role of alpha-synuclein in melanin synthesis in melanoma and dopaminergic neuronal cells. PloS One 2012;7(9), e45183.

57. Pan T, Xinqun L, Jankovic J. The association between Parkinson's disease and melanoma. International Journal of Cancer 2011;128:2251-2260.

58. Tessari I, Bisaglia M, Valle F, Samori B, Bergantino E, et al. The reaction of alpha-Syn with tyrosinase: possible implications for Parkinson disease. J Biol Chem 2008; 283: 16808–16817.

59. Liu D, Jin L, Wang H, Zhao H, Zhao C, et al. Silencing alpha-Syn gene expression enhances tyrosine hydroxylase activity in MN9D cells. Neurochem Res 2008; 33: 1401–1409.

60. Zhang X, Monroe ME, Chen B, et al. Endogenous 3,4-dihydroxyphenylalanine and dopaquinone modifications on protein tyrosine: links to mitochondrially derived oxidative stress via hydroxyl radical. Mol Cell Proteomics 2010;9:1199–208.

61. Sasaki M, Shibata E, Tohyama K, *et al*. Neuromelanin magnetic resonance imaging of locus coeruleus and substantia nigra in Parkinson's disease. Neuroreport 2006; 17: 1215-1218.

62. Sasaki M, Shibata E, Kudo K, Tohyama K. Neuromelanin sensitive MRI. Clin Neuroradiol 2008; 18: 147-153.

63. Kashihara K, Shinya T, Higaki F. Neuromelanin magnetic resonance imaging of nigral volume loss in patients with Parkinson's disease. J Clin Neurosci 2011; 18: 1093-1096.

64. Martin W. Magnetic Resonance Imaging in Movement Disorders. Cambridge University Press 2013; p.14

65. Zecca L, Shima T, Stroppolo A, et al. Interaction of neuromelanin and iron in substantia nigra and other areas of human brain. Neuroscience 1996; 73:407-415.

66. Gerlach M, Double KL, Ben-Shachar D et al. Neuromelanin and its interaction with iron as a potential risk factor for dopaminergic neurodegeneration underlying Parkinson's disease. Neurotox Res 2003;5:35-43.

67. Schenck JF, Zimmerman EA. High-field magnetic resonance imaging of brain iron: birth of a biomarker? NMR Biomed 2004;17:433-445.

68. Haacke EM, Cheng NY, House MJ et al. Imaging iron stores in the brain using magnetic resonance imaging. Magn Reson Imaging 2005;23:1-25.

69. Dexter DT, Wells FR, Lee AJ et al. Increased nigral iron content and alterations in other metal ions occurring in brain in Parkison's disease. J Neurochem 1989;52:1830-1836.

70. Sofic E, Riederer P, Heinsen H et al. Increased iron (III) and total iron content in post mortem substantia nigraof parkinsonian brain. J Neural Transm 1988;74:199-205.

71. Good PF, Olanow CW, Perl DP. Neuromelanin-containing neurons of the substantia nigra accumulate iron and aluminum in Parkinson's disease: a LAMMA study. Brain Res 1992;593:343-364.

72. Castellani RJ, Siedlak SL, Perry G, Smith MA. Sequestration of iron by Lewy bodies in Parkinson's disease. Acta Neuropathol 2000;100:111-114.

73. Griffiths PD, Dobson BR, Jones GR, Clarke DT. Iron in the basal ganglia in Parkinson's disease: an in vivo study using extended X-ray absortion fine structure and cryo-electron microscopy. Brain 1999;122:667-673.

74. Schenck JF. Magnetic resonance imaging of brain iron. J Neurol Sci 2003;207:99-102.

75. Chen JC, Hardy PA, Kucharczyk W, et al. MR of human postmortem brain tissue: correlative study between T2 and assays of iron and ferritin in Parkinson and Huntington disease. AJNR Am J Neuroradiol 1993;14:275–281.

76. Benarroch EE. Brain iron homeostasis and neurodegenerative disease. Neurology 2009;72:1436–40.

77. Zecca L, Youdim MB, Riederer P, Connor JR, Crichton RR. Iron, brain ageing and neurodegenerative disorders. Nat Rev Neurosci. 2004;5:863–73.

78. Langkammer C, Krebs N, Goessler W et al. Quantitative MR imaging of brain iron: a postmortem validation study. *Radiology* 2010;257:455-62.

79. Haacke EM, Mittal S, Wu Z, Neelavalli J, Cheng Y-CN. Susceptibility-weighted imaging: technical aspects and clinical applications, Part 1. AJNR Am J Neuroradiol 2009;30:19–30.

80. Martin W, Wieler M,Gee M. Midbrain iron content in early Parkinson disease: a potential biomarker of disease status. Neurology 2008;70:1411-1417.

81. Martin W. Quantitative estimation of regional brain iron magnetic resonance imaging. Parkinsonism Relat Disord 2009;15(Suppl3):S215-8.

82. Lotfipour AK, Wharton S, Schwarz ST, et al. High resolution magnetic susceptibility mapping of the substantia nigra in Parkinson's disease. J Magn Reson Imaging 2012;35:48–55.

83. Wang Y, Butros SR, Shuai X, et al. Different iron-deposition patterns of multiple system atrophy with predominant parkinsonism and idiopathic Parkinson's disease demonstrated by phase-corrected susceptibility-weighted imaging. AJNR Am J Neuroradiol 2012;33(2):266-73.

84. Dusek P, Jankovic J, Le W. Iron dysregulation in movement disorders. Neurobiol Dis 2012; 46: 1–18.

85. Zecca L, Tampellini D, Gatti A, et al. The neuromelanin of human substantia nigra and its interact with metals. J Neural Transm 2002; 109: 663–672.

86. Enochs WS, Sarna T, Zecca L, Riley PA, Swartz HM. The roles of neuromelanin, binding of metal ions, and oxidative cytotoxicity in the pathogenesis of Parkinson's disease: an hypothesis. J Neural Transm Park Dis 1994; Dement Sect 7: 83–100.

87. Stepien K, Dzierzega-Lecznar A, Tam I. The role of neuromelanin in Parkinson's disease–new concepts. Wiad Lek 2007; 60: 563–569.

88. Fasano M, Bergamasco B, Lopiano L. Modifications of the ironneuromelamin system in Parkinson's disease. J Neurochem 2006; 96: 909–916.

89. Zecca L, Zucca FA, Albertini A, Rizzio E, Fariello RG. A proposed dual role of neuromelanin in the pathogenesis of Parkinson's disease. Neurology 2006; 67(7 Suppl 2): S8–11.

90. Le Bihan D, Mangin J, Poupon C, et al. Diffusion tensor imaging concepts and applications. J Magn Reson Imaging 2001;13:534-46

91. Le Bihan D, Breton E, Lallemand D, et al. MR imaging of intravoxel incoherent motions: application to diffusion and perfusion in neurologic disorders. Radiology 1986;161:401–407.

92. Boska MD, Hasan KM, Kibuule D, et al. Quantitative diffusion tensor imaging detects dopaminergic neuronal degeneration in a murine model of Parkinson's disease. Neurobiol Dis 2007;26:590–596.

93. Vaillancourt DE, Spraker MB, Prodoehl J, et al. High-resolution diffusion tensor imaging in the substantia nigra of de novo Parkinson disease. Neurology 2009;72:1378–1384.

94. Yoshikawa K, Nakata Y, Yamada K, Nakagawa M. Early pathological changes in the parkinsonian brain demonstrated by diffusion tensor MRI. J Neurol Neurosurg Psychiatry 2004;75:481–484.

95. Du G, Lewis MM, Sterling NW, et al. Microstructural changes in the substantia nigra of asymptomatic agricultural workers. Neurotoxicol Teratol 2014;41:60-64.

96. Rolheiser T, Fulton H, Good K, et al. Diffusion tensor imaging and olfactory identification testing in early-stage Parkinson's disease. J Neurol 2011;258(7):1254-60.

97. Chan I, Rumpel H, Yap K, e tal. Case control study of diffusion tensor imaging in Parkinson's disease. J Neurol Neurosurg Psychiatry 2007;78:1383-1386.

98. Kendi A, Lehericy S, Luciana M, et al. Altered diffusion in the frontal lobe in Parkinson's disease. AJNR Am J Neuroradiol 2008;29:501-05.

99. Gattellaro G, Minati L, Grisoli M, et al. White matter involvement in idiopathic Parkinson Disease: a diffusion tensor imaging study. AJNR Am J Neuroradiol 2009;30:1222-26.

100. Menke RA, Jbabdi S, Miller KL, Matthews PM, Zarei M. Connectivity-based segmentation of the substantia nigra in human and its implications in Parkinson's disease. Neuroimage 2010;52:1175–1180.

101. Salamon N, Sicotte N, Drain A et al. White matter fiber tractography and color mapping of the normal human cerebellum with diffusion tensor imaging. Journal of Neuroradiology 2007;34:115-128.

102. Press GA, Murakami J, Courchesne E et al. The cerebellum: Anatomic-MR correlation in the coronal plane. AJNR Am J Neuroradiol 1990;11(1):41-50.

103. Schocke MF, Seppi K, Esterhammer R et al. Trace of diffusion tensor differentiates the Parkinson variant of multiple system atrophy and Parkinson's disease. Neuroimage 2004; 21:1443–1451.

104. Schrag A, Kingsley D, Phatouros C et al. Clinical usefulness of magnetic resonance imaging in multiple system atrophy. J Neurol Neurosurg Psychiatry 1998;65:65–71.

105. Nilsson C, Markenroth Bloch L, Brockstedt S et al, Tracking the neurodegeneration of parkinsonian disorders – a pilot study. Neuroradiology 2007; 49:111-119.

106. Kitamura K, Nakayama K, Kosaka et al. Diffusion tensor imaging of the cortico-ponto-cerebellar pathway in patients with adult-onset ataxic neurodegenerative disease. Neuroradiology 2008;50:285-292.

107. Ito M, Watanabe H, Kawai Y et al. Usefulness of combined fractional anisotropy and apparent diffusion coefficient values for detection of involvement in multiple system atrophy. J Neurol Neurosurg Psychiatry 2007;78:722-728.

108. Quattrone A, Nicoletti G, Messina D et al. MR imaging index for differentiation of progressive supranuclear palsy from Parkinson Disease and the Parkinson Variant of Multiple System atrophy. Radiology 2008;214-221.

109. Mandelli ML, De Simone T, Minati L et al. Diffusion tensor imaging of Spinocerebellar ataxias types 1 and 2. AJNR Am J Neuroradiol 2007;28:1996-2000.

110. Yoon B, Kim JS, Lee KS et al. Early pathological changes in the cerebellum of patients with pure cerebellar syndrome demonstrated by diffusion-tensor imaging. European Neurology 2006;56:166-171.

111. Yekhlef F, Ballan G, Macia F et al. Routine MRI for the differential diagnosis of Parkinson's disease, MSA, PSP, and CBD. J Neural Transm 2003;110:151–169.

112. Salamon N, Sicotte N Alger J et al. Analysis of the brain-stem white-matter tracts with diffusion tensor imaging. Neuroradiology 2005;47:895–902.

113. Nicoletti G, Lodi R, Condino F, et al. Apparent diffusion coefficient measurements of the middle cerebellar peduncle differentiate the Parkinson variant of MSA from Parkinson's disease and progressive supranuclear palsy. Brain 2006;129:2679-2687.

114. Oba H, Yagishita A, Terada H, et al. New and reliable MRI diagnosis for progressive supranuclear palsy. Neurology 2005;64: 2050-2055.

115. Bergeron C, Pollanen MS, Weyer L, Black SE, Lang AE. Unusual clinical presentations of cortical-basal ganglionic degeneration. Ann Neurol 1996;40:893–900.

116. Schneider JA, Watts RL, Gearing M et al. Corticobasal degeneration: neuropathologic and clinical heterogeneity. Neurology 1997;48:959–969.

117. Soliveri P, Monza D, Paridi D et al. Cognitive and magnetic resonance imaging aspects of corticobasal degeneration and progressive supranuclear palsy. Neurology 1999;53:502.

118. Della Nave R, Foresti S, Tessa C et al. ADC mapping of neurodegeneration in the brainstem and cerebellum of patients with progressive ataxias. Neuroimage 2004;22:698-705.

119. Stieltjes B, Kaufmann WE, van Zijl PC et al. Diffusion tensor imaging and axonal tracking in the human brainstem. Neuroimage 2001;14:723–735.

120. DaSilva AF, Tuch DS, Wiegell MR, Hadjikhani N. A primer on diffusion tensor imaging of anatomical substructures. Neurosurg Focus 2003;15:1–4.

121. Péran P, Cherubini A, Assogna F et al. Magnetic resonance imaging markers of Parkinson's disease nigrostriatal signature. Brain 2010;133:3423–3433.

122. Nikolaou N, Papamarkos N. Color Reduction for Complex Document Images. International Journal of Imaging Systems and Technology 2009; 19(1):14-26.

123. Sun X, Zhang H, Duan H. 3D Computerized Segmentation of Lung Volume with Computed Tomography. Academic Radiology 2006; 13(6): 670-677.

124. Birkmayer W, Birkmayer JD. Dopamine action and disorder of neurotransmitter balance. Gerontology 1987; 33 : 168-171.

125. Ohtsuka C, Sasaki M, Konno K et al. Changes in substantia nigra and locus coeruleus in patients with early-stage Parkinson's disease using neuromelanin-sensitive MR imaging. Neuroscience Letters 2013; 541: 93-98.

126. Berg D. Transcranial sonography in the early and differential diagnosis of Parkinson's disease. J Neural Tansm Suppl 2006; 70; 249-54.

127. Ogisu K, Kudo K, Sasaki M et al. 3D neuromelanin-sensitive magnetic resonance imaging with semi-automated volume measurement of the substantia nigra pars compacta for diagnosis of Parkinson's disease. Neuroradiology 2013; 55(6): 719-24.

128. Schwarz ST, Rittman T, Gontu V et al. T1-weighted MRI shows stage-dependent substantia nigra signal loss in Parkinson's disease. Mov Disord 2011; 26: 1633-1638.

129. Graham JM, Paley MN, Grünewald RA et al. Brain iron deposition in Parkinson's disease imaged using the PRIME magnetic resonance sequence. Brain 2000; 123: 2423-2431.

130. Enochs WS, Petherick P, Bogdanova A et al. Paramagnetic metal scavenging by melanin: MR imaging. Radiology 1997; 204: 417-423.

131. Tosk JM, Holshouser BA, Aloia RC et al. Effects of the interaction between ferric iron and L-dopa melanin on T1 and T2 relaxation times determined by magnetic resonance imaging. Magn Reson Med 1992; 26: 40-45.

132. Blazejewska AL, Schwarz ST, Pitiot A et al. Visualization of nigrosome 1 and its loss in PD: pathoanatomical correlation and in vivo 7 T MRI. Neurology 2013;81(6):534-40.

133. Ohtsuka C, Sasaki M, Konno K, Kato K, Takahashi J et al. Differentiation of early-stage parkinsonisms using neuromelanin-sensitive magnetic resonance imaging. Parkinsonism Relat Disord 2014;20(7):755-760.

134. de la Fuente-Fernandéz R. Role of DaTSCAN and clinical diagnosis in Parkinson disease. Neurology 2012;78:696-701.

135. Calne DB, Snow BJ, Lee C (1992) Criteria for diagnosing Parkinson's disease. Ann Neurol 32(Suppl):S125-7.

136. Sawle GV, Playford ED, Brooks DJ et al. Asymmetrical presynaptic and post-synaptic changes in the striatal dopamine projection in dopa naive parkinsonism. Diagnostic implications of the D2 receptor status. Brain 1993;116:853-67.

137. Vlaar AM, van Kroonenburgh MJ, Kessels AG et al. Meta-analysis of the literature on the diagnostic accuracy of SPECT in parkinsonian syndromes. BMC Neurol 2007;1:27.

138. Bouwmans AE, Vlaar AM, Mess WH, Kessels A, Weber WE. Specificity and sensitivity of transcranial sonography of the substantia nigra in the diagnosis of Parkinson's disease: prospective cohort study in 196 patients. BMJ Open 2013;2;3(4).pii:e002613.

139. Reimão S, Pita Lobo P, Neutel D, et al. Substantia nigra neuromelanin magnetic resonance imaging in de novo Parkinson's disease patients. Eur J Neurol 2014; Dec 22 [Epub ahead of print].

140. DuMouchel WH, O'Brien FL. Integrating a Robust Option into a Multiple Regression Computing Environment. *Computer Science and Statistics*: *Proceedings of the 21st Symposium on the Interface*. Alexandria, VA: American Statistical Association, 1989.

141. Uitti RJ, Baba Y, Whaley NR, Wszolek ZK, Putzhe JD. Parkinson disease: handedness predicts asymmetry. Neurology 2005;64(11):1925-1930.

142. Faucheux BA, Martin ME, Beaumont C et al. Neuromelanin associated redox-active iron is increased in the substantia nigra of patients with Parkinson's disease. J Neurochem 2003;86(5):1142-1148.

143. Enochs WS, Petherick P, Bogdanova A, Mohr U, Weissleder R (1997): Paramagnetic metal scavenging by melanin: MR imaging. Radiology 2004:417– 423.

144. Zecca L, Casella L, Albertini A et al. Neuromelanin can protect against iron-mediated oxidative damage in system modeling iron overload of brain aging and Parkinson's disease. J Neurochem 2008;106:1866-75.

145. Du G, Lewis MM, Styner M, et al. Combined R2* and diffusion tensor imaging changes in the substantia nigra in Parkinson's disease. Mov Disord 2011; 26:1627–1632.

146. Baudrexel S, Nürnberger L, Rüb U, et al. Quantitative mapping of T1 and T2* discloses nigral and brainstem pathology in early Parkinson's disease. Neuroimage 2010;51:512–520.

147. Haacke EM, Cheng NY, House MJ, et al. Imaging iron stores in the brain using magnetic resonance imaging. Mag Reson Imaging 2005;23(1):1-25.

148. Antonini A, Leenders KL, Meier D et al. T2 relaxation time in patients with Parkinson's disease. Neurology 1993;43:697-700.

149. Vymazal J, Righini A, Brooks RA, et al. T1 and T2 in the brain of healthy subjects, patients with Parkinson's disease, and patients with multiple system atrophy: relation to iron content. Radiology 1999;211:489-495.

150. Gorell JM, Ordidge RJ, Brown GG, et al. Increased iron-related MRI contrast in the substantia nigra in Parkinson's disease. Neurology 1995;45:1138–1143.

151. Wallis LI, Paley MN, Graham JM, et al. MRI assessment of basal ganglia iron deposition in Parkinson's disease. J Magn Reson Imaging 2008;28:1061–1067.

152. Xu X, Wang Q, Zhang M. Age, gender, and hemispheric differences in iron deposition in the human brain: an in vivo MRI study. Neuroimage 2008;40(1):35-42.

153. Prakash BD, Sitoh YY, Tan LC, Au WL. Asymmetrical diffusion tensor imaging indices of the rostral substantia nigra in Parkinson's disease. Parkinsonism Relat Disord 2012;18(9):1029-1033.

154. Chan RM, von Deuster C, Giese D et al. Characterization and correction of eddy-current artifacts in unipolar and bipolar diffusion sequences using magnetic field monitoring. J Magn Reson 2014;244:74-84.

155. Tijssen RH, Jansen JF, Backes WH. Assessing and minimizing the effects of noise and motion in clinical DTI at 3 T. Hum Brain Mapp 2009;30(8):2641-2655.

156. Bisdas S, Bohning DE, Besenski N, Nicholas JS, Rumboldt Z. Reproducibility, interrater agreement, and age-related changes of fractional anisotropy measures at 3T in healthy subjects: effect of the applied b-value. AJNR Am J Neuroradiol 2008; 29(6):1128-1133.

157. Teipel SJ, Reuter S, Stieltjes B et al. Multicenter stability of diffusion tensor imaging measures: a European clinical and physical phantom study. Psychiatry Res 2011;194(3):363-371.

158. Vollmar C, O'Muircheartaigh J, Barker GJ et al. Identical, but not the same: intra-site and inter-site reproducibility of fractional anisotropy measures on two 3.0T scanners. Neuroimage 2010;51(4):1384-1394.

159. Huang L, Wang X, Baliki MN, Wang L, Apkarian AV, Parrish TB. Reproducibility of structural, resting-state BOLD and DTI data between identical scanners. PLoS One 2012;7(10):e47684.

160. Bonekamp D, Nagae LM, Degaonkar M et al. Diffusion tensor imaging in children and adolescents: reproducibility, hemispheric, and age-related differences. Neuroimage 2007;34(2):733-742.

161. Cole J, Farmer R, Rees E et al. Test-retest reliability of diffusion tensor imaging in Huntington's disease. PLoS One 2014;6. pii:ecurrents.hd.f19ef63fff962f5cd9c0e88f4844f43b.

162. Müller HP, Grön G, Sprengelmeyer R et al. Evaluating multicenter DTI data in Huntington's disease on site specific effects: An ex post facto approach. Neuroimage Clin 2013;2:161-167.

163. Marenco S, Rawlings R, Rohde GK et al. Regional distribution of measurement error in diffusion tensor imaging. Psychiatry Res 2006;147(1):69-78.

164. Brander A, Kataja A, Saastamoinen A et al. Diffusion tensor imaging of the brain in a healthy adult population: Normative values and measurement reproducibility at 3 T and 1.5 T. Acta Radiol 2010;51(7):800-807.

165. FMRIB Software Library. FSL and FreeSurfer Course. *FMRIB Anal Gr MGH, Bost*. 2014. Available at: http://fsl.fmrib.ox.ac.uk/fslcourse/Accessed December 14, 2011

166. Jenkinson M, Beckmann CF, Behrens TEJ, Woolrich MW, Smith SM. FSL. Neuroimage 2012;62(2):782–790.

167. Bland JM, Altman DG. Statistical methods for assessing agreement between two methods of clinical measurement. Lancet 1986;1(8476):307-310.

168. Jansen JF, Kooi ME, Kessels AG, Nicolay K, Backes WH. Reproducibility of quantitative cerebral T2 relaxometry, diffusion tensor imaging, and 1H magnetic resonance spectroscopy at 3.0 Tesla. Invest Radiol 2007 Jun;42(6):327-337.

169. Fox RJ, Sakaie K, Lee JC, Debbins JP et al. A validation study of multicenter diffusion tensor imaging: reliability of fractional anisotropy and diffusivity values. AJNR Am J Neuroradiol 2012 Apr;33(4):695-700.

170. Pfefferbaum A, Adalsteinsson E, Sullivan EV. Replicability of diffusion tensor imaging measurements of fractional anisotropy and trace in brain. J Magn Reson Imaging *2*003;18:427–433.

171. Müller MJ, Mazanek M, Weibrich C et al. Distribution characteristics, reproducibility, and precision of region of interest-based hippocampal diffusion tensor imaging measures, AJNR Am J Neuroradiol 2006;27:440-445.

172. Yoshikawa K, Nakata Y, Yamada K, Nakagawa M. Early pathological changes in the parkinsonian brain demonstrated by diffusion tensor MRI. J Neurol Neurosurg Psychiatry 2004;75:481–484.

173. Menke RA, Scholz J, Miller KL et al. MRI characteristics of the substantia nigra in Parkinson's disease: a combined quantitative T1 and DTI study. Neuroimage 2009;47:435–441.

174. Magnotta VA, Matsui JT, Liu D et al. Multicenter reliability of diffusion tensor imaging. Brain Connect 2012;2(6):345-355.

175. Ozturk A, Sasson AD, Farrell JAD et al. Regional differences in diffusion tensor imaging measurements: assessment of intra-rater and interrater variability, AJNR Am J Neuroradiol 2008;29:1124-1127.

176. Cummings JL, Fine MJ, Grachey ID et al. Effective and efficient diagnosis of parkinsonism: the role of dopamine transporter SPECT imaging with ioflupane I-123 injection (DaTscan™). Am J Manag Care 2014;20(5 Suppl):97-109.

177. Volkow ND, Rosen B, Farde L. Imaging the living human brain: magnetic resonance imaging and positron emission tomography. Proc Natl Acad Sci USA 1997;94:2787–2788.

178. Antonini A, Biundo R. Parkinson's disease: Can dopamine transporter imaging define early PD? Nat Rev Neurol 2014:10(8):432-3.

179. Louis ED, Ferreira JJ. How common is the most common adult movement disorder? Update on the worldwide prevalence of essential tremor. Mov Disord 2010;25:534–541.

180. Louis ED. Re-thinking the biology of essential tremor: From models to morphology. Parkinsonism Related Disord 2014;20(Suppl 1):S88–S93.

181. Pahwa R, Koller WC. Is there a relationship between Parkinson's disease and essential tremor? Clin Neuropharmacol 1993;16:30-35.

182. Marshall VL, Reininger CB, Marquardt M et al. Parkinson's disease is overdiagnosed clinically at baseline in diagnostically uncertain cases: a 3 year European multicenter study with repeat [^{123}I]-FP-CIT SPECT. Mov Disord 2009;24:500-508.

183. Bhalsing KS, Saini J, Pal PK. Understanding the pathophysiology of essential tremor through advanced neuroimaging: A review. J Neurol Sci 2013;335:9–13.

184. Passamonti L, Cerasa A, Quattrone A. Neuroimaging of Essential Tremor: What is the Evidence for Cerebellar Involvement? Tremor Other Hyperkinet Mov 2012;2:

185. Louis ED, Huang CC, Dyke JP, Long Z, Dydak U. Neuroimaging studies of essential tremor: how well do these studies support/refute the neurodegenerative hypothesis? Tremor Other Hyperkinet Mov 2014;28:4:235.

186. Novelino F, Cherubini A, Chriaco C et al. Brain iron deposition in essential tremor: a quantitative 3-Tesla magnetic resonance imaging study. Mov Disord 2013;28(2):196-200.

187. Nicoletti G, Manners D, Novellino F et al. Diffusion tensor MRI changes in cerebellar structures of patients with familial essential tremor. Neurology 2010;74:988–994.

188. Prodoehl J, Li H, Planetta P et al. Diffusion tensor imaging of Parkinson's disease, atypical parkinsonism, and essential tremor. Mov Disord 2013;28(13):1816-1822.

189. Bach JP, Ziegler U, Deuschl G, Dodel R, Doblhammer-Reiter G. Projected numbers of people with movement disorders in the years 2030 and 2050. Mov Disord 2011;26:2286-2290.

190. Louis ED, Thawani SP, Andrews HF. Prevalence of essential tremor in a multiethnic, community-based study in northern Manhattan, New York, N.Y. Neuroepidemiology 2009;32:208–214.

191. Benito-León J, Bermejo-Pareja F, Morales JM, Vega S, Molina JA. Prevalence of essential tremor in three elderly populations of central Spain. Mov Disord 2003;18:389–394.

192. Benito-León J. Essential tremor: one of the most common neurodegenerative diseases? Neuroepidemiology 2011;36:77-78.

193. Louis ED. Age of onset: can we rely on essential tremor patients to report this? Data from a prospective, longitudinal study. Neuroepidemiology 2013;40:93–98.

194. Hardesty DE, Maraganore DM, Matsumoto JY, Louis ED. Increased risk of head tremor in women with essential tremor: longitudinal data from the Rochester Epidemiology Project. Mov Disord 2004;1:529–533.

195. Schrag A, Münchau A, Bhatia KP et al. Essential tremor: an overdiagnosed condition? J Neurol 2000;245:955-999.

196. Jain S, Lo SE, Lewis ED. Common misdiagnosis of a common neurological disorder: how are we misdiagnosing essential tremor? Arch Neurol 2006;63:1100-1104.

197. Geraghty JJ, Jankovic J, Zetusky WJ. Association between essential tremor and Parkinson's disease. Ann Neurol 1985;17:329 –333.

198. Benamer HTS, Patterson J, Grosset DG. Accurate differentiation of parkinsonism and essential tremor using visual assessment of [^{123}I]- FP-CIT SPECT imaging: the [^{123}I]- FP-CIT SPECT study group. Mov Disord 2000;15:503-510.

199. Pagan FL, Butman JA, Dambrosia JM, Hallett M. Evaluation of essential tremor with multi-voxel magnetic resonance spectroscopy. Neurology 2003;60:1344 –1347.

200. Quattrone A, Cerasa A, Messina D, et al. Essential head tremor is associated with cerebellar vermis atrophy: a volumetric and voxel-based morphometry MR imaging study. AJNR Am J Neuroradiol 2008;29:1692–1697.

201. Louis ED. Essential tremor: evolving clinicopathological concepts in an era of intensive post-mortem enquiry. Lancet Neurol 2010;9:613-622.

202. Stockner H, Sojer M, Seppi K, et al. Midbrain sonography in patients with essential tremor. Mov Disord 2007;22:414-417.

203. Stockner H, Wurster I. Transcranial sonography in essential tremor. Int Rev Neurobiol 2010;90:189-197.

204. Deuschl G, Bain P, Brin M. Consensus statement of the Movement Disorder Society on Tremor. Ad Hoc Scientific Committee. Mov Disord 1998;13(suppl 3):2–23.

205. Paulus W, Jellinger K. The neuropathologic basis of different clinical subgroups of Parkinson's disease. J Neuropathol Exp Neurol 1991;50(6):743-55.

206. Jellinger KA. Post mortem studies in Parkinson's disease- is it possible to detect brain areas for specific symptoms? J Neural Transm Suppl. 1999;56:1-29.

FACSIMILE

The Neuroradiology Journal 24: 177-186, 2011 www.centauro.it

Diffusion Tensor Imaging in Movement Disorders: Review of Major Patterns and Correlation with Normal Brainstem/cerebellar White Matter

S. REIMÃO[1], C. MORGADO[1], L. NETO[1], J. FERREIRA[2], M. COELHO[2], M. ROSA[2], J. CAMPOS[1]
[1]Neurological Imaging Department and [2]Neurology Department of Hospital Santa Maria; Lisbon, Portugal

Key words: diffusion tensor imaging, movement disorders, brainstem, cerebelum, while matter

SUMMARY – *The authors reviewed the diffusion tensor imaging (DTI) and tractography (DTT) of the normal brainstem and cerebellar white matter in normal volunteers, correlating it with structural magnetic resonance (MR) imaging and DTI data obtained in patients evaluated in our institution with movement disorders, including multisystem atrophy (MSA), spinocerebellar ataxia (SCA), progressive supra-nuclear palsy (PSP) and idiopathic Parkinson's disease (PD). DTI and tractography data demonstrated major white-matter fibers within the brain stem and cerebellum, including cortico-spinal tracts, transverse pontine fibers, medial lemniscus and cerebellar peduncles. Visualization of selective degeneration of these individual fibre tracts with DTI, in our cases, added qualitative data to the differential diagnosis of movement disorders.*

Introduction

Diffusion tensor imaging (DTI) and diffusion tensor tractography (DTT) have been used to map the normal anatomy of the brainstem/cerebellum, not only of the white matter but also allowing the study of gray matter structures [1]. DTI data has enabled detailed imaging of major afferent and efferent pathways of the cerebellar and their connections with the brainstem [1,2]. The increased sensitivity of DTI in demonstrating changes in the brainstem and cerebellum white matter has been shown in a wide number of pathologies. This information combined with structural MR imaging has proven useful in the detection of impairment in extra-pyramidal circuits, particularly in movement disorders [3,4].

The idiopathic parkinsonian movement disorders are a group of distinct neurodegenerative diseases, including idiopathic Parkinson's disease (PD), and atypical parkinsonian disorders (APD), comprising multiple system atrophy (MSA), progressive supranuclear palsy (PSP) and corticobasal degeneration (CBD). In the early stages of disease, the differential diagnosis between PD and APD remains a clinical problem, with APD comprising up to 20% of patients presenting with parkinsonism [5]. Although conventional magnetic resonance imaging (MR) can demonstrate changes in APD, these are essentially present in advanced stages of disease and have low specificity and sensitivity in the differential diagnosis [6]. The potential of DTI combined with DTT for the differential diagnosis and evaluation of the neurodegeneration of specific pathways in parkinsonian disorders has highlighted DTI as a potential useful tool in the clinical routine [7,8]. We reviewed DTI imaging of the normal brainstem and cerebellar white matter and the characteristic DTI patterns in the more frequent movement disorders. A retrospective review of the DTI studies performed in patients evaluated in Hospital de Santa Maria (Lisbon) with movement disorders was made, trying to ascertain the results obtained and correlating them with the published literature.

Paper presented at the XIX Symposium Neuroradiologicum, 2010.

Methods

The authors made a retrospective review of structural MR imaging and DTI/DTT of brainstem and cerebellar white matter in healthy volunteers and patients with clinically proven movement disorders including idiopathic Parkinson's disease (PD), multisystem atrophy (MSA), corticobasal degeneration (CBD), spinocerebellar ataxia (SCA), and Progressive Supra-nuclear palsy (PSP), evaluated in Hospital de Santa Maria - Lisbon with DTI studies in the last two years.

Subjects

Two healthy volunteers aged 42 and 54 years, and thirteen patients with early/advanced stage MSA, PSP, CBD, SCA, and PD.

Table1 Summary of patient data (*NA* not applicable; ↓ decreased; FA; MCP; TPF; SCP, SN)

Clinical Diagnosis	*Age (years)*	*Sex (M/F)*	*Disease Duration*	*T1/T2-weighted MR Changes*	*DTI*
Control	42	M	NA	Normal	Normal
Control	54	F	NA	Normal	Normal
MSA-C	62	M	Long	– Pontine-cerebellar Atrophy – T2 hyperintensity MCP – Pontine Cruciform Signal	– ↓ ↓↓ FA MCP and TPF – MCP Atrophy/green Color Lost – TPF red color lost
MSA-C	69	F	Long	– Pontine-cerebellar Atrophy – T2 hyperintensity MCP – Pontine Cruciform Signal	– ↓ ↓↓ FA MCP and TPF – MCP Atrophy/green Color Lost – TPF Red Color Lost
MSA-C	59	F	Short	– Pontine-cerebellar Atrophy	– ↓ FA MCP and TPF – ↓ MCP Green Color
MSA-C	63	M	Short	Normal	– ↓ FA MCP and TPF – ↓ MCP Green Color
MSA-C	72	F	Short	Normal	↓ FA MCP and TPF – ↓ MCP Green Color
MSA-P	71	M	Long	Atrophy and T2/T2* hypointensity Putamen	– ↓ FA MCP
MSA-P	63	M	Short	Normal	– ↓ FA MCP
MSA-P	70	F	Short	Normal (Basal Ganglia T2 hypointensity Normal for Age Group)	– ↓ FA MCP
PSP	64	M	Long	Midbrain Atrophy	– ↓ FA SCP – SCP Blue Color Lost – Absence SCP Decussation Red Color – Normal MCP and TPF
PSP	68	M	Short	Normal	– ↓ FA SCP – SCP Blue Color Reduction – SCP Decussation Red Color Reduction – Normal MCP and TPF
CBD	70	F	Long	– Asymmetric Parietal Atrophy (Left>Right) – "Eye of Tiger" Signal – T2 hyposignal External Putamen	– ↓ FA MCP – Normal TPF and SCP
SCA1	56	M	Long	– Pontine Cerebellar Atrophy	– ↓ Cerebellar Hemispheric Fibers – ↓ FA MCP and TPF
PD	62	M	Short	Normal	– SN FA Changes

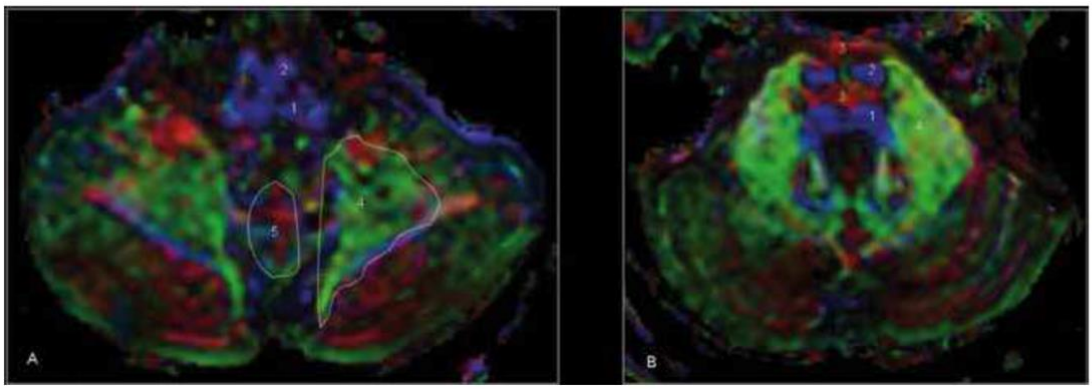

Figure 1 DTI on horizontal sections: at the level of upper medulla (A) the main cerebellar tract, below the level of the dentate are visible by their green color. At the level of the mid part of the pons (B) the ascending fibers of the medial lemniscus and corticospinal tract can be followed easily; laterally the two middle cerebellar peduncles are outlined by their green color, around the dentate nucleus. 1-medial leminscus. 2-pyramidal tract. 3-transverse pontine fibers. 4-middle cerebellar peduncle. 5-vermian transverse fibers.

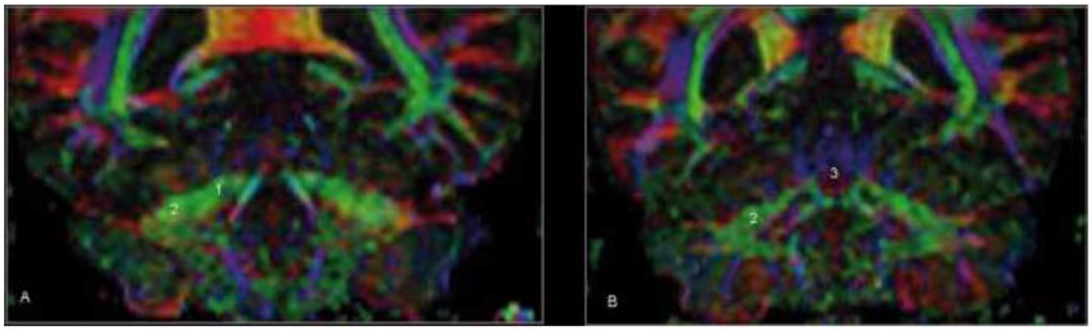

Figure 2 DTI coronal sections of the cerebellum behind the floor of the IV ventricle (A) and more posterior, at the level of the dentate nucleus (B). The afferent fibers of the middle cerebellar peduncle and the fibers to the dentate are clearly visible. The afferent fibers of the dentate are visible on section B, located more posteriorly. 1-dentate fibers. 2-middle cerebellar peduncle. 3-vermian transverse fibers.

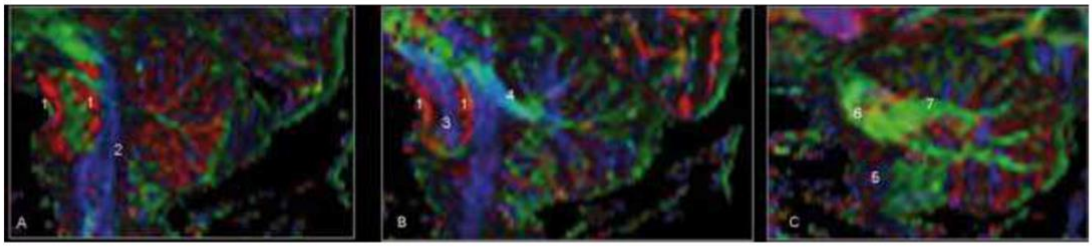

Figure 3 DTI sagittal sections of the brainstem and cerebellum on the midline (A), 5mm (B) and 10mm (C) from the midline. In the midline section almost all the vermian cerebellar surface corresponds to transverse fibers. More laterally the main fibers are directed from the cerebellar hemispheres to the main cerebellar nuclei. Above the level of the lateral part of the IV ventricle the superior cerebellar peduncle is well outlined. The two components of transverse pontine fibers are clearly visible by their red color. 1- transverse pontine fibers. 2-medial lemniscus 3-pyramidal tract.4-superior cerebellar peduncle. 5-inferior cerebellar peduncle. 6-middle cerebellar peduncle. 7-hemispheric cortical fibers to dentate and emboliform nuclei.

The diagnosis was made clinically, using established criteria [5]. Control and patient data are summarized in Table 1.

Imaging protocol

All the studies reviewed were performed in a 3.0-T Philips® MR scanner, using an eight channel head coil. DTI was performed with 5 mm thickness using a single-shot EPI sequence. The diffusion encoding used in the studies varied between 15 and 24 directions (b values 0-800 s/mm²). In all the studies reviewed a T1-weighted and a T2-weighted axial scan have also been acquired.

Post-processing

DTI data were analysed using DTI Studio® or the PRIDE fibre-tracking tool supplied by Philips Medical Systems®. In all cases FA maps with grey-scale and colour coding were generated. The colour-coding was assigned as: red - left to right, blue – craniocaudal, green – rostral-dorsal directions.

Using the same post-processing tools both single and multiple regions of interest (ROIs) were selected for tractography in the pons, midbrain or ina anatomical structure to be studied. The tracts were visualized by setting the tractography colour algorithm to show the principal anisotropy and direction with a threshold FA of less than 0.2.

Results

Conventional Imaging data

No anatomical or signal intensity abnormalities were seen in T1- and T2-weighted images in controls, patients with early MSA and PSP, the patient with PD or SCA1.

In the advanced MSA-C patients a significant atrophy of the pons and cerebellum was seen as well as T2 hyperintensity of the middle cerebellum peduncles and pontine cruciform signal. Small linear T2 hypointensity of the putamen was identified in patients with MSA-P and the "eye-of the tiger signal" and asymmetrical parietal atrophy in the CBD patients. Atrophy of the mesencephalon was seen in advanced PSP.

DTI/DTT

Controls

Transverse fibers of the vermis were apparent in red and are visible in all sections (Figures 1-3). On parasagittal color maps the main tracts have a green color, with anteroposterior direction, connecting the cerebellar cortex and the emboliform and dentate nuclei (Figure 3). The inferior cerebellar peduncle (ICP) can be identified in coronal and sagittal sections, with blue color, lateral to the medial lemniscus (Figure 3). The middle cerebellar peduncle (MCP) projects to pontine nuclei and appears as a large symmetric green area, clearly visible in all planes, intermingling with fibers of the dentate nucleus (Figures 1-5). The superior cerebellar peduncles (SCP) were easily identified in axial and sagittal planes (Figures 3-6), and the decussation of the SCP was visible in red color on horizontal sections (Figure 7) at the level of the midbrain.

Patients

DTI imaging with FA and colour coded maps in MSA cases of the cerebellar type (MSA-C) showed a significant decreased in fractional anisotropy (FA) in the transverse pontine fibers (TPF) and MCP, with preservation of the pyramidal tract and medial lemniscus (Figure 8), similar to the previous reported cases [9]. In sagittal images of the brain stem, atrophy and severe degeneration of both the MCP and TPF could be seen in all patients with advanced MSA, which was not seen in any of the controls or other patient groups. In MSA of the parkinsonian type (MSA-P) there was decreased FA of the MCP with only a slight decrease in the pontocerebellar fibers (Figure 9).

Table 2 Fractional anisotropy values in ROIs placed in the SN (rostral, middle and caudal portions) in a healthy control and PD patient. The PD patient reduced FA was greater in the caudal compared with the rostral ROI.

	FA values	
ROIs SN	PD	Control
rostral	0,49	0,56
middle	0,40	0,54
caudal	0,42	0,60

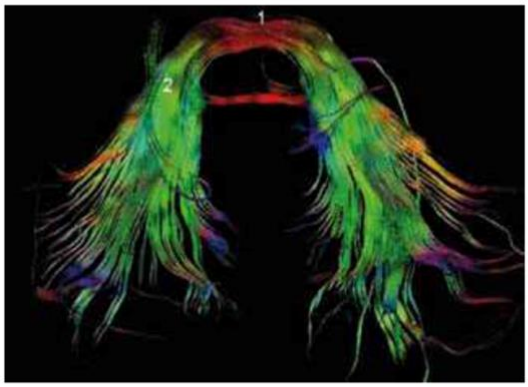

Figure 4 Selective tracking of the middle cerebellar peduncle on axial projection (ROI in the mid portion of the middle cerebellar peduncles bilaterally).1- transverse pontine fibers. 2-middle cerebellar peduncle.

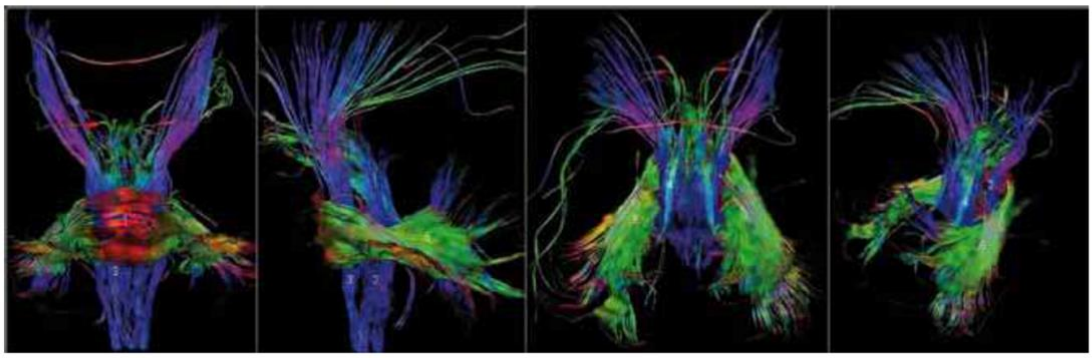

Figure 5 Selective tracking of the middle and superior cerebellar peduncle (ROI in the mid pons).1- transverse pontine fibers. 2-medial lemniscus 3-pyramidal tract.4-superior cerebellar peduncle. 5-middle cerebellar peduncle.

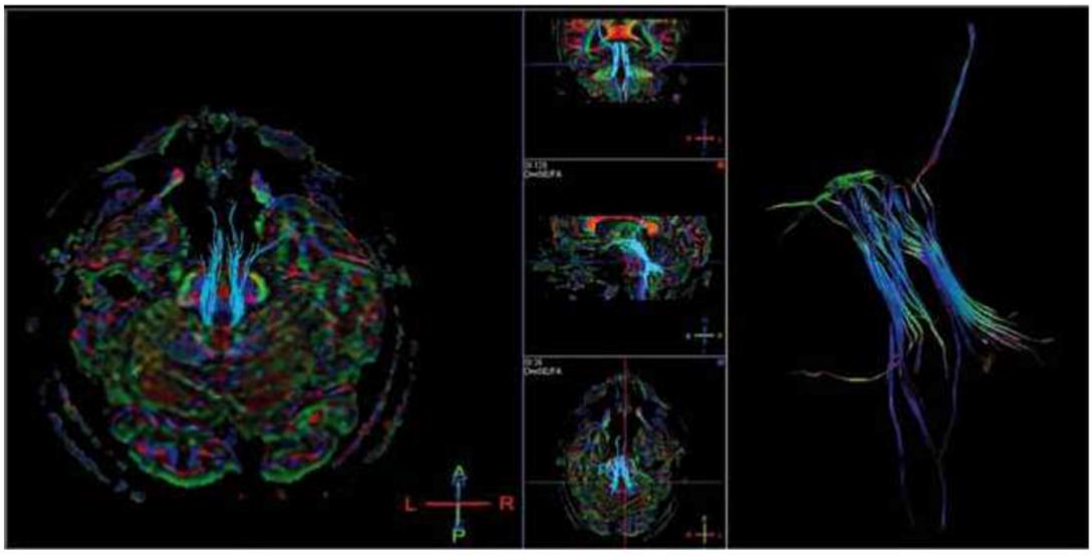

Figure 6 Selective tracking of the superior cerebellar peduncle (ROI in the superior cerebellar peduncle).

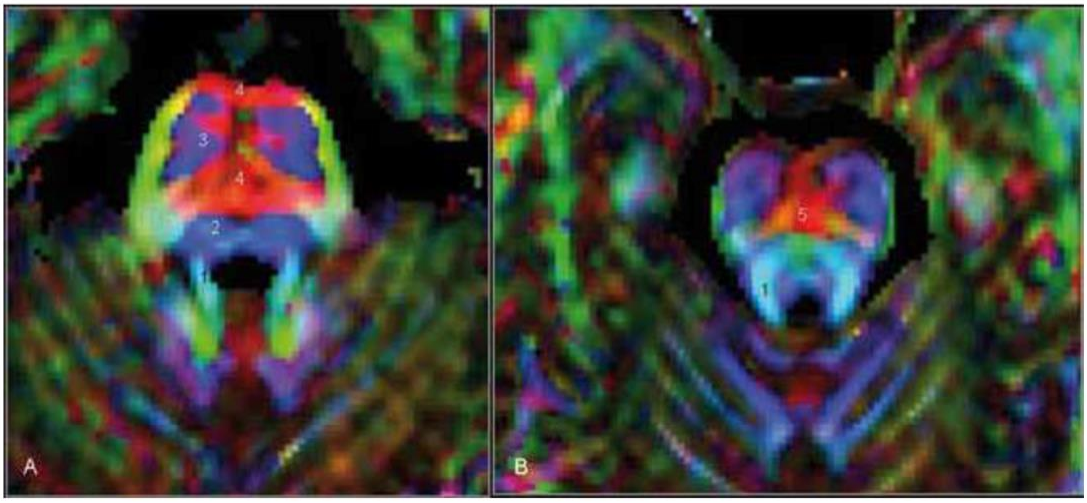

Figure 7 DTI horizontal sections of the superior pons (A) and midbrain (B). 1-superior cerebellar peduncle. 2-medial lemniscus. 3-pyramidal tract. 4-transverse pontine fibers. 5 superior cerebellar peduncle decussation.

In PSP, we found a decreased FA in the SCP (significant in advanced cases and less prominent in early disease progression), as well as blue color decrease in the SCP and loss of the normal red color of the SCP decussation in the advanced case (Figure 10); contrary to MSA cases there was relative integrity of TPF and MCP [10].

In the corticobasal degeneration patient we found only a slight FA decrease in the MCP, with no identifiable changes in the color coded map and no significant FA changes in the TPF or SCP.

In SCA changes are reported as variable, not allowing the differentiation between the different subtypes [11] but differing from healthy controls. Some studies in SCA type 1 and 2 have shown loss of cerebellar hemispheric fibers and decrease FA in the cerebellar peduncles and TPF [11,12], similar to what we found in a genetically confirmed SCA type 1 case (Figure 11).

In Idiopathic Parkinson's Disease (PD) we found FA reduction in the substancia nigra compared with one of the controls (Table 2), with a lateral to medial gradient, similar to the one found by Vaillancourt [13].

Discussion

Many studies have been published in the last 10 years investigating MR imaging in the differential diagnosis of parkinsonian disorders especially PD from the atypical disorders as MSA and PSP. Several morphological changes have been described as characteristic of MSA or PSP but, in general, these conventional MR signs have a low sensitivity for the diagnosis [14,15]. Recently some studies using DTI/DTT have shown a greater sensitivity of this technique in the differential diagnosis of parkinsonian disorders compared to conventional MR, rendering it attractive not only for future research but introducing it into the clinical practice [7,11].

The results of our review, with a small number of patients, are in accordance with previous DTI data. In patients with late stage MSA we found the characteristic morphology changes especially prominent pontine/cerebellar atrophy, pontine cruciform sign and MCP signal changes [14]. DTI data showed marked changes in the MCP and TPF in advanced cases but also MCP/TPF FA and color reduction in the early stages of the disease, similar to published studies [16], indicating that DTI data might be important in the distinction of MSA from controls as well as from PSP and Parkinson's disease [17].

The characteristic morphological MR changes of PSP were identified only on late stages of the disease, with prominent atrophy of the midbrain and SCP [18]. Similar to previous studies [10] in our patient with advanced disease we found a decreased FA in the SCP and loss of the normal red color of the SCP decussation with relative integrity of the TPF and MCP, enabling

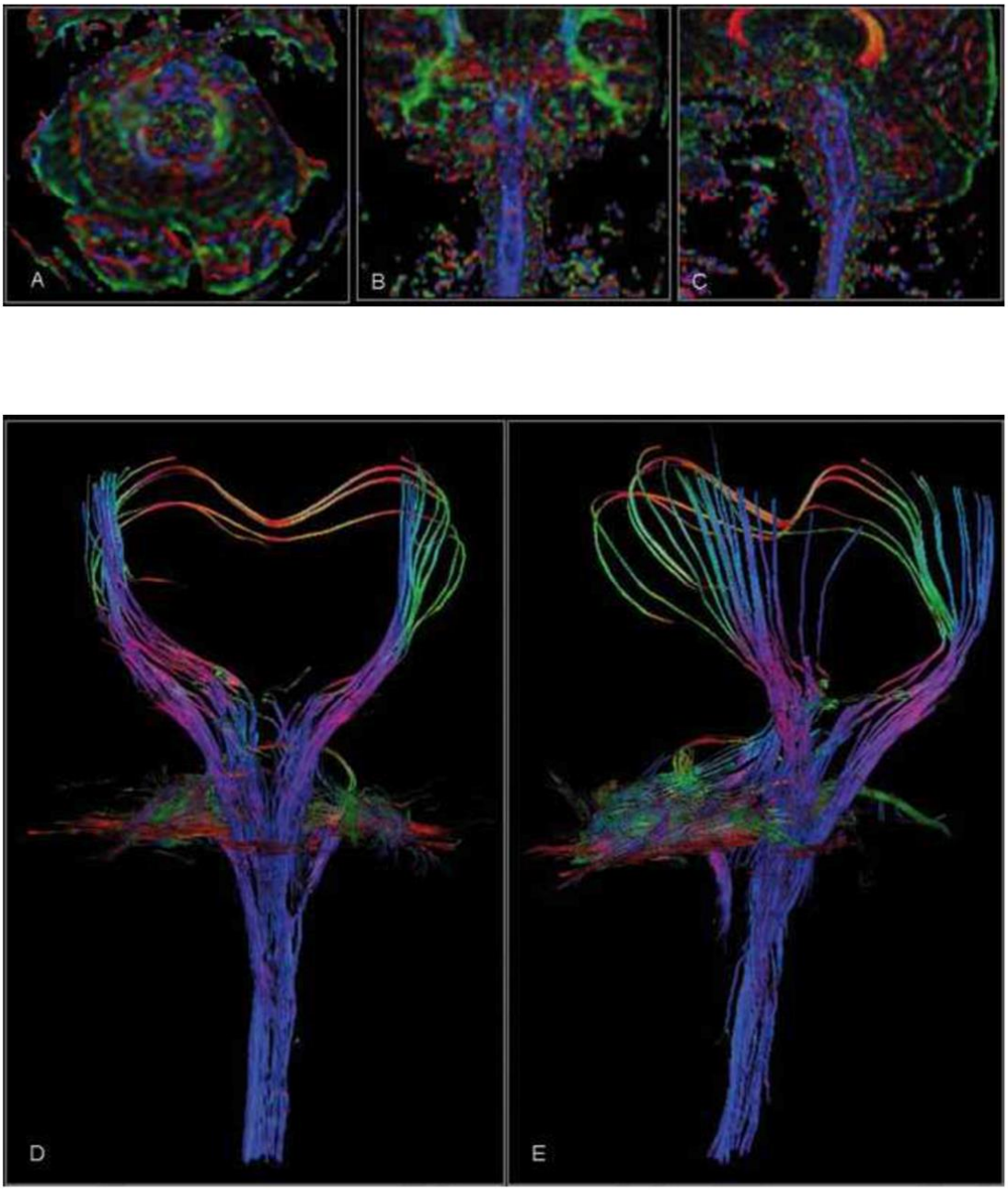

Figure 8 DTI horizontal section of the mid pons (A), coronal section of anterior pons (B), midline sagittal section (C) and tractography (D,E) in a patient with MSA-C showing significant decrease of the pontocerebellar fibers and transverse pontine fibers, with atrophy of the middle cerebellar peduncle. Relative integrity of pyramidal tract and medial lemniscus.

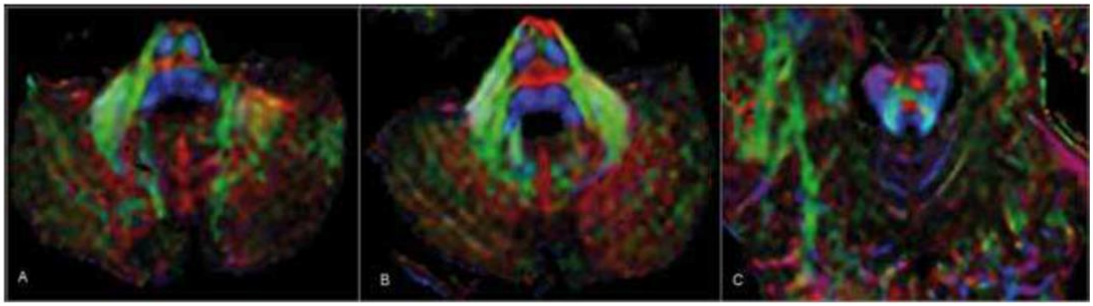

Figure 9 DTI horizontal sections in the inferior (A), mid pons (B) and midbrain (C) in a patient with MSA-P, showing slight decrease of pontocerebellar fibers color, with decreased FA of the middle cerebellar peduncle. Integrity of pyramidal tract, medial lemniscus and superior cerebellar peduncle decussation.

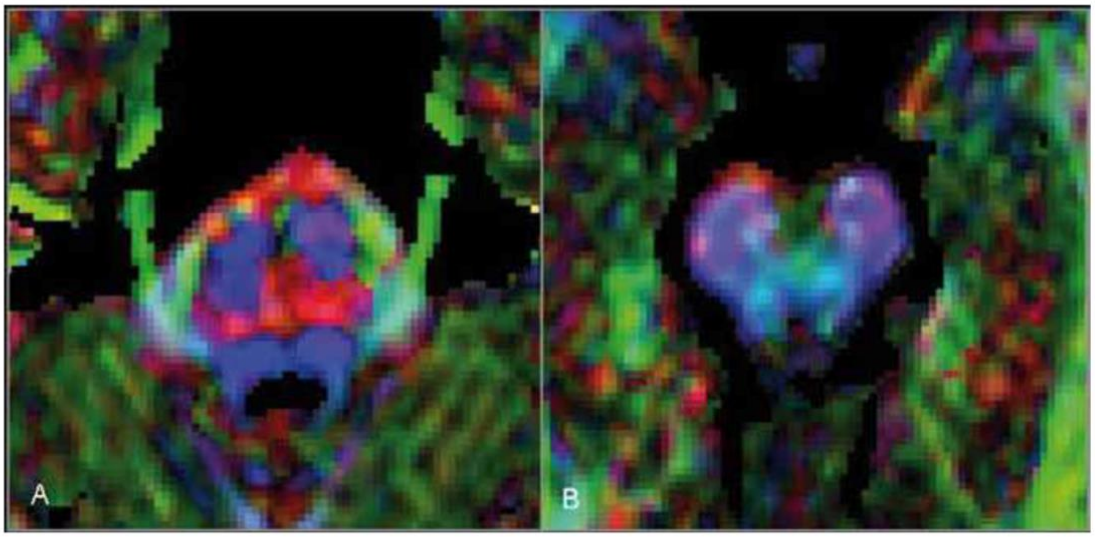

Figure 10 DTI horizontal sections in the mid pons (A) and midbrain (B) in a patient with PSP, showing a thin superior cerebellar peduncle with no identifiable red color at the superior cerebellar peduncle decussation level. Integrity of transverse pontine fibers and middle cerebellar peduncle.

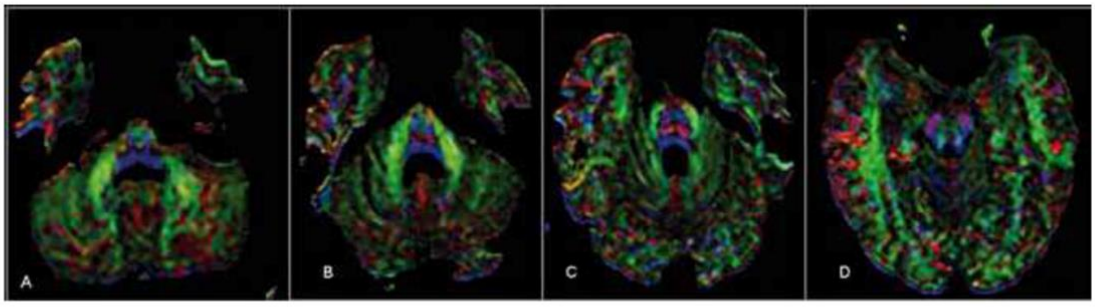

Figure 11 DTI horizontal sections at the level of the medulla (A), mid (B), superior pons (C), midbrain (D) in a patient with SCA 1, showing decreased color of transverse pontine fibers. Integrity of middle cerebellar peduncle, pyramidal tract, medial lemniscus and superior cerebellar peduncle decussation.

www.centauro.it The Neuroradiology Journal 24: 177-186, 2011

a differential diagnosis of this patient not only with controls but also with PD and MSA cases.

Corticobasal degeneration (CBD) has a distinctive clinical picture in late stages of the disease, but diagnosis is often uncertain at disease onset [19], with studies showing incorrect clinical diagnoses as well as pathologic overlap with other neurodegenerative diseases, namely PSP [20]. In late stages CBD has characteristic asymmetric frontoparietal atrophy as was found in our patient, with less consistent putaminal signal changes on MR studies [21]. On DTI there was only a slight FA decrease in the MCP but there were no significant changes in the TPF or SCP as seen in late stages MSA or PSP.

Conventional imaging differentiation of the different subtypes of SCAs is difficult and structural imaging can be normal in the early stages of the disease [11] with atrophy and signal changes of the brainstem and cerebellum appearing late in the disease [22]. DTI studies in SCA have not enabled differentiation between SCA subtypes, namely SCA1 and SCA2 but have shown strong differences with controls as was found in our case and correlating with clinical scores [11].

PD is known for its paucity of abnormal findings on conventional MR imaging (3). The DTI study of Vaillancourt [13] found changes in the substancia nigra (SN) in PD patients with a lateral to medial gradient that was also found in our only patient with recent onset PD.

Diffusion tensor tractography is an excellent tool for imaging individual white matter tracts of the brainstem [23,16], however the technical limitations of this method need to be considered, especially the problems concerning fiber crossing, delineation of tracts using manually drawn ROIs [24], distortion of axonal and neuronal architecture in neurodegenerative diseases, making it more difficult for the tracking algorithm to follow the fibres over longer distances or changes in direction. Tractography has also been less used in the study of movement disorders because data often require extensive manual postprocessing work, lacks standardization and is not easily reproducible for comparison.

Our work was just a retrospective review with a very small number of patients, based only on clinical diagnosis with no neuropathology confirmation, intended to evaluate the protocols used, the applicability, feasibility and relevance in clinical cases of the results obtained with DTI and DTT as part of the MR investigation in the differential diagnosis of disorders. We found DTI changes in advanced as well as early cases that had normal morphological imaging; these changes enabled patient differentiation from controls and MSA patients from PSP. However, there is the need for prospective studies with a significant number of patients trying to evaluate the sensitivity and specificity of DTI imaging in the diagnosis of parkinsonian movement disorders, especially in early stages of disease.

In the majority of previous DTI studies field strengths of 1.5 T and fewer directions have mostly been used [23,16]. In this review all the studies were performed in a 3.0T field strength magnet, using 15 or 24 independent diffusion encoding directions in order to increase the directional resolution as well as being tolerable for the patient and less susceptible to movement artifacts. The limited data of our review do not enable us to draw any conclusions as to the number of optimal directions to be used.

The DTI protocols we reviewed are easy to implement in a clinical setting, offering the possibility to study, in vivo, the major connections of the brainstem-cerebellum in healthy individuals as well as offering a unique possibility to study pathological changes unidentifiable in conventional MR sequences. In the cases we reviewed, DTI data supplemented routine T1-weighted, T2-weighted and FLAIR images in the differential diagnosis of movement disorders.

Although DTI/DTT have not yet become a routine procedure in the clinical setting, DTI/DTT protocols can be easily implemented and yield clinically relevant information. The different DTI patterns in movement disorders appears to be complementary to conventional structural MR [8], and in the future can be a useful tool for specific movement disorders identification in the clinical practice.

Furthermore, quantitative data on the diffusion properties of specific white matter tracts can be elicited, which might be of use in future studies of disease progression and effects of treatment in future research.

Conclusion

DTI imaging is very useful in identifying the normal brainstem and cerebellar white matter. White matter water-molecule disturbance in the brain-stem and cerebellar fibers in different types of movement disorders can be identified by DTI and provide a functional evaluation of the impaired extra-pyramidal circuits. Our

limited review is in accordance with other series indicating that DTI is a useful tool in the evaluation of the status of white matter fibers and gray matter structures, and in combination with structural imaging may have diagnostic value in patients with movement disorders.

References

1 Salamon N, et al. White matter fiber tractography and color mapping of the normal human cerebellum with diffusion tensor imaging. Journal of Neuroradiology. 2007; 34: 115-128.
2 Press GA, et al. The cerebellum: Anatomic-MR correlation in the coronal plane. Am J Neuroradiol. 1990; 11 (1): 41-50.
3 Schocke MF, et al. Trace of diffusion tensor differentiates the Parkinson variant of multiple system atrophy and Parkinson's disease. Neuroimage. 2004; 21: 1443-1451.
4 Yoshikawa K, et al. Early pathological changes in the parkinsonian brain demonstrated by diffusion tensor MRI. J Neurol Neurosurg Psychiatry. 2004; 75: 481-484.
5 Litvan I, et al. Movement Disorders Society Scientific Issues Committee report: SIC Task Force appraisal of clinical diagnostic criteria for Parkinsonian disorders. Mov Disord. 2003; 18: 467-486.
6 Schrag A, et al. Clinical usefulness of magnetic resonance imaging in multiple system atrophy. J Neurol Neurosurg Psychiatry. 1998; 65: 65-71.
7 Nilsson C, et al, Tracking the neurodegeneration of parkinsonian disorders - a pilot study. Neuroradiology. 2007; 49: 111-119.
8 Kitamura K, Nakayama K, Kosaka, et al. Diffusion tensor imaging of the cortico-ponto-cerebellar pathway in patients with adult-onset ataxic neurodegenerative disease. Neuroradiology. 2008; 50: 285-292.
9 Ito M, Watanabe H, Kawai Y, et al. Usefulness of combined fractional anisotropy and apparent diffusion coefficient values for detection of involvement in multiple system atrophy. J Neurol Neurosurg Psychiatry. 2007; 78: 722-728.
10 Aquattrone A, et al. MR imaging index for differentiation of progressive supranuclear palsy from Parkinson Disease and the Parkinson Variant of Multiple System atrophy. Radiology. 2008; 214-221.
11 Mandelli ML, et al. Diffusion tensor imaging of Spinocerebellar ataxias types 1 and 2. Am J Neuroradiol. 2007; 28: 1996-2000.
12 Yoon B, et al. Early pathological changes in the cerebellum of patients with pure cerebellar syndrome demonstrated by diffusion-tensor imaging. European Neurology. 2006; 56: 166-171.
13 Vaillancourt DE, et al. High-resolution diffusion tensor imaging in the substantia nigra of de novo Parkinson disease. Neurology. 2009; 72: 1378-1384.
14 Yekhlef F, et al. Routine MRI for the differential diagnosis of Parkinson's disease, MSA, PSP, and CBD. J Neural Transm. 2003; 110: 151-169.
15 Schrag A, et al. Clinical usefulness of magnetic resonance imaging in multiple system atrophy. J Neurol Neurosurg Psychiatry. 1998; 65: 65-71.
16 Salamon N, et al. Analysis of the brain-stem white-matter tracts with diffusion tensor imaging. Neuroradiology. 2005; 47: 895-902.
17 Nicoletti G, Lodi R, Condino F, et al. Apparent diffusion coefficient measurements of the middle cerebellar peduncle differentiate the Parkinson variant of MSA from Parkinson's disease and progressive supranuclear palsy. Brain. 2006; 129: 2679-2687.
18 Oba H, Yagishita A, Terada H, et al. New and reliable MRI diagnosis for progressive supranuclear palsy. Neurology. 2005; 64: 2050-2055.
19 Bergeron C, Pollanen MS, Weyer L, et al. Unusual clinical presentations of cortical-basal ganglionic degeneration. Ann Neurol. 1996; 40: 893-900.
20 Schneider JA, Watts RL, Gearing M, et al. Corticobasal degeneration : neuropathologic and clinical heterogeneity. Neurology 1997; 48: 959-969.
21 Soliveri P, et al. Cognitive and magnetic resonance imaging aspects of corticobasal degeneration and progressive supranuclear palsy. Neurology. 1999; 53: 502.
22 Della Nave R, et al. ADC mapping of neurodegeneration in the brainstem and cerebellum of patients with progressive ataxias. Neuroimage. 2004; 22: 698-705.
23 Stieltjes B, et al. Diffusion tensor imaging and axonal tracking in the human brainstem. Neuroimage. 2001; 14: 723-735.
24 DaSilva AFM, et al. A primer on diffusion tensor imaging of anatomical substructures. Neurosurg Focus. 2003; 15: 1-4.

Sofia Reimão, MD
Department of Neurological Imaging
Hospital de Santa Maria
Avenida Professor Egas Moniz
1649-035 Lisboa, Portugal
E-mail: sofiapcr@gmail.com

ORIGINAL ARTICLE

Substantia nigra neuromelanin magnetic resonance imaging in *de novo* Parkinson's disease patients

S. Reimão[a,b], P. Pita Lobo[b,c], D. Neutel[b,c], L. Correia Guedes[b,c], M. Coelho[b,c], M. M. Rosa[b,c,d], J. Ferreira[e], D. Abreu[b], N. Goncalves[b], C. Morgado[a], R. G. Nunes[e], J. Campos[a] and J. J. Ferreira[b,c,d]

[a]*Neurological Imaging Department, Hospital de Santa Maria – Centro Hospitalar Lisboa Norte, Lisbon;* [b]*Clinical Pharmacology Unit, Instituto de Medicina Molecular, Lisbon;* [c]*Neurology Department, Hospital de Santa Maria – Centro Hospitalar Lisboa Norte, Lisbon;* [d]*Laboratory of Clinical Pharmacology and Therapeutics, Faculty of Medicine, University of Lisbon, Lisbon; and* [e]*Institute of Biophysics and Biomedical Engineering, Faculty of Sciences, University of Lisbon, Lisbon, Portugal*

Keywords:
locus coeruleus, magnetic resonance imaging, neuromelanin, Parkinson's disease, substantia nigra

Received 22 June 2014
Accepted 7 October 2014

European Journal of Neurology 2014, **0:** 1–7

doi:10.1111/ene.12613

Background: Depigmentation of the substantia nigra (SN) and locus coeruleus (LC) is a conspicuous pathological feature of Parkinson's disease (PD) and is related to the loss of neuromelanin, whose paramagnetic properties result in high signal on specific T1-weighted magnetic resonance imaging (MRI). Recent studies have suggested that neuromelanin decrease in the SN and LC of PD patients may emerge as a possible diagnostic biomarker. The SN neuromelanin signal in *de novo* and early stage PD patients was studied to assess its diagnostic accuracy. This is the first study based on a semi-automated MRI analysis of the neuromelanin signal in *de novo* PD patients.

Methods: The inclusion criteria were untreated *de novo* PD and a 2–5 year disease duration; in addition, age matched healthy controls were enrolled. These were studied with a high-resolution T1-weighted MRI sequence at 3 T to visualize neuromelanin. The primary outcome was SN high signal area, length and neuromelanin/midbrain ratio obtained with semi-automated methods.

Results: A total of 12 *de novo* PD patients and 10 PD patients with a 2–5 year disease duration were evaluated. The area, length of the SN T1 high signal and the SN neuromelanin/midbrain ratio were markedly decreased in the PD groups compared with age-matched controls, with a substantial overlap between the two PD groups.

Conclusions: Neuromelanin-sensitive MRI techniques can discriminate PD patients from healthy individuals with high sensitivity and specificity. Our findings are consistent with recent findings showing that PD neuromelanin changes remain stable during the course of the disease.

Introduction

Parkinson's disease (PD) is a neurodegenerative condition characterized by depletion of dopaminergic neurons in the substantia nigra (SN) pars compacta (SNpc) and noradrenergic neurons in the locus coeruleus (LC) [1]. Pathological changes in the LC and SN occur early in the course of PD and have been described in pre-clinical stages [2]. Depigmentation of the SN and LC is a conspicuous pathological feature of PD and is related to the loss of a melanin pigment known as neuromelanin.

Neuromelanin is a by-product of dopamine and noradrenaline metabolism and is thought to protect neurons from oxidative stress mediated by free metals or free radicals [3]. This pigment has paramagnetic properties resulting in high signal on specific T1-weighted magnetic resonance imaging (MRI), enabling its identification *in vivo* [4,5]. Recent studies have described a reduction in MRI neuromelanin-generated signal in the SN and LC in patients with PD [4,6].

Correspondence: J. J. Ferreira, Laboratório de Farmacologia Clínica e Terapêutica, Faculdade de Medicina de Lisboa, Av. Prof. Egas Moniz, 1649-028 Lisboa, Portugal (tel.: +351 21 7802120; fax: +351 21 7802129; e-mail: joaquimjferreira@gmail.com).

EUROPEAN JOURNAL OF NEUROLOGY

Neuromelanin-sensitive MRI in *de novo* untreated PD patients and in PD patients with a 2–5 year disease duration was examined to study the diagnostic accuracy of this MRI sequence at clinical presentation and to determine whether it is possible to obtain objective measurements of the SN T1 high signal area and length using semi-automated methods that will discriminate PD patients from controls.

To our knowledge, this is the first study based on neuromelanin semi-automated MRI in *de novo* untreated PD patients.

Patients and methods

Patients and control subjects

The study was a cross-sectional case−control analysis (prospective follow-up ongoing) that included 32 subjects: 12 *de novo* patients with PD, 10 PD patients with a 2−5 year disease duration and 10 healthy subjects. Patients were recruited from the Movement Disorders Unit of the University Hospital of Santa Maria-Lisbon. *De novo* PD patients were included at the time of clinical diagnosis if they were not on antiparkinson medications, and all had <6 months since the beginning of clinical symptoms. Parkinson's disease patients with 2–5 year disease duration since clinical medical diagnosis were receiving optimal pharmacotherapy with levodopa or dopamine agonists. All patients were diagnosed with PD by a movement disorders specialist according to the UK Brain Bank criteria [7] and were rated using the Unified Parkinson's Disease Rating Scale (UPDRS). The healthy control subjects were recruited from local hospital staff and relatives. Dementia, psychiatric illness or contraindications to MRI were the exclusion criteria.

The examinations were performed with the understanding and written consent of each subject, with approval from the local ethics committee, and in compliance with national legislation and the Declaration of Helsinki guidelines.

Magnetic resonance imaging protocol

Imaging protocol

All data were acquired with a 3.0-T Phillips scanner (Phillips Achieva; Philips Medical Systems, Best, Netherlands). The following pulse sequence was used as previously described by Sasaki *et al.* [4]: T1-weighted fast spin echo; repetition time/effective echo time 633/10 ms; echo train length 3; number of slices 20; slice thickness 2.5 mm; intersection gaps 0 mm; matrix size 548 × 474; field of view 220 mm (pixel size 0.40 × 0.40 mm); and acquisition time 8 min. The sections were carefully set in the oblique axial plane perpendicular to the fourth ventricle floor with coverage from the posterior commissure to the inferior border of the pons.

T1- and T2-weighted images of the entire brain were additionally obtained in all subjects and evaluated by an experienced neuroradiologist to exclude other pathological imaging findings, namely changes in the parkinsonian index and other atypical parkinsonian syndrome changes, and lesions in the LC and SN areas that might interfere with further assessment.

Imaging analysis

Images were transferred to a Linux workstation for analysis, and an edge preserving filter [8] was applied using Matlab (R2012a, The Math Works, Natick, MA, USA) to reduce image noise. This is an adaptive mean filter where the intensity of each pixel in the filtered image $\hat{u}(i)$ is determined from the neighbourhood V_i of each pixel i (eight neighbours in two dimensions). The weight $w(i, j)$ given to each neighbouring pixel depends on the intensity difference between i and its neighbour j:

$$\hat{u}(i) = \frac{\sum_{j \in V_i} w(i,j)u(j)}{\sum_{j \in V_i} w(i,j)} \quad \text{where}$$

$$w(i,j) = 1 - \frac{|u(j) - u(i)|}{3 \times 255} \quad \text{and} \quad w(i,i) = 0$$

In this way pixels with similar intensity levels are given a higher weight, reducing blurring across different anatomical structures.

To account for subject-dependent signal fluctuations, a circular region of interest (ROI) was drawn in the central part of the *crus cerebri* of each neuromelanin-sensitive image, which was then normalized by the mean signal intensity within this ROI. T1 high signal in the SN region was visible in three slices, and the middle slice corresponding to the greatest SN volume was selected.

A rectangular region containing the mesencephalon was then selected in this slice, and two symmetrical seed points were manually defined on the most medial part of the high intensity area in the SN. A region-growing algorithm [9] was used for segmentation starting from each seed point, and the area of interest (AOI) was automatically drawn. Pixels with a signal intensity within the interval $I_{seed} \pm 0.035 \times (I_{max} - I_{min})$ were labelled as belonging to the AOI, where I_{seed} is the intensity at the seed point and I_{max} and I_{min} are the maximum and minimum signal intensities within the rectangular mesencephalon ROI. The threshold used to delimit the AOI was chosen following a preliminary optimization study where the thresh-

old was varied using a batch process with tests performed on several example images; the final value of 3.5% was selected as it was the one that provided a better visual fit to the anatomical area. The AOI was automatically drawn, and the maximal length was then calculated.

Additionally the global midbrain area and the ratio of SN neuromelanin T1 high signal area to total midbrain area (neuromelanin ratio) were calculated. Images were transferred to a PACS system and the slice where the neuromelanin area measurements were made was selected; in this slice the midbrain contours were manually drawn and the global area was calculated. Using this measure the SN neuromelanin ratio for each patient was then calculated.

Statistical analysis

The area, length and SN neuromelanin ratio obtained for each group were compared using non-parametric analysis. Kruskal–Wallis tests, with pairwise comparisons in which the resulting P values were corrected according to the Bonferroni method, and Mann–Whitney U tests were used as appropriate.

A P value of 0.05 was considered significant. Statistical analysis was performed with R 2.15.2 (R Foundation for Statistical Computing, Vienna, Austria).

Receiver operator characteristic curve analysis was conducted for the comparison between PD patients and normal subjects, and the specificity and sensitivity of the tests and the optimal cut-off point as well as the area under the curve (AUC) were also assessed.

Differences in the clinical characteristics amongst these groups were assessed. Differences in the sex distribution amongst groups were evaluated with the chi-squared test. The Kruskal–Wallis test was performed for comparison of the median age between groups as well as for the UPDRS total score and UPDRS part III.

Results

Magnetic resonance imaging was performed on all subjects, and the image quality allowed the clear identification of the high signal area in the SN region (Fig. 1). Automated analysis was possible on all subjects except one patient in the 2–5 year disease duration group whose MRI had significant artifacts and had to be excluded. Therefore, 12 patients with *de novo* PD, nine patients with 2–5 year disease duration and 10 healthy controls were eligible for further analysis. The clinical characteristics of these subjects are shown in Table 1. No significant differences were observed in age and sex amongst the three groups, and there were also no significant differences in Hoehn and Yahr (H&Y) stage and UPDRS scores between the *de novo* and the 2–5 year disease duration PD patients.

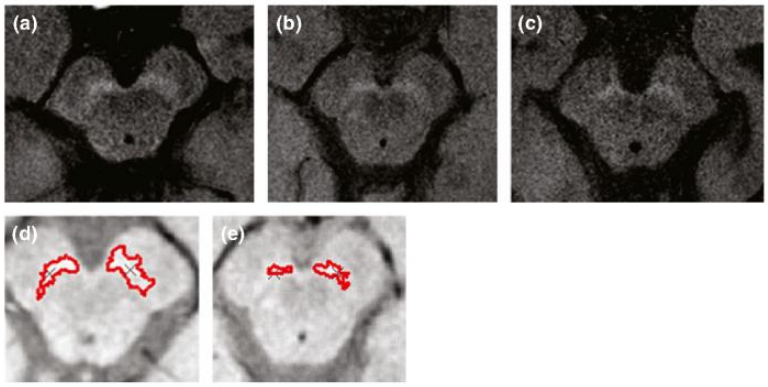

Figure 1 Neuromelanin-sensitive magnetic resonance images of the SN of a healthy control (a), a *de novo* PD patient (b) and a 2–5 year PD patient (c) and segmented images of a healthy control (d) and of a 2–5 year PD patient (e), showing diminished size of the T1 high intensity area of the SN in PD patients compared with that in controls.

Table 1 Demographics for Parkinson's and control subjects

	De novo PD	2–5 year PD	Controls	*P* value
No. (female/male)	12 (7/5)	9 (2/7)	10 (4/6)	0.186
Age, years (mean ± SD)	63.23 (±11.9)	67.22 (±6.7)	61.2 (±7.3)	0.289
H&Y (mean ± SD)	2 (2–2)	2 (2–2)	–	–
Total UPDRS (mean ± SD)	44.46 (±26.0)	49.86 (±14.0)	–	0.149
UPDRS III motor score (mean ± SD)	29.08 (±14.2)	27.43 (±10.4)	–	0.498

PD, Parkinson's disease; H&Y, Hoehn and Yahr; UPDRS, Unified Parkinson's Disease Rating Scale.

The median area and length obtained for *de novo* PD patients were 19.88 mm^2 and 33.41 mm, respectively. For the 2–5 year PD group, the median area was 12.58 mm^2 and the median length was 23.14 mm; for healthy controls, an area of 25.40 mm^2 and a length of 52.75 mm were observed.

The area and maximal length were markedly decreased in *de novo* and the 2–5 year PD groups compared with the healthy control group (Fig. 1) with a *P* value of 0.003 and a *P* value of 0.002, respectively, for area and length in *de novo* patients compared with controls and a *P* value <0.001 for area and length in the 2–5 year PD group compared with controls (Fig. 2). However, substantial overlaps were observed between the *de novo* and the 2–5 year disease duration groups (Fig. 2), with no significant difference observed between the two groups (*P* value of 0.22 for area and of 0.62 for length), although the median area and length of the *de novo* PD group tended to be slightly higher than those of the 2–5 year PD group.

No significant differences were found in the global midbrain area between the three groups (*P* value >0.205). The SN neuromelanin ratio was markedly decreased in the *de novo* and the 2–5 year PD groups compared with the healthy control group (*P* value of 0.014 and of <0.001, respectively) (Table 2). The ratio also had a substantial overlap between the *de novo* and the 2–5 year disease duration groups with no significant difference observed between the two groups (*P* value of 0.141).

Receiver operating characteristic analyses for the area showed an AUC of 0.73 in patients with *de novo* PD, whereas it was 0.85 in patients with 2–5 year disease duration. AUC values obtained for length were 0.79 for *de novo* PD and 0.82 for the 2–5 year PD group.

Amongst these, the sensitivity and specificity of the SN high signal area for discriminating the *de novo* PD group from the healthy control group were 70% and 65%, respectively, when the cut-off value for the area was set at 23 mm^2. The sensitivity and specificity for discriminating the 2–5 year PD group from the control group were 60% and 100%, respectively, with an area cut-off value of 21 mm^2. The sensitivity and specificity for the maximal length of the SN high signal for discriminating the *de novo* PD group from the control group were 83.3% and 70%, respectively, for a length cut-off value of 45.73 mm. For discriminating the 2–5 year PD group from the control group, the sensitivity and specificity were 83% and 70%, respectively, with a length cut-off value of 45.6 mm (Table 3 and Fig. 3).

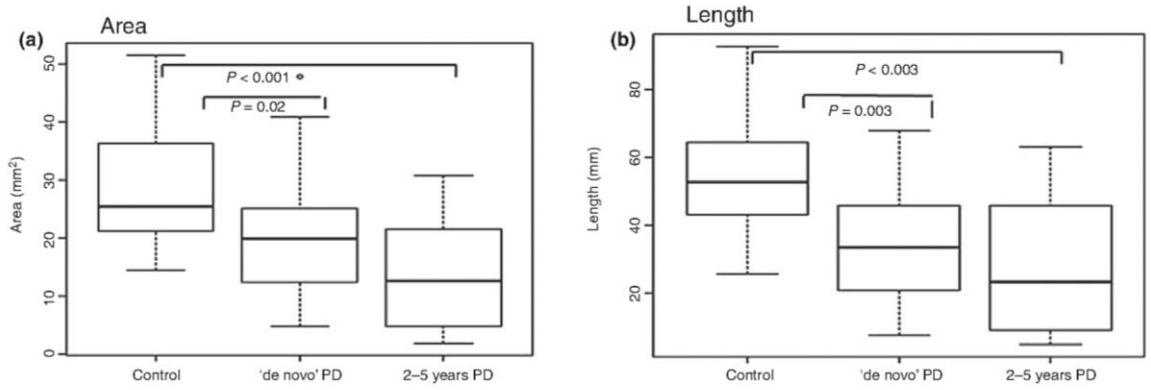

Figure 2 Area (a) and maximal length (b) of the SN high intensity region on neuromelanin-sensitive MR images in patients with *de novo* and 2–5 year PD and healthy controls: *P* values, Mann–Whitney *U* test.

Table 2 SN neuromelanin T1 high signal and midbrain measurements

	De novo PD	2–5 year PD	Controls	*P* value[a]
SN neuromelanin area (mm^2), median (range)	19.88 (4.78–47.84)	12.58 (1.85–28.86)	25.4 (14.51–51.55)	<0.001
SN neuromelanin length (mm), median (range)	33.41 (7.40–67.89)	23.14 (4.70–63.07)	52.75 (25.53–92.76)	<0.001
Midbrain area (mm^2), median (range)	60.30 (51.88–72.19)	63.20 (56.96–70.42)	59.30 (56.55–66.84)	0.205
SN neuromelanin ratio, median (range)	0.36 (0.08–0.85)	0.19 (0.03–0.53)	0.42 (0.24–0.83)	<0.001

PD, Parkinson's disease; SN, substantia nigra; SN neuromelanin ratio = SN T1 high signal area/midbrain area.
[a]Comparisons using Kruskal–Wallis test.

Table 3 Receiver operator characteristic analysis of neuromelanin-sensitive magnetic resonance imaging for discriminating patients with *de novo* PD and 2–5 year PD duration from healthy subjects

	Cut-off value	Sensitivity (%)	Specificity (%)	AUC
De novo PD vs. control				
Area	23.0 mm^2	70	65	0.73
Length	45.8 mm	83.3	70	0.79
2–5 year PD duration vs. control				
Area	21.1 mm^2	60	100	0.85
Length	45.6 mm	83	70	0.82

PD, Parkinson's disease; AUC, area under the curve.

Discussion

In the present study, with semi-automated MRI measures, significant changes could be detected in the area and length of the T1 high signal area of the SN corresponding to the neuromelanin in early stage PD compared with healthy individuals. Clinical symptoms of PD are generally apparent when a substantial part of the dopaminergic neurons of the SN are lost [10,11] and therefore it is expected that even in early disease stages a substantial loss of neuromelanin-containing

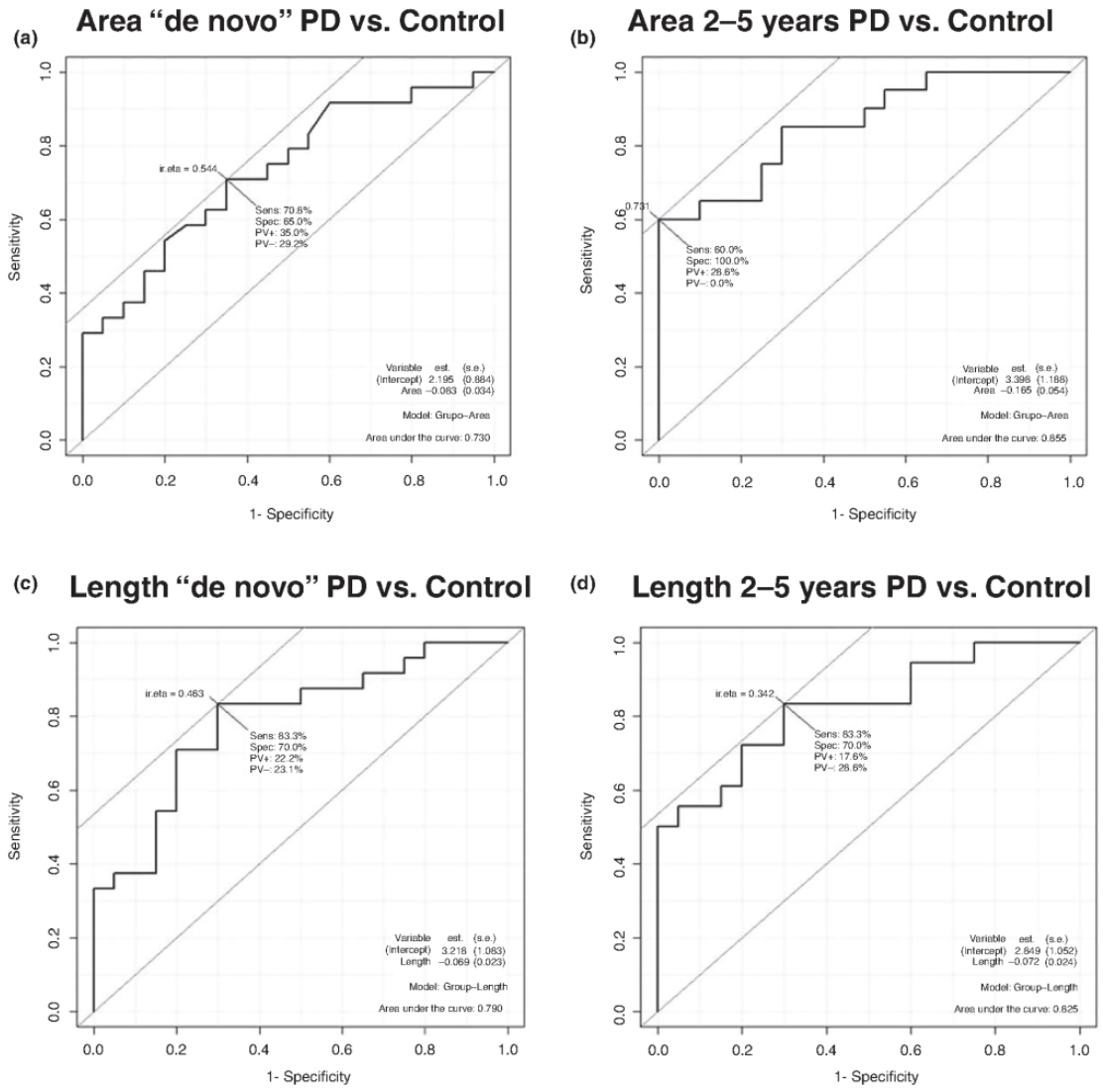

Figure 3 Receiver operator characteristic (ROC) curves of the area for differentiating between *de novo* PD and healthy subjects (a) and between 2–5 year PD patients and healthy controls (b); ROC curves of the length to differentiate between *de novo* PD and healthy subjects (c) and between 2–5 year PD patients and healthy controls (d).

neurons would be detectable by MRI-sensitive sequences. It is also known from pathological studies that the neuronal loss in PD is more pronounced in the ventrolateral region of the SNpc with relative preservation of the dorsal region [11] and so both the area and length of the SN T1 high signal region were studied because the maximal length gives a measure of the longitudinal extension additional to the global area.

In the present study, both the area and the maximal length of the SN T1 high signal region were significantly reduced, suggesting neuronal depletion in patients with early PD compared with healthy individuals. Moreover, high sensitivity and specificity of the values of both of our measurements were obtained when differentiating patients with early PD from controls. The sensitivity and specificity of the maximal length are higher than the sensitivity and specificity obtained for the area measurements for discriminating the *de novo* PD group from the healthy controls. This finding supports the longitudinally expected difference of the SN with greater ventrolateral neuronal loss in early stage PD.

To evaluate the possible impact of midbrain volume reduction in PD patients that might influence neuromelanin measurements the ratio of SN neuromelanin T1 high signal area to total midbrain area was calculated for each group. As expected the midbrain area was similar between the groups and the calculated ratios showed a significant reduction of SN neuromelanin in *de novo* and 2–5 year PD patients, demonstrating that the individual midbrain area does not influence the detection of neuromelanin changes in PD.

In our study, significant differences were not observed in the area or length of the SN neuromelanin between the groups with *de novo* and 2–5 year disease duration PD. These findings, using semi-automated methods, are consistent with recent findings in a study that investigated signal intensity changes in SN neuromelanin [12], which also found no difference between untreated and advanced stage (H&Y 3–5) PD patients. Interestingly, these findings are also consistent with transcranial sonography studies in PD demonstrating that the ultrasound signal does not change in the course of the disease [13]. The area and length of the SN T1 high signal region were studied, and these measures are similar to the signal intensity changes recently reported in the SNpc [12], providing two different measures of the reduction of SN neuromelanin in early PD.

Our sensitivity and specificity results are consistent with previous reports [12,14]. The semi-automated method used in our study is less operator dependent and less time consuming than the manual SN segmentation for neuromelanin estimation [12]. The use of a region-growing algorithm for SN segmentation increases accuracy and reduces the time required for image analysis. To improve the signal-to-noise ratio of this algorithm a previous group performed image smoothing applying a Gaussian filter on a three-dimensional sequence [14]. As Gaussian filters lead to edge blurring an alternative filtering approach was used that gives more accurate area estimations and enabled semi-automated measurements of SN T1 high signal on two-dimensional images with only a few required operator-dependent steps (signal normalization and definition of seed points).

The correlation of neuromelanin decrease with the known pathological changes associated with disease duration and progression of clinical severity [11] needs to be investigated. The different imaging and measurement methods in previous studies might explain the inconsistent findings in neuromelanin patterns in relation to disease duration [6,15]. Additionally, the correlation of iron load with the SN neuromelanin-sensitive MRI needs further analysis, as it is known that iron content in the SN increases in PD and during its progression [16]. Neuromelanin exhibits paramagnetic properties when bound to iron that result in the acceleration of T1 relaxation [17,18], and therefore the increased iron load in the SN in PD patients might enhance neuromelanin-related contrast. Variations in the neuromelanin-related signal of the SNpc related to the iron content are currently being investigated by our group with a direct correlation of the neuromelanin signal with iron quantification with a relaxometry sequence.

However, our study has several limitations, namely the small number of patients in each group and the absence of pathological confirmation because the PD diagnosis was only clinical. Another aspect is related to the disadvantages of the imaging technique, including the long acquisition time, the relatively low spatial resolution and the existence of in-plane signal inhomogeneity. In addition, the region-growing post-processing technique used in this study for semi-automated measurement of volumes requires the determination of seed points and normalization of signal intensity that could not be completely automated. The total imaging analysis is relatively time consuming and requires the implementation of post-processing software that is not widely available. However, only two operator-dependent steps are required, and the rest of the analysis is automated and operator independent. Motion artifacts were not a problem in our early stage patients, with few involuntary movements, but advanced stage patients might have problems that will need to be addressed.

Further prospective studies are required to address all of these issues.

Conclusions

Magnetic resonance neuromelanin-sensitive images were sufficient for detecting significant changes in the SN at the time of clinical diagnosis of PD. Our findings suggest that the neuromelanin changes remain stable with disease progression, consistent with previous findings based on sonography. MRI neuromelanin-sensitive techniques might become a useful diagnostic tool with high sensitivity and specificity for the diagnosis of PD.

Acknowledgements

The authors thank all of the patients and control subjects for their time and commitment to this research. We are also grateful for all the help and expertise from engineer Nuno Loucão in the MRI sequence optimization.

Disclosure of conflicts of interest

The authors declare no financial or other conflicts of interest.

References

1. Mann DM, Yates PO. Pathological basis for neurotransmitter changes in Parkinson's disease. *Neuropathol Appl Neurobiol* 1983; **9:** 3–19.
2. Braak H, Del Tredici K, Rüb U, *et al*. Staging of brain pathology related to sporadic Parkinson's disease. *Neurobiol Aging* 2003; **24:** 197–211.
3. Double KL, Gerlach M, Schünemann V, *et al*. Iron-binding characteristics of neuromelanin of the human substantia nigra. *Biochem Pharmacol* 2003; **66:** 489–494.
4. Sasaki M, Shibata E, Tohyama K, *et al*. Neuromelanin magnetic resonance imaging of locus coeruleus and substantia nigra in Parkinson's disease. *NeuroReport* 2006; **17:** 1215–1218.
5. Sasaki M, Shibata E, Kudo K, Tohyama K. Neuromelanin sensitive MRI. *Clin Neuroradiol* 2008; **18:** 147–153.
6. Kashihara K, Shinya T, Higaki F. Neuromelanin magnetic resonance imaging of nigral volume loss in patients with Parkinson's disease. *J Clin Neurosci* 2011; **18:** 1093–1096.
7. Huges AJ, Daniel SE, Kilford L, Lees AJ. Accuracy of clinical diagnosis of idiopathic Parkinson's disease: a clinic-pathological study of 100 cases. *J Neurol Neurosurg Psychiatry* 1992; **55:** 181–184.
8. Nikos Nikolaou NP. Color reduction for complex document images. *Int J Imaging Syst Technol* 2009; **19:** 14–26.
9. Sun X, Zhang H, Duan H. 3D computerized segmentation of lung volume with computed tomography. *Acad Radiol* 2006; **13:** 670–677.
10. Birkmayer W, Birkmayer JD. Dopamine action and disorder of neurotransmitter balance. *Gerontology* 1987; **33:** 168–171.
11. Fearnley JM, Lees AJ. Ageing and Parkinson's disease: substantia nigra regional selectivity. *Brain* 1991; **114:** 2283–2301.
12. Ohtsuka C, Sasaki M, Konno K, *et al*. Changes in substantia nigra and locus coeruleus in patients with early-stage Parkinson's disease using neuromelanin-sensitive MR imaging. *Neurosci Lett* 2013; **541:** 93–98.
13. Berg D. Transcranial sonography in the early and differential diagnosis of Parkinson's disease. *J Neural Tansm Suppl* 2006; **70:** 249–254.
14. Ogisu K, Kudo K, Sasaki M, *et al*. 3D neuromelanin-sensitive magnetic resonance imaging with semi-automated volume measurement of the substantia nigra pars compacta for diagnosis of Parkinson's disease. *Neuroradiology* 2013; **55:** 719–724.
15. Schwarz ST, Rittman T, Gontu V, *et al*. T1-weighted MRI shows stage-dependent substantia nigra signal loss in Parkinson's disease. *Mov Disord* 2011; **26:** 1633–1638.
16. Graham JM, Paley MN, Grünewald RA, Hoggard N, Griffiths PD. Brain iron deposition in Parkinson's disease imaged using the PRIME magnetic resonance sequence. *Brain* 2000; **123:** 2423–2431.
17. Enochs WS, Petherick P, Bogdanova A, Mohr U, Weissleder R. Paramagnetic metal scavenging by melanin: MR imaging. *Radiology* 1997; **204:** 417–423.
18. Tosk JM, Holshouser BA, Aloia RC, *et al*. Effects of the interaction between ferric iron and L-dopa melanin on T1 and T2 relaxation times determined by magnetic resonance imaging. *Magn Reson Med* 1992; **26:** 40–45.

RESEARCH ARTICLE

Substantia Nigra Neuromelanin-MR Imaging Differentiates Essential Tremor From Parkinson's Disease

Sofia Reimão, MD,[1,2] Patrícia Pita Lobo, MD,[2,3,4] Dulce Neutel, MD,[2,3] Leonor Correia Guedes, MD,[2,3,4] Miguel Coelho, MD,[2,3] Mário M. Rosa, MD,[2,3,5] Pedro Azevedo, MSc,[6] Joana Ferreira, MSc,[6] Daisy Abreu, MSc,[2] Nilza Gonçalves, MSc,[2] Rita G. Nunes, PhD,[6] Jorge Campos, PhD,[1] and Joaquim J. Ferreira, PhD[2,3,4,5]*

[1]*Neurological Imaging Department, Hospital de Santa Maria, Centro Hospitalar Lisboa Norte, Portugal*
[2]*Clinical Pharmacology Unit, Instituto de Medicina Molecular, Faculty of Medicine, University of Lisbon, Portugal*
[3]*Neurology Department, Hospital de Santa Maria, Centro Hospitalar Lisboa Norte, Portugal*
[4]*CNS—Campus Neurológico Sénior, Torres Vedras, Portugal*
[5]*Laboratory of Clinical Pharmacology and Therapeutics, Faculty of Medicine, University of Lisbon, Portugal*
[6]*Instituto de Biofísica e Engenharia Biomédica, Faculdade de Ciências, Universidade de Lisboa, Portugal*

ABSTRACT: Essential tremor (ET) is a very common movement disorder that has no diagnostic markers. Differentiation with Parkinson's disease (PD) can be clinically challenging in some cases, with a high rate of misdiagnosis. Magnetic resonance imaging (MRI) studies have been able to identify neuromelanin changes in the substantia nigra (SN) of PD patients, but they have thus far not been investigated in ET. In this study, we aimed to characterize neuromelanin-MR signal changes in ET and evaluate its diagnostic accuracy in the differential diagnosis with PD. The inclusion criteria were patients with ET and untreated "de novo" PD patients; in addition, age-matched controls were enrolled. These were studied with a high-resolution T1-weighted MRI sequence at 3.0 Tesla to visualize neuromelanin. The primary outcomes were the area and width of the SN region with high signal. A total of 15 ET patients and 12 "de novo" PD patients were evaluated. The area and width of the T1 high signal in the SN region were markedly decreased in the PD group compared with the ET and age-matched controls, and a greater decrease was seen in the ventrolateral segment. The neuromelanin measures in the ET group, although slightly lower, were not significantly different from the healthy control group. We obtained a sensitivity of 66.7% and a specificity of 93.3% in discriminating ET from early-stage PD. Neuromelanin-sensitive MRI techniques can discriminate ET from early-stage tremor-dominant PD and can be a useful clinical tool in the evaluation of tremor disorders. © 2015 International Parkinson and Movement Disorder Society

Key Words: essential tremor; Parkinson's disease; neuromelanin; *substantia nigra*; MRI

Essential tremor (ET) is a very common neurological disorder[1-4] that has an estimated prevalence of approximately 5% in the population older than 65 years.[5,6] Essential tremor is clinically characterized by a symmetric 4-Hz to 8-Hz action tremor that most frequently affects the hands and arms, but it also can involve the head.[7] Typical ET cases can be easily diagnosed and distinguished from Parkinson's disease (PD), which is characterized by an asymmetrical 3-Hz to 5-Hz resting tremor.[8] However, the clinical differentiation between these conditions can be challenging, and considerable overlap is seen in the clinical features, particularly in the early stages of the disease.[8,9] This differentiation is very important in defining prognosis and treatment decisions and in identifying patients for research, but a high rate of ET misdiagnosis has been described in several studies,[10-13] emphasizing the need for additional diagnostic evaluation.

*Correspondence to: Dr. Joaquim J. Ferreira, Laboratório de Farmacologia Clínica e Terapêutica, Faculdade de Medicina da Universidade de Lisboa, Av. Prof. Egas Moniz, 1649-028 Lisboa, Portugal, E-mail: joaquimjferreira@gmail.com

Funding agencies: This work had no financial support.

Relevant conflicts of interest/financial disclosures: Nothing to report. Full financial disclosures and author roles may be found in the online version of this article.

Received: 20 August 2014; **Revised:** 21 January 2015; **Accepted:** 26 January 2015

Published online 00 Month 2015 in Wiley Online Library (wileyonlinelibrary.com). DOI: 10.1002/mds.26182

The etiology of ET is unknown, and its pathophysiology is still poorly understood. Several magnetic resonance imaging (MRI) studies have investigated morphological and functional brain alterations in ET patients,[14-16] and some pathological studies have recently shown evidence of structural brain changes in this disease that might be associated with neurodegeneration.[17]

Recent imaging studies have reported changes in the SN of ET patients with an increased echogenicity in sonography studies[18,19] and MR T2*-relaxometry signal reduction,[20] suggesting the involvement of the SN and nigrostriatal degeneration as in PD.

Parkinson's disease is characterized by depigmentation of the substantia nigra pars compacta (SNpc) and of the locus coeruleus, which is related to the loss of neuromelanin.[21] Over the few last years, new MRI sequences have been able to detect a significant reduction in the SN neuromelanin signal in PD,[22-25] and these changes have a high diagnostic sensitivity and specificity for PD diagnosis, even in the very early clinical stages.

Despite the identified SN changes in ET, the SN neuromelanin changes in ET have not previously been studied. In this study, we analyzed the neuromelanin MR signal pattern in ET and the accuracy of this imaging technique in the differential diagnosis with early-stage PD. To the best of our knowledge, this is the first study of MR neuromelanin imaging in ET.

Patients and Methods

Patients and Control Subjects

The study had a cross-sectional case-control design that included 37 subjects; 15 patients had ET, 12 patients had de novo PD, and 10 were control subjects. Patients were recruited from the Movement Disorders Unit of the University Hospital of Santa Maria-Lisbon. The PD patients were included at the time of clinical diagnosis if they were not on antiparkinson medications. All patients were diagnosed by a movement disorders specialist and fulfilled the ET criteria of the Movement Disorder Society on Tremor[26] or the PD UK Brain Bank criteria.[27] The healthy control subjects were recruited from local hospital staff and relatives. Dementia, psychiatric illness, or contraindications to an MRI were the exclusion criteria.

All examinations were performed with the understanding of and written consent from each subject, with approval from the local ethics committee, and in compliance with national legislation and the Declaration of Helsinki guidelines.

MRI Protocol

Imaging Protocol

All data were acquired using a 3.0Tesla Phillips scanner (Phillips Achieva). The following neuromelanin-sensitive pulse sequence was used as previously described by Sasaki et al.[22]: T1-weighted fast spin echo (FSE): repetition time/effective echo time, 633/10 ms; echo train length, 3; number of slices, 20; slice thickness, 2.5 mm; intersection gaps, 0 mm; matrix size, 548 × 474; field of view, 220 × 190 mm^2 (pixel size: .40 × .40 mm^2); and acquisition time, 8 min. The sections were carefully set in the oblique axial plane perpendicular to the fourth ventricle floor, with coverage from the posterior commissure to the inferior border of the pons.

T1- and T2-weighted images of the entire brain were additionally obtained in all subjects and evaluated by an experienced neuroradiologist to exclude other pathological imaging findings, namely, changes in the parkinsonian index and other atypical parkinsonian syndrome changes as well as lesions in the locus coeruleus and SN areas that could interfere with further assessment.

Imaging Analysis

Images were transferred to a Linux workstation for analysis, and an edge-preserving filter[28] was applied using Matlab (R2012a, The Math Works, Natick, MA, USA) to reduce the image noise. T1 high signal in the SN region was visible in three slices, and the middle slice corresponding to the greatest SN volume was selected (Fig. 1A-C). A rectangular region was then selected in this slice, and two symmetrical seed points were manually defined on the most medial part of the high-intensity area in the SN. A region growing algorithm[29] was used for segmentation starting from each seed point, and the area of interest (AOI) was automatically drawn. Pixels with a signal intensity within the interval $I_{seed} \pm 0.035 \times (I_{max} - I_{min})$ were labeled as belonging to the AOI, where I_{seed} is the intensity at the seed point, and I_{max} and I_{min} are the maximum and minimum signal intensities, respectively, within the rectangular mesencephalon region of interest (ROI). The threshold used to delimit the AOI was chosen after a preliminary optimization study using healthy controls and PD patients,[30] in which the threshold was varied using a batch process; the final value of 3.5% was selected because it provided a better visual fit to the anatomical area. The optimal threshold value depends on the contrast and signal-to-noise ratio of the input images, and so it should be adjusted for each specific set of acquisition conditions, imaging sequence, and coils used for signal reception. The AOI was automatically calculated (Fig. 1D-1F). Because no significant differences were found regarding side for the SN area measurements, the median value was obtained from an average between the left and right neuromelanin area obtained for each subject.

Additional manual measures were performed in the same slice used for the automatic measurements. The high signal region was selected in this slice, and a line

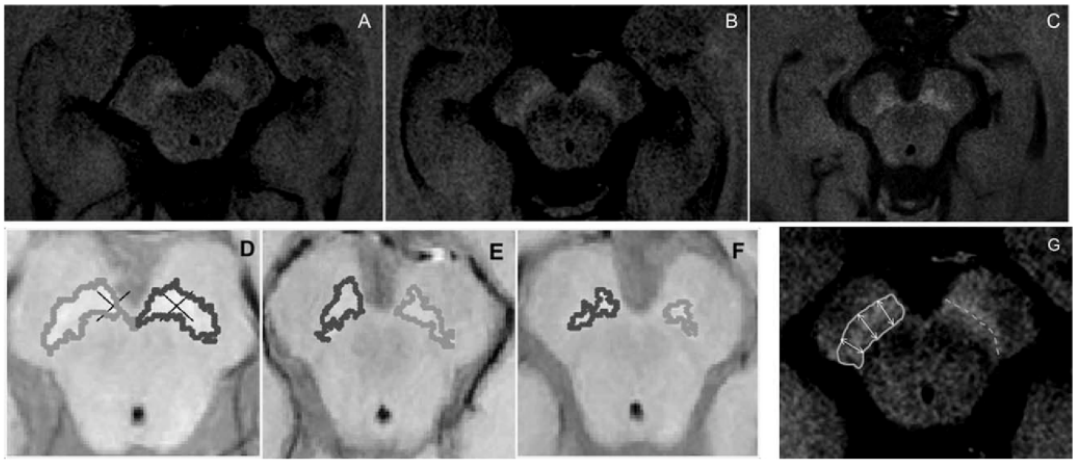

FIG. 1. SN neuromelanin-MRI of (**A**) control, (**B**) ET, and (**C**) PD patients; segmented areas in the same groups: (**D**) control, (**E**) ET, and (**F**) PD patients; the crosses in (**D**) represent the placement of the seed points in that specific subject; (**G**) width measurement example in an ET patient. SN = substantia nigra; MRI = magnetic resonance imaging; ET =essential tremor; PD = Parkinson's disease.

was defined following the maximal longitudinal length of the SN area. This line was divided into three equal segments defining the lateral, central, and medial SN parts. One of the authors (R.S.), who was blinded to the subject information, performed manual measurements of the maximal width of the T1 high signal area perpendicular to the length line for the three SN parts, as shown in Figure 1G. Measurements were performed on both sides, and because no significant differences were found between the left and the right sides, the averaged value was used.

Statistical Analysis

The SN high signal area and width obtained for each group were compared using nonparametric analysis. Kruskal-Wallis tests, with pairwise comparisons in which the resulting p-values were corrected according to Bonferroni method, and Mann-Whitney U tests were used as appropriate. A p-value below 0.05 was considered significant. Receiver operation characteristics curve analysis was conducted to assess the discrimination capacity of the measures SN area and width, for ET and PD as well as PD patients and controls; additionally, specificity and sensitivity values were obtained. Optimal cutoff points were assessed through a method that simultaneously maximized the sensitivity and specificity. The area under the curve also was assessed. All statistical analysis was performed with R 2.15.2.

Results

The obtained MRI quality allowed for the clear identification of the high-signal area in the SN region in all subjects. The automated analysis and manual width measurements were possible on all acquired images. We analyzed 15 patients with ET, 12 patients with de novo PD, and 10 controls. The clinical characteristics of these subjects are shown in Table 1. The ET patients were older than the de novo PD patients and controls; no significant differences were observed in sex among the three groups ($p = 0.925$). Essential tremor patients had a median disease duration of 10 y (3-21 y). Parkinson's disease patients had a mild disease severity, with Hoehn and Yahr score of 2 and a mean Unified Parkinson's Disease Rating Scale motor score of 29.08. Tremor of the hands was the presenting symptom in 11 of the 12 PD patients, with only one patient presenting with an akinetic-rigid form. Symptoms at onset were predominantly unilateral, with half of the patients presenting criteria for asymmetric disease on Unified Parkinson's Disease Rating Scale part III.[31]

Using an automated analysis of the SN high signal, we obtained a median area of 19.76 mm^2 for the "de novo" PD patient group, 25.77 mm^2 for the ET group, and 27.78 mm^2 for the controls. We found no significant differences between left and right SN areas ($p = 0.630$).

In the lateral part of the SN, the manually measured median width of the T1 high signal was 1.5 mm, 2.0

TABLE 1. Demographics for essential tremor, Parkinson's disease, and control subjects

	ET	PD	Controls	*P* Value
No. (female/male)	15 (8/7)	12 (7/5)	10 (4/6)	0.925
Age, y (mean ± SD)	70.5 (±12.5)	63.2 (± 11.9)	61.2 (±7.3)	0.036
UPDRS-III motor score (mean ± SD)	—	29.1 (±14.2)	—	—

ET, essential tremor; PD, Parkinson's disease; SD, standard deviation.

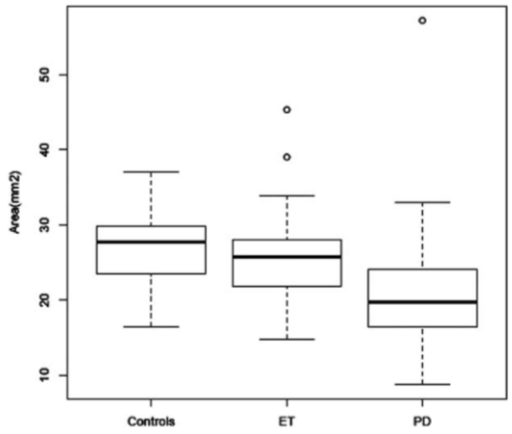

FIG. 2. Area of the SN high-intensity region on neuromelanin-sensitive MR images in patients with ET, "de novo" PD, and controls; *P* values, Mann-Whitney *U*-test. SN = substantia nigra; MR = magnetic resonance; ET = essential tremor; PD = Parkinson's disease.

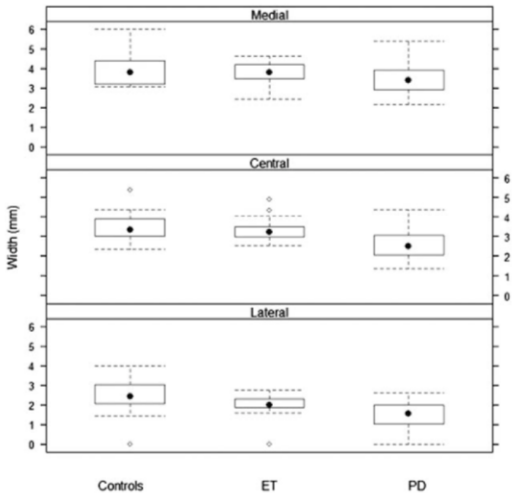

FIG. 3. Width of the SN high-intensity region on neuromelanin-sensitive MR images in patients with ET, "de novo" PD, and healthy controls, *P* values, Mann-Whitney *U*-test. SN = substantia nigra; MR = magnetic resonance; ET = essential tremor; PD = Parkinson's disease.

mm, and 2.4 mm in the PD, ET, and healthy control groups, respectively. In the central part, the median width was 2.5 mm, 3.2 mm, and 3.3 mm in the PD, ET, and healthy control groups, respectively. In the medial segment, the median widths were 3.4 mm, 3.8 mm, and 3.8 mm in the PD, ET, and healthy control groups, respectively. If we considered all of the SN segments, the average width of the manually measured T1 high signal was 2.5 mm in the de novo PD patients, 3.2 mm in ET group, and 3.2 mm in the healthy control group.

The measured area of the SN T1-high signal was only slightly reduced in the ET patients compared with controls, with $P > 0.05$, but it was markedly decreased in the PD group compared with the ET and healthy control groups ($P < 0.001$ for both comparisons; Fig 2).

In the ET group, we identified two outliers whose SN area was above the superior level of the control group (Fig. 2). To see how the outlying observations could influence the results, we removed them and performed a sensitivity analysis. Excluding the outliers, the SN neuromelanin median area in ET patients was 25.54 mm^2, and the group comparisons yielded similar results with a significant reduction in the neuromelanin SN high-signal area in PD patients compared with ET and controls ($P < 0.001$), and no significant differences between the ET patients compared with controls ($P = 0.909$). The SN neuromelanin manual width measurements were reduced in the PD group compared with ET and controls with *P* values of 0.002 and <0.001, respectively. The greatest reduction was evident at the lateral and central SN segments, with $P < 0.001$ and $P = 0.005$, respectively (Fig. 3). Two outliers were identified in the lateral SN segment (1 control and 1 ET patient) (Fig. 3), with measured width close to zero. We reviewed these images and the lateral midbrain region had reduced image quality, which might have influenced the visual identification of the T1 high signal area image and the manual measurement. We did not find any significant differences between the ET and control groups for the neuromelanin SN measurements ($P = 0.261$), using either method, although the median measurements of the ET group tended to be slightly lower than the controls (Figs. 2 and 3).

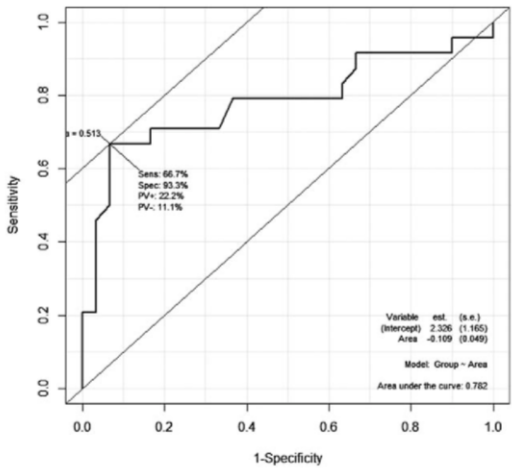

FIG. 4. ROC curve of the area for differentiating between ET and "de novo" PD patients. ROC = receiver operating characteristics; ET = essential tremor; PD = Parkinson's disease.

The sensitivity and specificity of the SN high signal area for discriminating the ET patients from the PD patients were 66.7% and 93.3%, respectively, when the cutoff value for the area was set at 24.08 mm^2.

The sensitivity and specificity for discriminating the de novo PD group from the control group were 70.8% and 80%, respectively, with an area cutoff value of 24.08 mm^2 (Fig. 4).

Discussion

In this MRI study, we were able to detect significant differences in the neuromelanin SN pattern of ET compared with PD. In ET, the neuromelanin in the SN was not significantly reduced compared with the healthy control group, but the PD patients, even at the time of clinical diagnosis, exhibited a significant reduction in the SN T1-high signal, which was more pronounced laterally in accordance with known pathological changes.[31] Using different SN neuromelanin signal measurement methods, manual and semi-automated, we obtained similar findings for the T1-high signal area and width, enabling the differentiation of ET patients from the de novo PD group with very high sensitivity and specificity.

We know from pathological studies that the neuronal loss in PD occurs asymmetrically and early in the course of PD or even in preclinical stages,[32] and that it is more pronounced in the ventrolateral region of the SNpc with relative preservation of the dorsal region.[33] We used manual width measurements additionally to the automated global area to study the pattern changes in the different segments of the SN T1 high signal region. In agreement with previous neuromelanin studies,[22-24,34] our neuromelanin data reproduce the SN pathological findings in PD, suggesting SN neuromelanin neuronal depletion in patients with early PD that is absent in ET or healthy individuals. We were not able to find a significant asymmetry in the SN area nor a correlation with the clinically most affected side in our PD patients. This may be attributable to the small number of subjects in our samples, which limits our power.

Considering the reported sonography changes of the SN in ET,[18,19] our data show that, contrary to the findings in PD, the increased echogenicity of the SN in ET is not related to reduced SN neuromelanin content. These sonography changes might only be related to the increased tissue iron content in ET, which has been recently documented in an MRI quantitative study.[20] Our results corroborate the hypothesis that iron deposition and neuromelanin loss might be separate processes that are related to different pathological processes and variable clinical manifestations, such as specific tremor characteristics. The correlation of neuromelanin and the iron content of the SN requires further investigation and the determination of the different disease pathological patterns that affect the SN in ET and PD and result in different clinical characteristics.

Although the clinical diagnosis of ET in typical cases requires no further diagnostic investigation, in the subset of patients with atypical signs and symptoms, particularly in the early disease stages, there can be a significant benefit from further diagnostic evaluation because the distinction with PD has important therapeutic and prognostic consequences. In this study, the obtained moderate sensitivity and high specificity for MRI neuromelanin studies are only slightly lower than those obtained in [^{123}I]-FP-CIT single photon emission computed tomography (SPECT) studies in discriminating ET from PD.[13,35,36] This MRI technique is safe and widely available; as a result, it might have the potential to become an alternative to the more expensive nuclear medicine techniques that have additional risks[36] in the diagnostic evaluation of tremor disorders.

However, our study has several limitations, including the small number of patients in each group and the absence of pathological confirmation. The small sample size of our study groups limits the precision of the obtained estimates of sensitivity and specificity, and so further studies are needed to strengthen the performance characteristics of this imaging method in the distinction between PD and ET patients.

Another aspect is related to the disadvantages of the imaging technique, including the long acquisition time, the relatively low spatial resolution, and the existence of in-plane signal inhomogeneity. Slice positioning and partial voluming may be confounding factors in surface-based measurements, which could potentially be improved by using a three-dimensional acquisition.[37]

Additionally, the region-growing postprocessing technique used in this study for the semi-automated measurement of areas requires the determination of seed points and normalization of signal intensity that could not be completely automated. Although the same criteria were followed for the placement of the seed points on each image, in the future the impact of varying their position on the estimated neuromelanin SN area should be investigated to determine the reproducibility of this method.

The total imaging analysis is relatively time consuming and requires the implementation of postprocessing software that is not widely available. However, the manual analysis yields very similar results, and, although it is operator dependent, it is very fast and widely available without the need for postprocessing software. The within-subject and inter-rater reproducibility of MR neuromelanin measurements has not been fully established, and so the reproducibility of these parameters needs to be addressed in further studies,

especially concerning the manual analysis, to allow a wider implementation of this imaging technique.

Motion artifacts were not a problem in either the ET or PD groups, but these were early-stage patients. Advanced-stage patients with exuberant tremor might have artifact problems that will require further adjustments.

Two outliers (one control and one ET patient) had neuromelanin lateral SN widths close to zero, which could be related to the poor image quality in the lateral midbrain region. A possible source of subject-dependent contrast variation is the effective B1 field, which is determined by the electrical properties of the tissue (its conductivity and permittivity). In the future, the acquisition protocol should be further optimized, so as to improve image contrast and consistently enable good visualization of the SN.

The number of patients in our study did not allow statistical correlation with clinical severity or age group correction of the SN neuromelanin measurements. However, a previous neuromelanin MR study with 80 PD patients found no correlation between age and neuromelanin SN volumes in PD patients or control subjects,[24] and so age is not likely to be an influencing factor in our results, although we cannot completely exclude it. In the same study, the authors found an inverse correlation between neuromelanin-sensitive SN volume and the Hoehn and Yahr stage and disease duration in PD patients.

Our small sample does not allow PD patients' stratification in clinical subtypes for further analysis, but almost all of our PD patients had tremor as the presenting symptom. Akinetic-rigid and tremor-dominant subtypes of PD are known to have different neuropathological patterns,[38] with greater SN neuronal loss in akinetic-rigid patients (with ventrolateral predominance) compared with tremor-dominant patients (with medial predominance).[39] We found a significantly different SN neuromelanin pattern in ET versus PD patients, in agreement with the known absence of pathomorphological SN changes in ET, but further studies are needed to specifically investigate the difference in neuromelanin SN MRI changes in PD clinical subtypes. The obtained sensitivity for PD patients' discrimination was lower than the specificity, which might be intrinsically related to SN neuromelanin changes in PD. The current understanding of the relationship between the extent of dopamine cell loss and the clinical manifestations of PD remains unclear, and previous dopaminergic brain imaging studies have reported that some PD patients with mild symptoms have no evidence of dopaminergic dysfunction.[40] Also, the SN neuromelanin volume may not directly reflect the dopaminergic function because degenerated nigral cells might still contain neuromelanin granules,[33] influencing MRI signal measurements.

Conclusion

Magnetic resonance neuromelanin-sensitive images were able to accurately distinguish ET from tremor-dominant PD patients even at the time of PD clinical diagnosis. We detected significant neuromelanin changes in the SN of PD patients that are not present in ET, highlighting the different pathological processes in the SN of these two tremor conditions. Magnetic resonance imaging neuromelanin-sensitive techniques might become a useful diagnostic tool for the differentiation of ET from PD in very early clinical stages. ■

Acknowledgments: We thank all of the patients and control subjects for their time and commitment to this research. We are also thankful for all of the help and expertise provided by engineer Nuno Loução in the MRI sequence optimization and to Ana Teresa Santos for technical assistance.

References

1. Bach JP, Ziegler U, Deuschl G, Dodel R, Doblhammer-Reiter G. Projected numbers of people with movement disorders in the years 2030 and 2050. Mov Disord 2011;26:2286-2290.
2. Louis ED, Thawani SP, Andrews HF. Prevalence of essential tremor in amultiethnic, community-based study in northern Manhattan, New York, N.Y. Neuroepidemiology 2009;32:208-214.
3. Benito-León J, Bermejo-Pareja F, Morales JM, Vega S, Molina JA. Prevalence of essential tremor in three elderly populations of central Spain. Mov Disord 2003;18:389-394.
4. Benito-León J. Essential tremor: one of the most common neurodegenerative diseases? Neuroepidemiology 2011;36:77-78.
5. Louis ED, Ferreira JJ. How common is the most common adult movement disorder? Update on the worldwide prevalence of essential tremor. Mov Disord 2010;25:534-541.
6. Louis ED. Age of onset: can we rely on essential tremor patients to report this? Data from a prospective, longitudinal study. Neuroepidemiology 2013;40:93-98.
7. Hardesty DE, Maraganore DM, Matsumoto JY, Louis ED. Increased risk of head tremor in women with essential tremor: longitudinal data from the Rochester Epidemiology Project. Mov Disord 2004;1:529-533.
8. Pahwa R, Koller WC. Is there a relationship between Parkinson's disease and essential tremor? Clin Neuropharmacol 1993;16:30-35.
9. Marshall VL, Reininger CB, Marquardt M, et al. Parkinson's disease is overdiagnosed clinically at baseline in diagnostically uncertain cases: a 3 year European multicenter study with repeat [^{123}I]-FP-CIT SPECT. Mov Disord 2009;24:500-508.
10. Schrag A, Münchau A, Bhatia KP, et al. Essential tremor: an overdiagnosed condition? J Neurol 2000;245:955-999.
11. Jain S, Lo SE, Lewis ED. Common misdiagnosis of a common neurological disorder: how are we misdiagnosing essential tremor? Arch Neurol 2006;63:1100-1104.
12. Geraghty JJ, Jankovic J, Zetusky WJ. Association between essential tremor and Parkinson's disease. Ann Neurol 1985;17:329-333.
13. Benamer HTS, Patterson J, Grosset DG. Accurate differentiation of parkinsonism and essential tremor using visual assessment of [^{123}I]- FP-CIT SPECT imaging: the [^{123}I]- FP-CIT SPECT study group. Mov Disord 2000;15:503-510.
14. Pagan FL, Butman JA, Dambrosia JM, Hallett M. Evaluation of essential tremor with multi-voxel magnetic resonance spectroscopy. Neurology 2003;60:1344-1347.
15. Quattrone A, Cerasa A, Messina D, et al. Essential head tremor is associated with cerebellar vermis atrophy: a volumetric and voxel-based morphometry MR imaging study. AJNR Am J Neuroradiol 2008;29:1692-1697.

16. Nicoletti G, Manners D, Novellino F, et al. Diffusion tensor MRI changes in the cerebellar structures of patients with familial essential tremor. Neurology 2010;74:988-994.
17. Louis ED. Essential tremor: evolving clinicopathological concepts in an era of intensive post-mortem enquiry. Lancet Neurol 2010;9: 613-622.
18. Stockner H, Sojer M, Seppi K, et al. Midbrain sonography in patients with essential tremor. Mov Disord 2007;22:414-417.
19. Stockner H, Wurster I. Transcranial sonography in essential tremor. Int Rev Neurobiol 2010;90:189-197.
20. Novellino F, Cherubini A, Chriaco C, et al. Brain iron deposition in essential tremor: a quantitative 3-Tesla magnetic resonance imaging study. Mov Disord 2013;28;196-200.
21. Double KL, Gerlach M, Schünemann V, et al. Iron-binding characteristics of neuromelanin of the human substantia nigra. Biochem Pharmacol 2003;66:489-494.
22. Sasaki M, Shibata E, Tohyama K, et al. Neuromelanin magnetic resonance imaging of locus coeruleus and substantia nigra in Parkinson's disease. Neuroreport 2006;17:1215-1218.
23. Sasaki M, Shibata E, Kudo K, Tohyama K. Neuromelanin sensitive MRI. Clin Neuroradiol 2008;18:147-153.
24. Kashihara K, Shinya T, Higaki F. Neuromelanin magnetic resonance imaging of nigral volume loss in patients with Parkinson's disease. J Clin Neurosci 2011;18:1093-1096.
25. Blazejewska AL, Schwarz ST, Pitiot A, et al. Visualization of nigrosome 1 and its loss in PD: pathoanatomical correlation and in vivo 7 T MRI. Neurology 2013;81:534-540.
26. Deuschl G, Bain P, Brin M. Consensus statement of the Movement Disorder Society on Tremor. Ad Hoc Scientific Committee. Mov Disord 1998;13(suppl 3):2-23.
27. Huges AJ, Daniel SE, Kilford L, Lees AJ. Accuracy of clinical diagnosis of idiopathic Parkinson's disease: a clinic-pathological study of 100 cases. J Neurol Neurosurg Psychiatry 1992;55:181-184.
28. Nikolaou N, Papamarkos N. Color reduction for complex document images. International Journal of Imaging Systems and Technology 2009;19:14-26.
29. Sun X, Zhang H, Duan H. 3D computerized segmentation of lung volume with computed tomography. Acad Radiol 2006;13:670-677.
30. Reimão S, Pita Lobo P, Neutel D, et al. Substantia nigra neuromelanin magnetic resonance imaging in de novo Parkinson's disease patients. Eur J Neurol 2014; DOI: 10.1111/ene.1261 [Epub ahead of print].
31. Uitti RJ, Baba Y, Whaley NR, Wszolek ZK, Putzhe JD. Parkinson disease: handedness predicts asymmetry. Neurology 2005;64:1925-1930.
32. Braak H, Del Tredici K, Rüb U, et al. Staging of brain pathology related to sporadic Parkinson's disease. Neurobiol Aging 2003;24: 197-211.
33. Fearnley JM, Lees AJ. Ageing and Parkinson's disease: substantia nigra regional selectivity. Brain 1991;114:2283-2301.
34. Ohtsuka C, Sasaki M, Konno K, et al. Changes in substantia nigra and locus coeruleus in patients with early-stage Parkinson's disease using neuromelanin-sensitive MR imaging. Neurosci Lett 2013; 541:93-98.
35. Vlaar AM, van Kroonenburgh MJ, Kessels AG, et al. Meta-analysis of the literature on the diagnostic accuracy of SPECT in parkinsonian syndromes. BMC Neurol 2007;1:27.
36. de la Fuente-Fernandéz R. Role of DaTSCAN and clinical diagnosis in Parkinson disease. Neurology 2012;78:696-701.
37. Ogisu K, Kudo K, Sasaki M, et al. 3D neuromelanin-sensitive magnetic resonance imaging with semi-automated volume measurement of the substantia nigra pars compacta for diagnosis of Parkinson's disease. Neuroradiology 2013;55:719-724.
38. Paulus W, Jellinger K. The neuropathologic basis of different clinical subgroups of Parkinson's disease. J Neuropathol Exp Neurol 1991;50:743-755.
39. Jellinger KA. Post mortem studies in Parkinson's disease: is it possible to detect brain areas for specific symptoms? J Neural Transm Suppl. 1999;56:1-29.
40. Antonini A, Biundo R. Parkinson's disease: Can dopamine transporter imaging define early PD? Nat Rev Neurol 2014:10:432-433.